

BEAM LOADING IN A PROTON DRIVEN PLASMA WAKEFIELD ACCELERATOR

Veronica K. Berglyd Olsen

Department of Physics

University of Oslo

Norway



Dissertation Presented for the Degree of
Philosophiae Doctor (PhD) in Physics

June 2018

Abstract

Abstract

Acknowledgements

Acknowledgements

Contents

Preface	1
1 Introduction	3
1.1 Plasma Wakefield Acceleration	3
1.1.1 Laser Driven Acceleration	4
1.1.2 Beam Driven Acceleration	5
1.2 Beam and Plasma Interactions	5
1.2.1 Beam Emittance and Twiss Parameters	6
1.2.2 The Drive Beam	7
1.2.3 The Transformer Ratio	8
1.2.4 Plasma Regimes	9
1.2.4.1 The Linear Regime	9
1.2.4.2 The Non-Linear Regime	11
1.2.4.3 The Quasi-Linear Regime	12
1.2.5 Beam Loading	13
1.2.6 Beam Matching	13
1.2.7 Multiple Drive Bunches	14
1.3 Using a Proton Drive Beam	15
1.3.1 Protons vs. Electrons as Drive Beam	15
1.3.2 The Self-Modulation Instability	16
2 The AWAKE Experiment	19
2.1 Evolution of the Concept	20
2.2 AWAKE: A Design Overview	20
2.2.1 Plasma Source	20
2.2.2 Electron Source	21
2.3 Stages of the Experiment	22
2.3.1 AWAKE Run 1	23
2.3.1.1 The Self-Modulation Instability in AWAKE	23
2.3.2 AWAKE Run 2	23
3 AWAKE Data Acquisition	27
3.1 Experiment Measurements	27
3.2 Data Acquisition	28

CONTENTS

3.2.1	Front End Software Architecture (FESA)	29
3.2.2	AWAKE Integration with FESA	29
4	Simulation Method	31
4.1	Simulating the Drive Bunch	31
4.1.1	With a Pre-Modulated Beam	32
4.1.2	With a Single Drive Bunch	33
4.2	Simulating the Witness Bunch	34
4.2.1	Witness Bunch Size and Resolution	34
4.2.2	Witness Bunch Transverse Evolution	36
4.3	Simulating the Plasma	37
5	Simulation Analysis	39
5.1	Extracting Twiss Parameters from Particle Arrays	39
5.2	A Measure for Beam Quality	40
5.3	Full Scale Studies	41
5.4	Beam Loading and Energy Spread	42
5.5	Emittance Evolution	43
5.5.1	The Quasi-Linear Regime	43
5.5.2	The Quasi-Linear + Non-Linear Case	43
5.5.3	Convergence Scan	43
5.6	Optimising the Witness Beam	43
5.7	Summary of Simulation Studies	44
6	Summary and Conclusion	45

Publications

I	Loading of a Plasma-Wakefield Accelerator Section Driven by a Self-Modulated Proton Bunch, <i>Proceedings of IPAC 2015</i>	49
II	Loading of Wakefields in a Plasma Accelerator Section Driven by a Self-Modulated Proton Beam, <i>Proceedings of NAPAC 2016</i>	55
III	Data Acquisition and Controls Integration of the AWAKE Experiment at CERN, <i>Proceedings of IPAC 2017</i>	61
IV	Emittance Preservation of an Electron Beam in a Loaded Quasilinear Plasma Wakefield, <i>Physical Review Accelerators and Beams</i>	67

Appendices

A	Particle in Cell (PIC)	79
----------	-------------------------------	-----------

A.1	The Full Electromagnetic PIC Method	79
A.1.1	Numerical Cherenkov	81
A.2	The Quasi-Static Electromagnetic Method	82
A.3	Considerations	83
B	Data Analysis Tools	85
B.1	The Osiris Analysis Toolbox	85
B.1.1	Core Objects	86
B.1.2	Data Types	86
B.1.3	Graphical Interface and Plots	87
B.2	QuickPIC Analysis Framework	87
B.3	Additional Tools Extending MATLAB Functionality	88
	Bibliography	89

List of Figures

Figure 1.1	Illustration of a plasma wakefield accelerating structure with a single electron drive bunch. The drive bunch produces a series of focusing/defocusing and accelerating/decelerating regions, as seen for an electron witness bunch.	6
Figure 1.2	The phase space ellipse of bunch particles. The figure is recreated from Figure 3.23 by Klauss Wille in <i>The Physics of Particle Accelerators</i> [124].	7
Figure 1.3	Four sample simulations of a proton beam of varying density n_b with respect to the plasma density n_{pe} . Each simulation is representative for the four regimes. The longitudinal and perpendicular wakefields are normalised to their own maxima to illustrate their shape rather than their absolute magnitude.	10
Figure 1.4	The radial function $R(r)$ for a range of uniform beams cut off at a radius a up to twice the plasma skin depth k_{pe}^{-1} . The plot is reproduced from Katsouleas <i>et al.</i> [61].	11
Figure 1.5	Top: Relative on-axis plasma density perturbation for a n_b/n_{pe} density ratio corresponding to a linear, quasi-linear, non-linear and highly non-linear case. Bottom: Longitudinal wakefield per unit of beam charge for the same four cases. The four samples correspond to the four cases presented in Figure 1.3.	12
Figure 1.6	The evolution of the transverse RMS size of an initially matched electron beam as it accelerates through a plasma. The tail of the beam, in red, remains in a region where it is matched, while the head of the beam, in blue, does not. The black line corresponds to the theoretical spot size of the beam at nominal plasma density. Based on simulation data from Publication IV.	14
Figure 2.1	An overview of the CERN Accelerator Complex [77].	19
Figure 2.2	Drawing of the AWAKE experimental area with the key components labelled.	21
Figure 2.3	Drawing of the plasma stage and its related components, as presented in the 2016 AWAKE Status Report [10].	22
Figure 2.4	Drawing of the electron source and accelerating structure [90].	22

Figure 2.5	Resolved streak camera images of the SPS proton beam propagating through the Rb vapour in the AWAKE experiment. The read lines indicate the region of the laser pulse. Left: The laser on low power; that is, no plasma. Centre: The laser on high power, ionising the vapour and defocusing the beam. Right: A high resolution image of the defocused region, showing beam modulation. The image is borrowed from the thesis of M. Turner [111].	24
Figure 3.1	An overview of the CERN Control System structure. The system is layered and with standardised interfaces. The data acquisition happens on the Front End Layer where high performance PCs and PLCs provides real time processing of raw data, which is then fed up to the data logging layer, and then made available to the displays at the top layer. Illustration taken from Publication III, which is again recreated from [46].	28
Figure 3.2	Flow chart of the internal logic in all the FESA File Reader classes developed for AWAKE. Illustration taken from Publication III, and was originally presented at an AWAKE Technical Board meeting in 2016 [15].	29
Figure 4.1	Top: An example of a simulation of half SPS proton bunch before reaching plasma. Bottom: The same bunch after having undergone self-modulation in about 3 m of plasma. The halo of protons ejected from the defocusing regions can be clearly seen, leaving a core of micro bunches on the beam axis.	32
Figure 4.2	An example of a pre-modulated beam of 26 micro-bunches modulated at the plasma wavelength. This simulation set-up was used for Publication I. The density function (see Equation 4.3) is tuned to match the earlier self-modulation simulations shown in Figure 4.1.	34
Figure 4.3	An example of the simulation set-up used for Publication IV. These simulations used a single, rigid proton bunch in blue, with a charge large enough to generate a wakefield equivalent to what we expect from the SPS proton bunch in AWAKE Run 2. The electron witness bunch is shown in red, and the plasma density is shown in grey where the white region is the plasma bubble void of plasma electrons. Note that in the QuickPIC simulations the simulation box travels towards the left, towards $\xi = 0$	35

Figure 5.1	A wavelet analysis of the beam shown in Figure 4.1, at the same position in the plasma, using Morlet wavelet analysis [110]. The horizontal axis shows the position ξ in the simulation box. The vertical axis shows the Fourier period in units of the plasma wavelength λ_p . This density plot is the absolute value of the complex wavelet data, showing clearly the peak in frequency in the area around the plasma wavelength. The colour axis is saturated at amplitude 1 in order to show the fine structure of the harmonics. The contour plot overlay shows the full range of the density data in steps of 0.5.	41
Figure 5.2	A parameter scan for the 26 bunch pre-modulated studies where six different beam currents and four different beam lengths were considered. The energy gain $P_z - P_{z,0}$ after 1.1 m of plasma is shown with the error bars representing the RMS energy spread. The figure is presented in Publication II and in Adli <i>et al.</i> [2].	42
Figure A.1	The four main steps of the PIC algorithm. 1: Evolve the velocity and position of the particles using the Newton-Lorentz equations. 2: Interpolate and deposit the charge/current densities onto the grid. 3: Evolve the Maxwell's equations, or Poisson's equation if electrostatic. 4: Interpolate the fields from the grid onto the particles for the next push. Recreated from Vay <i>et al.</i> [117].	80
Figure A.2	Left: The staggered Yee grid. Current densities and electric fields are defined on the edges of the cells, and magnetic fields on the faces. Right: Leapfrog time integration uses alternating half time steps for electric and magnetic fields. Recreated from Vay <i>et al.</i> [117].	82
Figure B.1	A screen shot of the OsirisAnalysis GUI tool.	87

List of Tables

Table 1	Overview of notation used in this thesis.	2
Table 1.1	Accelerators world wide with proton beams with an energy higher than 10 GeV. The table was compiled by Adli and Muggli [3], and updated to include the planned upgrade to the LHC.	16
Table 2.1	Nominal AWAKE beam parameters for Run 1 [50, 51] and Run 2 [2].	23
Table 5.1	Convergence results for a reference simulations for Publication IV. The reference bunch has a charge of 250 pC, and the emittance tolerance criterion for the \tilde{Q} parameter is 5% (see Section 5.2).	44
Table 5.2	Overview of total simulation cost. 97% of the simulations were run on the supercomputer <i>Abel</i> , on Oct Core Intel Xeon E5-2670 CPUs. The remainder were run on older nodes with Quad Core AMD Opteron 2354 CPUs.	44

Preface

Plasma wakefield accelerators are complex. and there are many parameters to tweak in order to accelerate a beam of a quality that is useful for applications. What practical applications such accelerators may have depends on exactly what these parameters end up being and how they depend on each other, whether it is designs intended for in particle physics, medicine, or other types of research. As Terry Pratchett once said: *It is well known that a vital ingredient of success is not knowing that what you're attempting can't be done* [92]. Even if a useful particle collider cannot be built based on a plasma wakefield accelerator design, understanding how charged particle beams interact with plasmas may lead to other applications. The strong beam focusing forces produced by plasmas under certain conditions can be taken advantage of in for instance plasma lenses [107], and hollow electrons channels can for instance be used for beam collimation [106].

Computer simulations are a very useful tool to try and understand complex systems like these, where many factors interact. They can be used to find and study ideal cases, or they can be used to replicate experiments in order to better understand what is going on when you cannot measure all the properties of an experiment. The work presented in this thesis is aimed towards addressing some of the questions surrounding the design of Run 2 of the AWAKE experiment at CERN (see Chapters 1 and 2). While Run 1 addresses some of the principle properties of a proton driven plasma wakefield accelerator, like the interaction between the plasma and the beam itself, how the wakefields evolve, and how a sample of electrons behave in such a wakefield, Run 2 aims to accelerate a narrow, short electron beam to high energies while retaining a low energy spread and low emittance. The work is published in the following four papers:

- I Loading of a Plasma-Wakefield Accelerator Section Driven by a Self-Modulated Proton Bunch, *Proceedings of IPAC 2015* [17]
- II Loading of Wakefields in a Plasma Accelerator Section Driven by a Self-Modulated Proton Beam, *Proceedings of NAPAC 2016* [18]
- III Data Acquisition and Controls Integration of the AWAKE Experiment at CERN, *Proceedings of IPAC 2017* [19]
- IV Emittance Preservation of an Electron Beam in a Loaded Quasilinear Plasma Wakefield, *Physical Review Accelerators and Beams* [20]

The thesis also includes an introduction outlining some of the core concepts involved in plasma wakefield acceleration techniques in Chapter 1. The AWAKE experiment itself is outlined in more detail in Chapter 2. The simulations forming the basis for the publications are described in Chapters 4 and 5, where the approximations used are also described. In Chapter 3 some of the additional work of integrating the AWAKE experiment with the CERN Control System is outlined. A final summary and conclusions section is found in Chapter 6. The four publications are included in this thesis in an appendix titled Publications. Additional appendices outlining the principles of Particle in Cell codes used in this work, and the analysis code written, are also included.

Notation

TABLE 1: Overview of notation used in this thesis.

NOTATION	DESCRIPTION
n_0	The average or initial plasma density
n_{pe}	The density of plasma electrons
n_b	The density of a general particle beam
n_{eb}, n_{pb}	The density of an electron or a proton beam in particular
σ_r	The width of a Gaussian beam when it is assumed to be round
σ_x, σ_y	The transverse size of a Gaussian beam when it may not be round, or the value applies to only one plane.
α, β, γ	The Twiss parameters, also known as the Courant-Snyder parameters [34].
β_r, γ_r	Relativistic factors*

* These are indexed with r in this thesis to separate them from the Twiss parameters.

1 Introduction

The Advanced Wakefield Experiment (AWAKE) [12], located at the old CNGS¹ facility at CERN, became operational in December 2016. It is a proof-of-concept Proton Driven Plasma Wakefield Accelerator (PDPWFA) using the proton beam from the Super Proton Synchrotron (SPS) as its drive beam.

AWAKE is currently in Run 1, where the interaction between the proton drive beam and the plasma will be studied, and where a long electron witness beam will be injected to sample the wakefields. Run 2 is planned to start after the next Long Shutdown of the LHC [21] scheduled for 2019 and 2020, when significant upgrades will be made to the experiment. Run 2 will attempt to accelerate a short, intense electron beam to high energy while avoiding growth in emittance and large energy spread. In preparation for Run 2, a number of design choices needs to be made based on the results of Run 1 as well as simulations of Run 2. The work presented in this thesis primarily focuses on the beam loading of a short electron witness beam through simulations, in preparation for AWAKE Run 2.

The key results are presented in Publication IV, with the studies leading up to this presented in two conference papers: Publication I and II. A third conference paper, Publication III, covers the integration of the AWAKE experiment with the CERN control system, which is the main contribution to Run 1 in this PhD project.

In this chapter we will first cover some of the key concepts involved in plasma wakefield acceleration techniques relevant to the work presented in this thesis. The design of the AWAKE experiment itself is laid out in more detail in the next chapter, and the framework for the simulations is described in the third chapter. The fourth chapter outlines the work done in integrating AWAKE Run 1 with the control system at CERN.

1.1 Plasma Wakefield Acceleration

Accelerating particle beams in a plasma is an attractive concept as plasmas are capable of sustaining significantly higher accelerating fields than RF structures used in conventional accelerators can. Such RF structures suffer electrical breakdowns at very high electric fields, and these breakdowns can over time damage the structures [26]. This puts an upper limit on the accelerating

¹The CERN Neutrinos to Gran Sasso (CNGS) experiment was operational between 2006 and 2012.

gradient. As these breakdowns causes damage to the surfaces of the RF cavities, in practice the upper limit is determined by the statistical probability of a breakdown and the acceptable number of breakdowns in a given period of time [93], and the practical limit is therefore lower – around 100 MV/m [4].

While RF cavities use standing electromagnetic waves to accelerate particles, plasma accelerators use an energetic beam to drive strong electromagnetic wakefields in the plasma. The two main techniques for producing these strong accelerating fields are by the use of an intense laser beam, or by the use of a particle drive beam. Laser accelerator techniques were investigated in the early 1970s [29, 88], and wakefield acceleration techniques through the use of computer simulations at the end of the decade [108]. Using particle beams to drive accelerating wakefields were proposed some time later, in 1985 [31].

Both these beam and laser driver techniques utilise a neutral plasma where the collective motion of the free electrons define the main parameters of the accelerating structure. The characteristic time of the electron motion is related to the plasma frequency, ω_{pe} , and the characteristic length is related to the plasma wavelength, λ_{pe} .

$$\lambda_{pe} = \frac{2\pi c}{\omega_{pe}}, \quad \omega_{pe} = \sqrt{\frac{n_0 e^2}{m_e \epsilon_0}}, \quad (1.1)$$

where n_0 is the initial plasma electron density, e is the elementary charge, m_e is the electron mass, and ϵ_0 is the vacuum permittivity [40, 89, 109]. Here we ignore the ion mass and we assume the plasma is cold, i.e. we ignore the thermal motion of the electrons. The characteristic time and length of ion motion scales as the square root of the mass difference compared to the plasma electrons and tend, depending on the ion mass, to be a few orders of magnitude longer than those of the electrons. In the case of very long accelerating structures, the motion of the ions may become an issue [97].

Plasmas can in general sustain accelerating electric fields on the order of the non-relativistic wave-breaking field [35, 40]

$$E_{WB} = \frac{m_e c \omega_{pe}}{e}. \quad (1.2)$$

For instance, for a plasma density of 10^{18} cm^{-3} , the maximum field is on the order of 100 GV/m. This has been inferred by experiment in the mid 1990s when a few electrons was accelerated to over 40 MeV in about $300 \mu\text{m}$ of Helium plasma, driven by a 25 TW pico second laser [78].

Both techniques require a drive beam that deposits energy into the plasma in the form of wakefields. The drive beam is trailed by another beam which draws energy from the fields in order to accelerate. We thus see a transfer of energy from the drive beam to the witness beam through plasma as the intermediate medium [80]. Let us briefly introduce the core principle of the two methods of plasma wakefield acceleration.

1.1.1 Laser Driven Acceleration

In a laser wakefield driven plasma accelerator (LWFA), the plasma acts like a transformer, changing high frequency transverse field of the laser pulse into a low frequency longitudinal

wave [76]. The effect driving the accelerating fields was described by Tajima and Dawson in 1979, and can be summarised as follows: The ponderomotive force at the front of the laser pulse drives plasma electrons forward, while at the back of the pulse it pushes them backwards. This generates a longitudinal wave that is at its most efficient when the length of the laser pulse $L_{ph} = \lambda_{pe}/2$ [108]. A trailing particle beam can then be positioned on the accelerating flank of the field. In some instances plasma electrons can also be captured and accelerated instead.

1.1.2 Beam Driven Acceleration

In a beam driven plasma wakefield acceleration (PWFA) a drive beam of charged particles are sent through a section of neutral plasma. The space charge of the drive beam displaces the plasma electrons, which oscillate at the plasma frequency, creating periodic regions of low and high electron density generating strong wakefields. The longitudinal and transverse fields generated by this wake is then loaded by a trailing beam of particles. The principles behind this technique were formulated in the 1980s by Pisin Chen *et al.* [31].

Any type of charged particle beam can be used in such an accelerator. Most experiments to date have used electrons. It has been shown that energy can be transferred from one or more electron drive beams to a single electron witness beam in multiple past experiments [24, 60, 70, 86, 95]. In one experiment at the Stanford Linear Accelerator Center (SLAC), a 42 GeV electron beam passing through an 85 cm section of ionised Lithium vapour, saw the trailing part of the electron beam reach 85 GeV. This corresponds to a gradient of 52 GV/m [24].

A limitation using an electron beam with a similar initial charge and energy for both drive and witness beams is that the witness beam will rapidly gain energy, while the drive beam loses energy. This both causes the drive beam to quickly decelerate, while the witness beam undergoing acceleration will at the same time catch up with the drive beam. Typically propagation length of an electron drive beam is a few tens of centimetres of plasma.

1.2 Beam and Plasma Interactions

As a relativistic, charged beam propagates through plasma, it affects the local density of the plasma electrons. The charged beam generates strong transverse fields, pushing or pulling the plasma electrons away or towards the propagation axis of the beam [3, 68]. As the heavier plasma ions will move on a much longer time scale, due to inertia, the plasma electrons expelled from the axis will be pulled back towards it by the ion charge. The electrons will tend to overshoot the axis, creating an oscillation system. A positively charged drive beam will initially pull the electrons towards the axis, where they overshoot, creating a similar effect to a negative drive beam with a half-period phase offset. The oscillation period is determined by the plasma wavelength of the electrons [53, 79].

A conceptual illustration of an electron beam driven plasma accelerator is shown in Figure 1.1. Several regions of decreasing magnitude of accelerating/decelerating and focusing/defocusing are generated behind the drive beam. By positioning a trailing beam in an optimal phase, such a beam can be both accelerated and focused. The drive beam needs to be shorter than

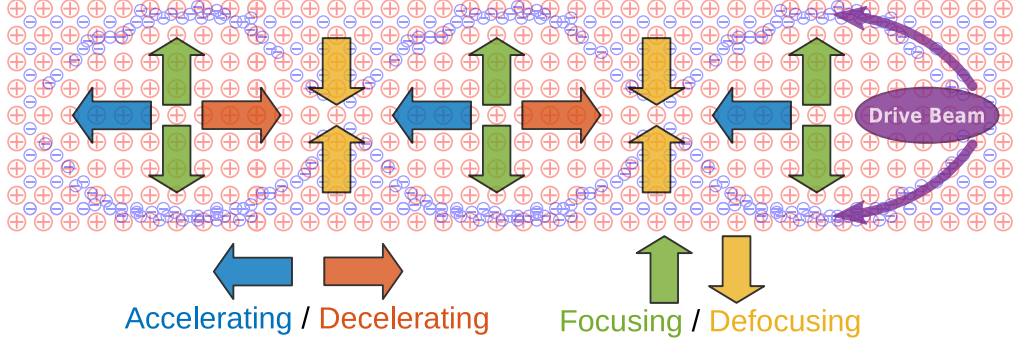


FIGURE 1.1: Illustration of a plasma wakefield accelerating structure with a single electron drive bunch. The drive bunch produces a series of focusing/defocusing and accelerating/decelerating regions, as seen for an electron witness bunch.

the plasma period for this structure to develop, but multiple short drive beams with a separation of the plasma wave length can resonantly amplify the wakefields.

1.2.1 Beam Emittance and Twiss Parameters

Before we continue, let us briefly introduce an important set of parameter when describing the evolution of a charged particle beam: the beam emittance, and the Twiss parameters also known as the Courant-Snyder parameters [34]. The Twiss parameters are useful quantities to describe the trajectory of particles in an accelerator in the transverse phase space. The following, brief, derivation is based on Klauss Wille, *The Physics of Particle Accelerators* [124].

The general solution to the trajectory of particles in an accelerator is given by

$$x(s) = \sqrt{\epsilon\beta(s)} \cos [\Psi(s) + \phi] \quad (1.3)$$

$$x'(s) = -\sqrt{\frac{\epsilon}{\beta(s)}} [\alpha(s) \cos (\Psi(s) + \phi) + \sin (\Psi(s) + \phi)], \quad (1.4)$$

where the parameter

$$\alpha(s) \equiv -\frac{\beta'(s)}{2}. \quad (1.5)$$

In order to arrive at an expression describing the particle motion in the $x-x'$ plane, we must eliminate the terms depending on Ψ . We thus obtain:

$$\epsilon = \frac{x^2}{\beta(s)} + \left(\frac{\alpha(s)}{\sqrt{\beta(s)}} x + \sqrt{\beta(s)} x' \right)^2. \quad (1.6)$$

By introducing the parameter

$$\gamma(s) \equiv \frac{1 + \alpha^2(s)}{\beta(s)}, \quad (1.7)$$

we obtain

$$\epsilon^2 = \gamma(s)x^2(s) + 2\alpha(s)x(s)x'(s) + \beta(s)x'^2(s). \quad (1.8)$$

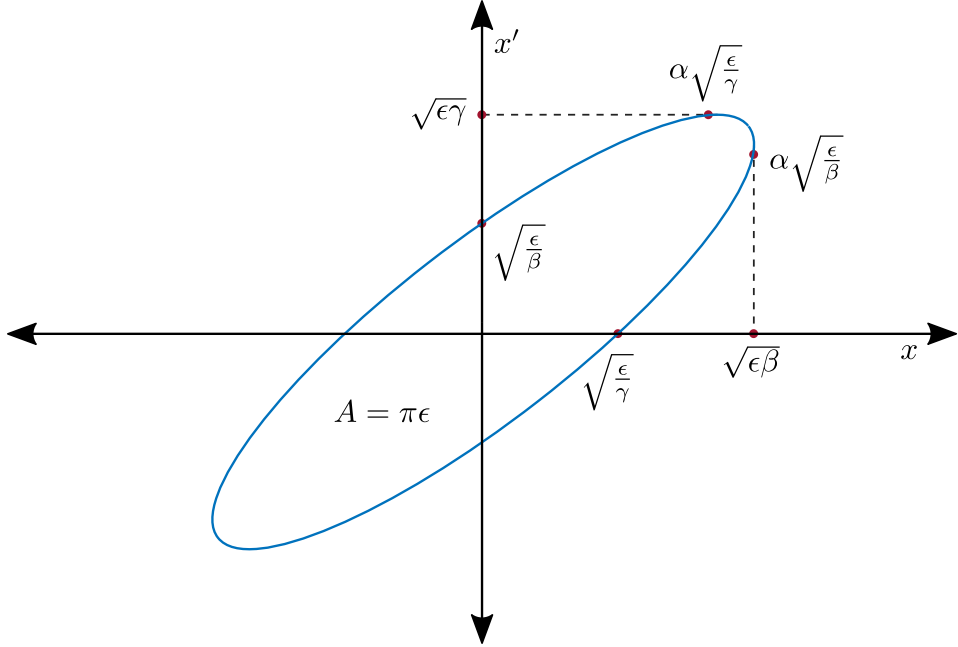


FIGURE 1.2: The phase space ellipse of bunch particles. The figure is recreated from Figure 3.23 by Klauss Wille in *The Physics of Particle Accelerators* [124].

This equation describes an ellipse in phase space, and how the Twiss parameters α , β and γ relates to the geometric emittance ϵ and the shape of the ellipse is illustrated in Figure 1.2. It is often useful to refer to normalised emittance, which is the geometric emittance multiplied with the relativistic factor

$$\epsilon_N = \epsilon\gamma_r. \quad (1.9)$$

1.2.2 The Drive Beam

The wakefields generated by a charged drive beam are given by the Lorentz force

$$\vec{W} = \frac{\vec{F}}{q_b} = \vec{E} + \vec{v}_b \times \vec{B}, \quad (1.10)$$

where q_b is the beam charge and \vec{v}_b is the beam velocity. We define the longitudinal coordinate in the frame of the beam along its direction of propagation as

$$\xi \equiv z - v_b t \approx z - ct, \quad (1.11)$$

and for the purpose of the following derivations, we use a cylindrical coordinate system (r, ξ) . It follows, then, that the longitudinal wakefield is only determined by the longitudinal component

of the electric field – to the first order – such that

$$W_{\parallel}(r, \xi) = E_z(r, \xi). \quad (1.12)$$

The transverse wakefield, on the other hand, also depends on the magnetic field such that

$$W_{\perp}(r, \xi) = E_r(r, \xi) - cB_{\theta}(r, \xi), \quad (1.13)$$

where we again take the velocity of the beam to be $v_b \approx c$.

A charged beam will diverge and lengthen due to space charge, but since the beam is relativistic the effect is of no significance over a few metres of plasma. In the transverse plane, however, the beam is subject to the Lorentz force given by the transverse component of Equation 1.10. Taking Maxwell's equations and $B_{\theta} = v_b E_r / c^2$ [101], the strength can be estimated using an infinitely long, uniform beam of density n_b :

$$F_{\perp} = q_b(E_r - v_b B_{\theta}) = q_b E_r \left(1 - \frac{v_b^2}{c^2}\right) = \frac{1}{\gamma^2} q_b E_r. \quad (1.14)$$

The implication of this is that for relativistic beams, the transverse dynamics are dominated by emittance and external forces. De-phasing is a potential concern in long plasma sections, and ΔL over a distance L can be estimated as

$$\frac{\Delta L}{L} \approx \frac{1}{\gamma^2} \frac{\Delta \gamma}{\gamma} \quad (1.15)$$

for two sample particles with energy difference $\Delta \gamma$ [79]. For a relativistic beam, this is also not a significant over a few metres.

1.2.3 The Transformer Ratio

The aim of plasma wakefield acceleration is to transfer energy from a drive beam to a witness beam via the plasma. The efficiency of the energy transfer is the ratio of accelerating field amplitude at the position of the witness beam to the decelerating field amplitude within the drive bunch.

Following Ruth *et al.* [99], let us consider a drive bunch of zero length, with N_d particles of individual energy E_d , and $W_e(\xi)$ is the wakefield per unit charge. The energy loss of the bunch in the decelerating field is given by:

$$\frac{d(N_d E_d)}{dz} = -N_d^2 e^2 W_e(0), \quad (1.16)$$

where $\xi_d = 0$ is the position of the drive bunch.

The trailing witness bunch at position ξ_w , will see the wakefield left by the drive bunch as well as its own wakefield:

$$\frac{d(N_w E_w)}{dz} = -N_w^2 e^2 W_e(0) - N_d N_w e^2 W_e(\xi_w), \quad (1.17)$$

where N_w is the number of particles in the witness bunch, and E_w is their individual energy.

As required by energy conservation, the total energy of the system cannot increase. It thus follows that

$$(N_d^2 + N_w^2)W_e(0) + N_d N_w W_e(\xi_w) \geq 0, \quad (1.18)$$

giving the requirement that the acceleration gradient experienced by a trailing particle satisfies

$$\frac{dE_w}{dz} \leq (2N_d - N_w)e^2 W_e(0). \quad (1.19)$$

Assuming the drive bunch transfers all of its energy to the wakefields, it would stop after a distance

$$L = \frac{E_d}{N_d e^2 W_e(0)}. \quad (1.20)$$

The energy a witness beam particle can gain must satisfy

$$\Delta E_w = \frac{dE_w}{dz} L \leq E_d \left(2 - \frac{N_w}{N_d} \right). \quad (1.21)$$

To maximise efficiency in the transfer of energy from the drive beam to the plasma, the beam should have a length $k_{pe}\sigma_z \simeq \sqrt{2}$ [67, 73]. Its transverse size should also stay within $k_{pe}\sigma_r \lesssim 1$ as wider beams will cause filamentation instabilities [5, 105].

The maximum energy gain approaches twice the energy of the drive bunch as $N_w \rightarrow 0$. In a wakefield accelerator we define the maximum accelerating field *behind* the drive bunch where the witness beam is positioned, to the maximum decelerating field *within* the drive bunch as the *transformer ratio* [79]

$$R = \frac{E_+}{E_-}. \quad (1.22)$$

While the maximum transformer ratio is 2, larger values can be achieved by for instance bunch ramping [13] or by a train of bunches [58].

1.2.4 Plasma Regimes

The effect of a beam on the plasma, as it travels through it, can be divided into a linear and a non-linear regime. In addition to these two there is a transitional region between these often referred to as *quasi-linear*. It is also useful in some contexts to distinguish between a non-linear and a highly non-linear regime. Figure 1.3 illustrates the four regimes considered here with representative proton drive beams.

1.2.4.1 The Linear Regime

When the charge density of the beam is smaller than that of the plasma, $n_b \ll n_{pe}$ (see Figure 1.3), the system is in the *linear regime*. The linear regime is not of much interest for accelerator applications as it does not utilise the full potential of the plasma for generating strong

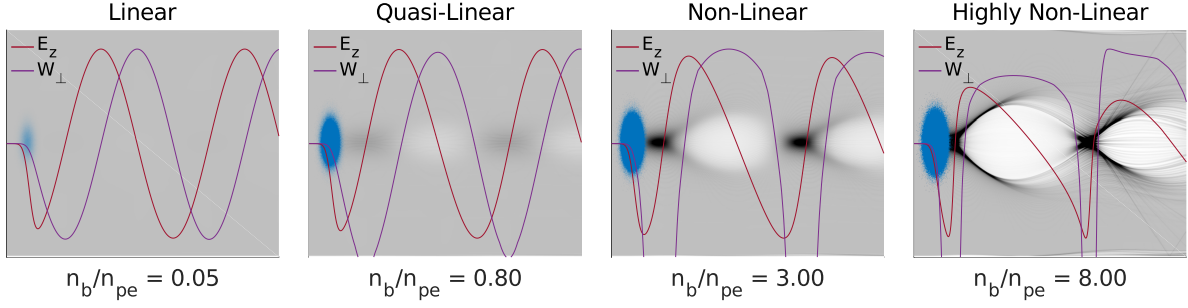


FIGURE 1.3: Four sample simulations of a proton beam of varying density n_b with respect to the plasma density n_{pe} . Each simulation is representative for the four regimes. The longitudinal and perpendicular wakefields are normalised to their own maxima to illustrate their shape rather than their absolute magnitude.

wakefields, and the transverse and longitudinal fields have continuous variations. These variations will strongly affect the energy spread and emittance of the witness beam. However, this regime is interesting from a theoretical perspective because it is well described analytically [79].

A linear theory for plasma accelerators can be derived using a cold, non-relativistic fluid model of the plasma. The response of the cold plasma can be found from the linearised equations of motion and continuity, and the Maxwell equations. (For examples of linearisation, see [30, 89].) The equations of motion and continuity are linearised assuming the perturbed plasma density, n_1 , is much smaller than the unperturbed density, $n_0 = n_{pe}$ [32]. By further combining the fluid equation and the Poisson equation [61], a wave equation for the plasma density perturbation by the beam can be derived [32, 79]:

$$\frac{\partial^2}{\partial \xi^2} n_1 + k_{pe}^2 n_1 = \frac{q_b}{e} k_{pe}^2 n_b, \quad (1.23)$$

where we still assume $n_b \ll n_{pe}$.

The solution to Eq. 1.23 in the longitudinal dimension is the Green's function for a harmonic oscillator in one dimension [61], and the radial dependency can be calculated from two-dimensional theory for different radial profiles [32]. For a beam that has a Gaussian profile in both dimensions, the wakefields are

$$W_{\parallel}(r, \xi) = \frac{e}{\epsilon_0} \int_{-\infty}^{\xi} n_{b\parallel}(\xi') \cos [k_{pe}(\xi - \xi')] d\xi' \cdot R(r) \quad (1.24)$$

$$W_{\perp}(r, \xi) = \frac{e}{\epsilon_0 k_{pe}} \int_{-\infty}^{\xi} n_{b\parallel}(\xi') \sin [k_{pe}(\xi - \xi')] d\xi' \cdot \frac{d}{dr} R(r), \quad (1.25)$$

where the transverse dependency $R(r)$ is

$$R(r) = k_{pe}^2 \int_0^r n_{b\perp}(r') I_0(k_{pe} r') K_0(k_{pe} r) r' dr' \\ + k_{pe}^2 \int_r^{\infty} n_{b\perp}(r') I_0(k_{pe} r) K_0(k_{pe} r') r' dr'. \quad (1.26)$$

Here I_0 and K_0 are the zeroth-order modified Bessel functions of the first and second kind, respectively [32, 79].

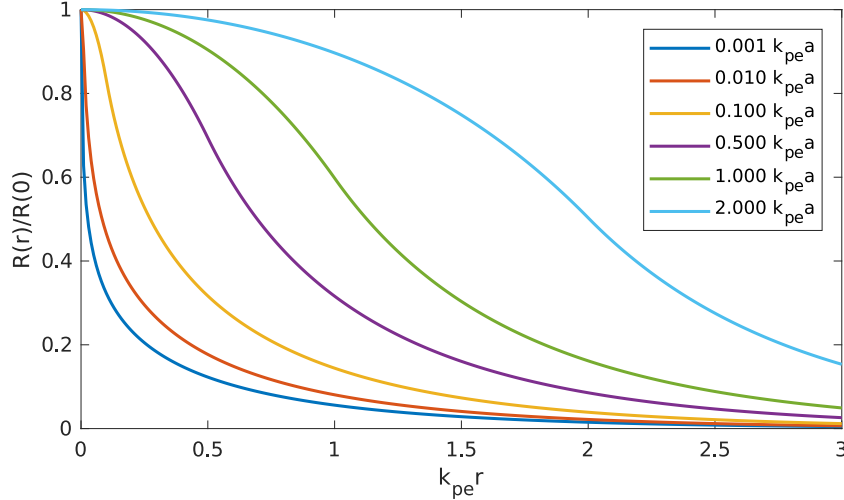


FIGURE 1.4: The radial function $R(r)$ for a range of uniform beams cut off at a radius a up to twice the plasma skin depth k_{pe}^{-1} . The plot is reproduced from Katsouleas *et al.* [61].

As can be seen from Figure 1.4, the longitudinal wakefield is at its maximum on-axis. For very wide beams, $\sigma_r \gg k_{pe}$, we converge at the one-dimensional result. For very narrow beams, $\sigma_r \ll k_{pe}$, the maximum decreases rapidly with radius causing different parts of the witness beam at different radii to see different accelerating fields. The cosine component of Equation 1.24 also implies longitudinal variations of the accelerating field. Combined, these produce a large energy spread for the accelerating beam. Additionally, the sinusoidally varying focusing field from Equation 1.25 produces emittance growth [61, 79].

1.2.4.2 The Non-Linear Regime

When the beam density $n_b > n_{pe}$, the system enters the non-linear regime, and becomes highly non-linear when $n_b \gg n_{pe}$ – often referred to as the *blowout regime* (see Figure 1.3). In this regime the plasma electrons are expelled entirely from the region around the axis to form a region populated by only plasma ions. As the ions are practically stationary on the time scale of the plasma electrons, they form a uniform column of positive charge. The electrons displaced by the space charge of the drive beam are pulled back on axis by the ions in the form a thin sheath with the shape of a bubble. Hence, this regime is also sometimes referred to as the *bubble regime*. The large transverse forces produced by the drive beam in this regime, followed by the strong restoring force of the ion channel, produces a large density spike behind the formed bubble [35, 96]. Using this regime for plasma wakefield acceleration was proposed by Rosenzweig *et al.* in 1991 [96].

The radial wakefield, W_r , produces linear focusing, while the accelerating wakefield, W_z , is uniform within the bubble. In other words: while the focusing prevents emittance growth, the

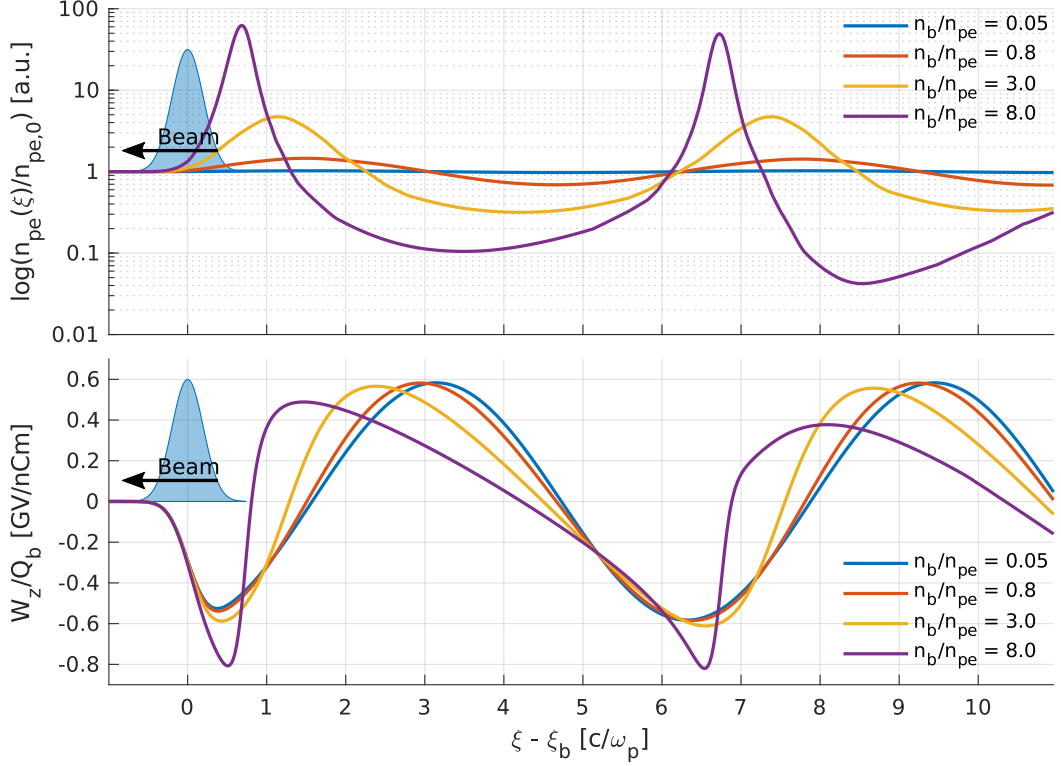


FIGURE 1.5: **Top:** Relative on-axis plasma density perturbation for a n_b/n_{pe} density ratio corresponding to a linear, quasi-linear, non-linear and highly non-linear case. **Bottom:** Longitudinal wakefield per unit of beam charge for the same four cases. The four samples correspond to the four cases presented in Figure 1.3.

accelerating gradient of the witness bunch, being independent of radial position for a range of positions, avoids large energy spreads – both disadvantages with the linear regime.

Unlike in the linear case, there is no full theory describing the non-linear case. However, a non-linear kinetic theory has been developed by Lu *et al.* that is valid under certain assumed conditions [74, 75].

1.2.4.3 The Quasi-Linear Regime

The quasi-linear regime, when $n_b \lesssim n_{pe}$ (see Fig. 1.3), can be interesting for some applications where multiple drive bunches are used. The regime is weakly non-linear in the sense that although a bubble in the plasma does not form, a significant depletion of electrons occur such that some of the beneficial effects are present in a narrower region around the axis than in the fully non-linear case. It is thus possible to have focusing fields as well as radially near uniform accelerating fields while at the same time have a non-linear wake that can be added linearly over multiple drive bunches, allowing for improved efficiency or transformer ratios [79, 98].

1.2.5 Beam Loading

A challenge with both the linear and the non-linear regime is the longitudinally varying accelerating field, producing energy spread in the accelerated bunch. Ideally, the accelerating field should be uniform in the region occupied by the witness bunch. As the witness bunch generates its own wakefield, these fields are combined with those from the drive bunch. It follows, then, that the properties of the witness bunch can both worsen and improve the flatness of the field.

Add beam loading plot, or combine with plot from previous subsection

In the linear case, the challenge is to create a uniform accelerating field in both the transverse and longitudinal direction. The non-uniformity challenges have been outlined, and solutions proposed, by Van der Meer [114] as well as Katsouleas *et al.* [61] in the 1980s. The latter suggesting triangular and trapezoidal witness bunches in order to exactly cancel the variations in the field within the bunch.

In the non-linear case, the radial accelerating field variation, $W_z(r)$, vanishes, provided witness bunch transverse size is within about $2\sigma_r$ of the drive bunch [96]. The longitudinal variation, however, remains.

A short bunch with respect to the accelerating phase of the wakefield, $L \leq \lambda_{pe}/4$, will affect the shape of the plasma electron sheath, but still allows the electrons to return to the axis while decreasing their transverse momentum. If the total momentum reaches zero, the witness beam has extracted all the energy of the accelerating field [74, 75]. As outlined by Tzoufras *et al.* [112], a trapezoidal witness bunch with a density maximum at its head, can theoretically both flatten the field and achieve a high transformer ratio. They further show that a flat top bunch is similarly efficient, and Gaussian bunches also have comparable properties – all being sensitive to fine tuning of position within the bubble, as well as its spot size.

Tzoufras *et al.* provides a solution for the energy absorbed per unit length for an ideal trapezoidal bunch, stating that

$$Q_{tr}E_t = \frac{\pi R_b^4}{16}, \quad (1.27)$$

where Q_{tr} is the total charge of the trapezoidal bunch, E_t is the longitudinal field at the head of the bunch, and R_b is the radius of the bubble. It immediately follows that at optimal beam loading, there is a trade-off between charge and the accelerating gradient and thus energy gain [112].

1.2.6 Beam Matching

In the non-linear case, where an ion column is formed, the focusing force it produces will cause a pinching effect on the beam. While the beam itself, assuming the normalised emittance $\epsilon_N > 0$, will try to expand, there exists a beam radius where the focusing force and the beam's tendency to expand are in equilibrium. For a highly relativistic beam, $\gamma_r \gg 1$, the equilibrium radius is given by [63]

$$\sigma_{r,eq} = \left(8 \frac{\epsilon_N^2 c^2}{\gamma_r \omega_p^2} \right)^{1/4}. \quad (1.28)$$

This follows from the general envelope equation [66] under the assumption that: the beam enters the plasma at focus (i.e. $d\sigma_r/dz = 0$), does not diverge significantly from a Gaussian transverse density profile, and that the focusing force is linear [63].

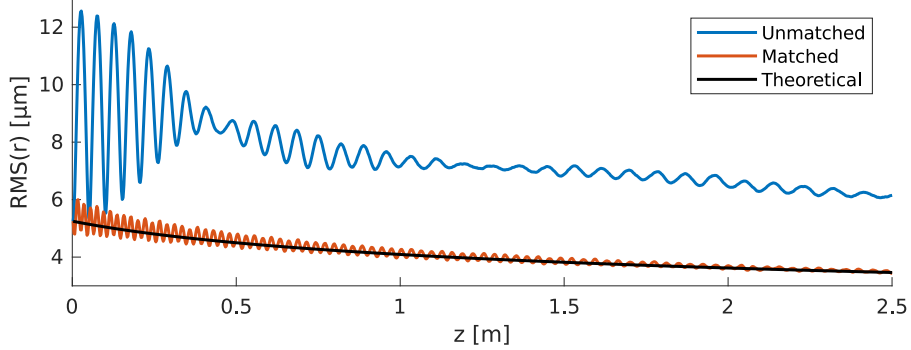


FIGURE 1.6: The evolution of the transverse RMS size of an initially matched electron beam as it accelerates through a plasma. The tail of the beam, in red, remains in a region where it is matched, while the head of the beam, in blue, does not. The black line corresponds to the theoretical spot size of the beam at nominal plasma density. Based on simulation data from Publication IV.

The simulation in Fig. 1.6 shows the evolution of the transverse RMS size of an electron beam as it travels through a plasma. The beam has a normalised emittance of $2 \mu\text{m}$, and is initially matched to a plasma density of $7 \times 10^{14} \text{ cm}^{-3}$ with a $\sigma_r = 5.24 \mu\text{m}$. The tail of the beam, in red, is in the plasma bubble and thus sees an ion density equal to the plasma density. The head of the beam, in blue, where the bubble is forming, sees a lower density. It is thus not matched, and instead oscillates around an equilibrium point at a larger radius. The black line is the predicted σ_r given by Eq. 1.28 at initial plasma density, and beam energy as a function of z as the beam is accelerated [20].

1.2.7 Multiple Drive Bunches

As discussed above, higher transformer ratios can be achieved with multiple drive bunches with a λ_{pe} separation. This happens because such a train of bunches will resonantly drive increasing wakefields.

As outlined by Kallos *et al.* [60], if the bunches are longitudinally square, the wakefields scale linearly with the number of bunches. The shape is of less importance if the bunch length is much less than λ_{pe} . However, this does not result in high efficiency as every trailing bunch will see the decelerating field of the earlier bunches. Efficiency is instead increased when each bunch experience a similar wake field.

This effect can be mitigated in two ways that will in turn maximise transformer ratio. The first option, named *Ramped Bunch Train*, is to position the bunches with a $1.5 \cdot \lambda_{pe}$ separation, such that each bunch is in the accelerating phase of the forward bunches, while at the same time ramp their charge such that the wakefield inside each bunch matches the decelerating field from the first bunch. This scheme has been demonstrated experimentally by Jing *et al.* [58, 59].

The second method described by Kallos *et al.*, called *Phased Bunch Train*, proposes using short, $k_{pelz} \ll 1$, equally charged bunches placed in a specific decelerating phase. The bunch separation needs to be tuned so that the fields inside each bunch matches that of the first bunch. The phase shift θ_M for the M -th bunch is described by Ruth *et al.* [99]:

$$\theta_M = \sum_{n=2}^M \tan^{-1} \left(\frac{1}{\sqrt{n-2}} \right), \quad M \geq 2. \quad (1.29)$$

This yields a maximum energy gain

$$\Delta E_w = E_{d,1} \left(2\sqrt{M} - \frac{N_w}{N_{d,1}} \right), \quad (1.30)$$

where $N_{d,1}$ is the first of M drive bunches. Compared to Eq. 1.21 this is an improvement, although not linearly increasing with the number of bunches [99].

1.3 Using a Proton Drive Beam

So far the theory presented has focused on short electron bunches as drivers for plasma wakefield acceleration. Electron bunches used in such experiments have a low energy and thus a limited propagation length in the plasma, as can be estimated using Equation 1.20.

One experiment, at the Stanford Linear Accelerator Center (SLAC) [24], achieved up to a doubling of energy of electrons with a 42 GeV driver with 1.8×10^{10} particles, corresponding to a total beam energy of 120 J. The propagation length of such a beam is on the order of a metre, and the experiment used an 85 cm lithium plasma cell to achieve the energy doubling, with a gradient of up to 52 GeV. Such short accelerator segments are suitable for multi staged accelerators, but they require multiple high energy electron drive beams.

1.3.1 Protons vs. Electrons as Drive Beam

As ultra-high energy electron bunches are not readily available, the possibility of using protons as drive beams instead has been of interest for some time [23, 27]. The much higher mass carries orders of magnitude more energy at relatively low gamma values. This effectively eliminates the problem with short propagation lengths in plasma as it scales linearly with the beam energy; see Equation 1.20. Several accelerators exist which delivers kJ-scale proton beams. See Table 1.1 for an overview.

However, in order to produce GV/m-scale plasma wakefield accelerators, the plasma density needs to be on the order of $\gtrsim 10^{14} \text{ cm}^{-3}$; see Equation 1.2. This corresponds to plasma wavelengths on the order of a few millimetres. To maximise efficiency in the transfer of energy from the drive beam to the plasma, as discussed in Section 1.2.3, the bunch must satisfy $k_{pe}\sigma_z \simeq \sqrt{2}$. Such short bunches are not readily available, but options for creating short bunches have been proposed [8]. On the other hand, the problem with $\gg \lambda_{pe}$ proton bunches can be

TABLE 1.1: Accelerators world wide with proton beams with an energy higher than 10 GeV. The table was compiled by Adli and Muggli [3], and updated to include the planned upgrade to the LHC.

ACCELERATOR	MAX ENERGY		BUNCH LENGTH	
	[GeV]	[J]	[ps]	[mm]
CERN PS, Geneva, Switzerland [8]	26	540	1 000	300
J-PARC, Ibaraki Prefecture, Japan [55]	30	130 000	15 000	4 500
IHEP U70, Protvino, Russia [57]	50	4 000	12 000	3 600
Fermilab Main Injector, Batavia, Illinois, USA [85]	120	2 100	600	180
CERN SPS, Geneva, Switzerland [8]	450	8 300	400	120
CERN LHC, Geneva, Switzerland [8]	7 000	124 000	250	75
CERN HL-LHC, Geneva, Switzerland [7]	7 000	247 000	270	81

solved by exploiting one of several instabilities that can occur when a long bunch propagates through plasma.

1.3.2 The Self-Modulation Instability

A long bunch with respect to the plasma wavelength will generate a density wave driven by its own head. This is true for both laser beams [39] and particle beams [64], and they are caused by the same underlying physics. For a laser beam, the self-modulation arises from alternating regions of focusing and diffraction. For a particle beam, the wakefields generated within the beam acts back on itself, breaking it up into short micro bunches with a surrounding, defocused halo.

In the 1980s, this self-modulating effect was taken advantage of in LWFA experiments as only long laser pulses were available. Advances in ultra short laser technology later removed the dependence of this effect [94], but for proton bunches, this remains a challenge. However, the self-modulation instability can also be exploited for proton bunches to generate high accelerating gradients [27, 102, 103].

Beam self-modulation is caused by a transverse two-stream instability which occurs for a bunch with a radius on the order of the plasma skin depth, $\sigma_r \simeq c/\omega_{pe}$ [119]. Much narrower bunches will see pinching effects, while wider bunches will experience filamentation instabilities [62].

The micro bunching caused by self-modulation is close to the plasma wavelength, but long bunches are also subject to hosing instabilities [123], and effect also seen in long laser beams [37, 38]. This may prove to be a limitation to beam stability over long propagation lengths. Hosing, however, can be prevented by the breaking up of the beam caused by self-modulation [122]. A sharp leading edge of the bunch can be used to seed modulation [41]. Seeding can significantly reduce the risk of hosing. This is also the case for long laser pulses, and resolved by seeding [119].

Self-modulation has been shown experimentally for long electron bunches at SLAC [82, 83]

as well halo formation on short and long positron bunches [54, 81]. Self-modulation has also recently been seen for proton bunches at AWAKE [84].

2 The AWAKE Experiment

AWAKE is the first proton driven wakefield accelerator experiment in the world. It is a proof-of-concept experiment aiming to inform a design for future high energy accelerators [51] and to prove the feasibility of such an accelerator. The proton drive beam for the experiment is delivered by the Super Proton Synchrotron (SPS) at CERN at an energy of 400 GeV, and joined by an electron witness beam in a 10 m plasma stage.

AWAKE is physically located at the former site of the CERN Neutrinos to Gran Sasso experiment (CNGS) [49] in a tunnel below the Swiss-French border, and is connected to the SPS at SPS Point 4. The connection of the AWAKE experiment to the rest of the CERN accelerator complex is illustrated in Fig. 2.1.

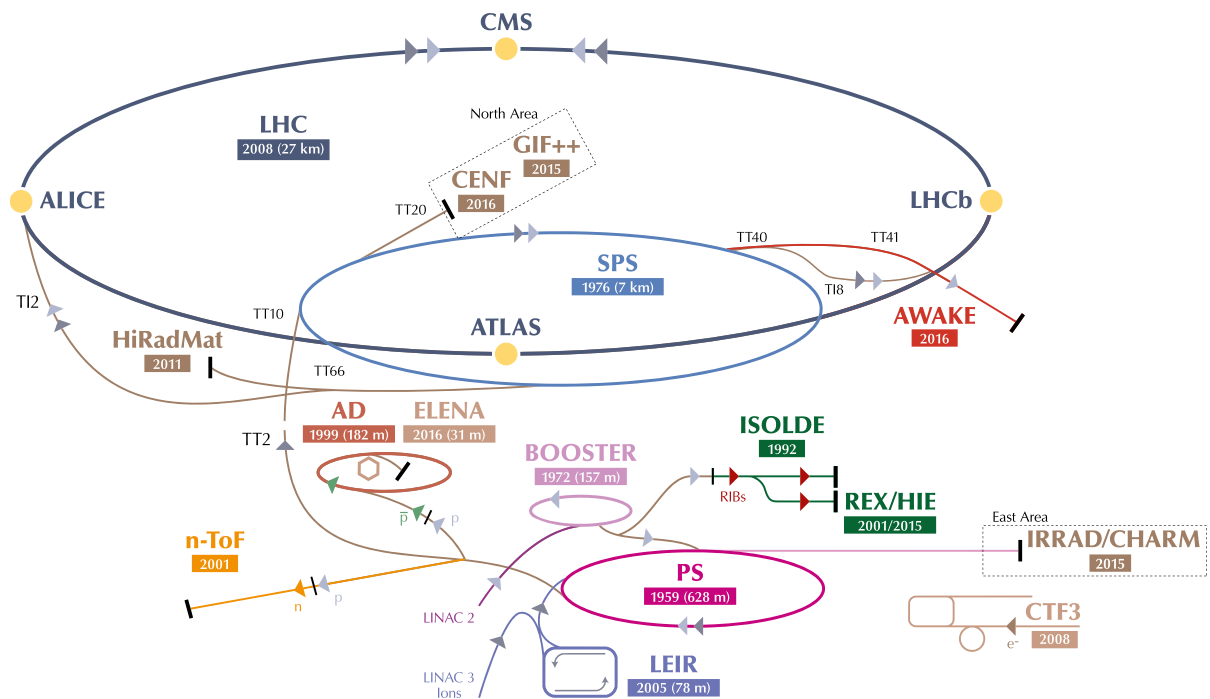


FIGURE 2.1: An overview of the CERN Accelerator Complex [77].

2.1 Evolution of the Concept

While AWAKE is the first proton driven wakefield experiment, a number of experiments with electron drive beams have confirmed the models produced by theory and simulations. The first experimental results of plasma wakefield acceleration were conducted at the Advanced Accelerator Test Facility at Argonne National Laboratory (ANL) outside Chicago, USA, and published in 1988 [95]. The experiment split an electron beam of a few nC into a drive and a witness beam, and demonstrated that the drive beam generates accelerating wakefields as well as strong transverse fields. The accelerating gradient they produced was modest, only a few MeV.

More recently, GeV level acceleration gradients have been achieved with an electron bunch at SLAC, where parts of a 42 GeV electron bunch saw energy doubling in an 85 cm plasma cell. The results were published in Nature in 2007 [24]. The plasma stage produced a continuous spread in energy up to about 85 GeV. However, only a small fraction of the charge was accelerated to these energies. An experiment at SLAC later produced a discrete, accelerated bunch with a core of 74 pC in an accelerating gradient of 4.4 GeV/m [70].

2.2 AWAKE: A Design Overview

AWAKE is, as of the writing of this thesis, operational and in Run 1. The proton beam line arriving from the SPS joins with the laser beam and the electron beam line, and connects to a 10 m plasma stage at the end of the tunnel. In addition, an electron source has been installed, and a new side tunnel had to be dug to fit the electron beam line connecting the source to the main assembly. Figure 2.2 gives an overview of the experimental layout in the tunnel. The old CNGS target is still present behind a shielding wall, as it is highly radioactive. This, unfortunately, has created some constraints for fitting the downstream beam line and diagnostics, and may pose additional challenges for Run 2 if longer or multiple plasma stages are needed.

2.2.1 Plasma Source

The requirements for the plasma source for AWAKE Run 1 were a 10 m long cell capable of a plasma electron density ranging from $1 - 10 \times 10^{14} \text{ cm}^{-3}$. The density variation should be within 0.2%, and the radius of the plasma channel should be $\geq 1 \text{ mm}$. The plasma should also consist of heavy ions to mitigate ion motion [28].

For the AWAKE vapour source, rubidium (Rb) was chosen. Rubidium has a low melting point, 39.3 °C; a low first ionisation energy, 4.18 eV; and a standard atomic weight of 85.47. The plasma wavelength of rubidium ions with a +1 charge is roughly 400 times that of the plasma electrons (see Equation 1.1), preventing significant ion motion for AWAKE application [120]. An additional benefit of using an alkaline metal like rubidium is that the second ionisation level is significantly higher, 27.3 eV, making it relatively easy to prevent further ionisation and thus a lower charge/mass ratio [11]. The rubidium vapour is created by heating the reservoir and the plasma cell to around 150 – 230 °C to reach the density range required for AWAKE [28, 84].

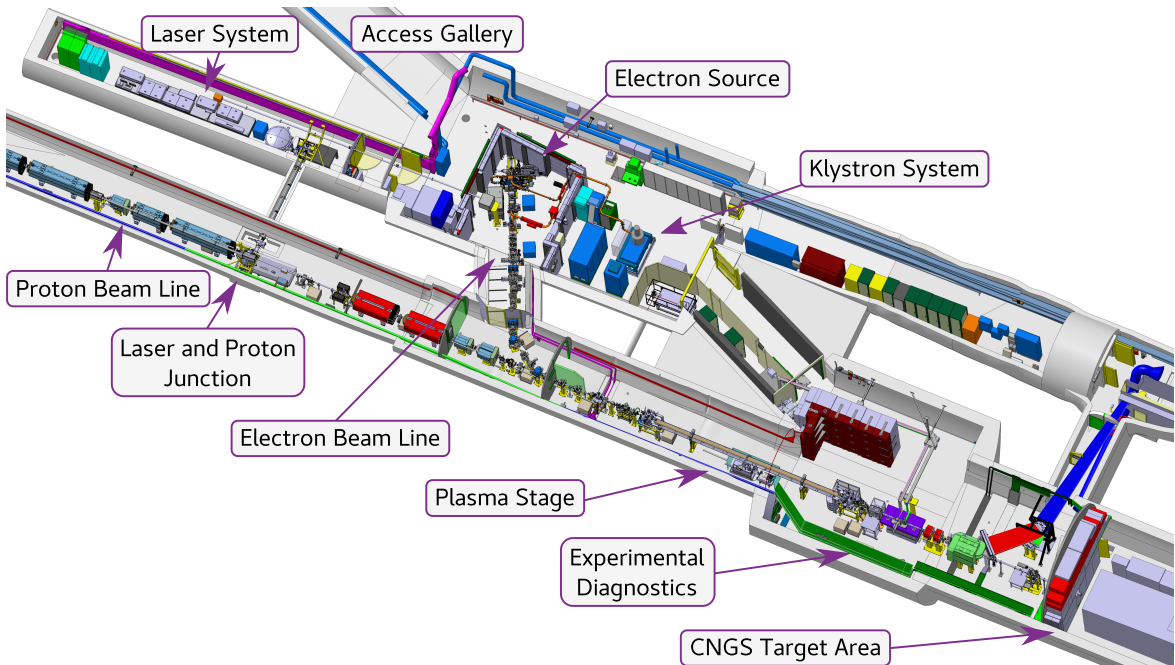


FIGURE 2.2: Drawing of the AWAKE experimental area with the key components labelled.

The ionisation of the Rb vapour is achieved with a short laser pulse co-propagating with the proton drive beam. The laser can be timed such that the plasma channel is created inside the beam itself. The short laser pulse produces a sharp plasma edge that provides a good seed for the self-modulation instability [121], as discussed in Section 1.3.2. The section of the proton beam ahead of the laser does not interact strongly with the neutral rubidium vapour, although a low level of impact ionisation does occur. However, this effect is not significant [11].

The ionisation laser used for AWAKE is a 780 nm Ti:Sapphire laser with a pulse length of 120 fs and a maximum compressed energy of 450 mJ. The peak intensity is around $1.2 \times 10^{14} \text{ W/cm}^2$, with a spot size radius of 1 mm [11]. The appearance intensity needed for ionisation of rubidium is around $1.7 \times 10^{12} \text{ W/cm}^2$ [9]. Ionisation of a second electron requires some 455 times higher intensity, so secondary ionisation is not expected [84].

The plasma density produced by the laser pulse is currently measured with a Mach-Zehnder type interferometers, which produces an interferogram that requires further processing to provide a density measurement [87]. There are also possible solutions proposed for real-time diagnostics using a Michelson-type interferometer [36].

2.2.2 Electron Source

The AWAKE electron source for Run 1 consists of a 2.5 cell RF-gun and a 1 m long booster structure, both operating at 3 GHz, a cathode transfer chamber, beam diagnostics, and a beam transport line connecting it to the proton beam line. The beam is boosted to up to 20 MeV by a constant gradient acceleration structure. The RF-gun and the booster are powered by a 30 MW klystron [11, 90]. Several of the components, including the RF-gun and klystron, were

2. THE AWAKE EXPERIMENT

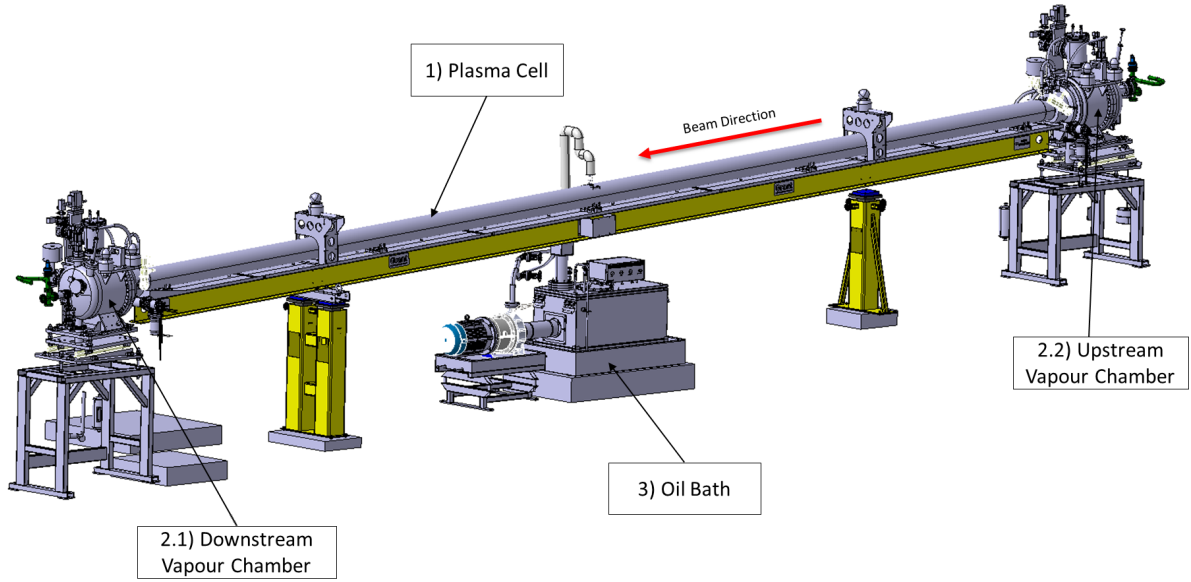


FIGURE 2.3: Drawing of the plasma stage and its related components, as presented in the 2016 AWAKE Status Report [10].

re-purposed from the former PHIN injector in the CLIC test facility [33]. An overview of the electron source and the accelerating structure can be seen in Figure 2.4.

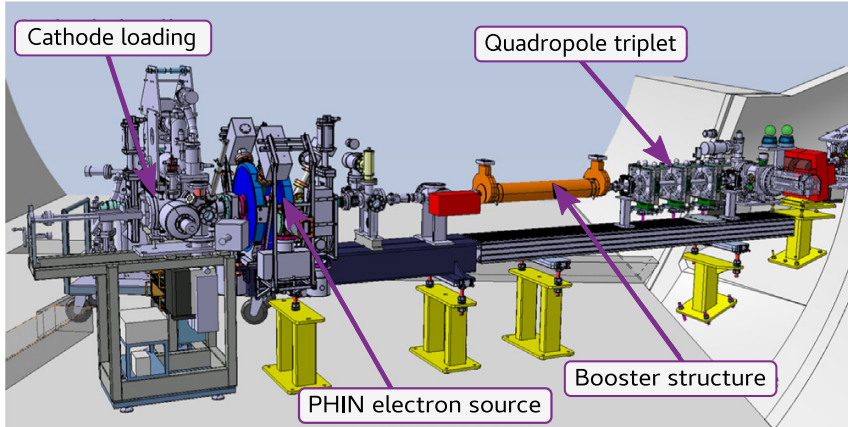


FIGURE 2.4: Drawing of the electron source and accelerating structure [90].

2.3 Stages of the Experiment

All stages of the AWAKE experiment has been studied in detail in simulations. Due to the large number of parameters for the plasma and laser, and the drive and witness beams, the range of interest of these have both been determined by previous experiments and AWAKE specific simulations.

The key, nominal parameters for Run 1, and the planned parameters for Run 2, are listed in Table 2.1.

TABLE 2.1: Nominal AWAKE beam parameters for Run 1 [50, 51] and Run 2 [2].

EXPERIMENT	PROTONS	ELECTRONS	
PARAMETERS	RUN 1&2	RUN 1	RUN 2
Momentum	400 GeV	16 MeV	$\gtrsim 50$ MeV
Charge	4.8 nC	200 pC	67 – 200 pC
Particles	3×10^{11}	1.25×10^9	$0.42 - 1.25 \times 10^9$
Bunch length (σ_z)	12 cm	1.2 mm	40 – 60 μ m
Bunch size ($\sigma_{x,y}$)	200 μ m	250 μ m	—
Normalised emittance (ϵ_N)	3.5 μ m	2 μ m	$\lesssim 10$ μ m
Relative energy spread ($\Delta p/p$)	0.035%	0.5%	few %
Beta function ($\beta_{x,y}^*$)	4.9 m	0.4 m	—
Dispersion ($D_{x,y}^*$)	0	0	—

2.3.1 AWAKE Run 1

The primary focus of Run 1 of AWAKE was to study the wakefields generated by the SPS proton beam in the 10 m Rubidium plasma stage. In the first phase the main focus was on measuring the self-modulation instability and the frequency of this modulation in relation to the plasma density. The second phase aims to sample the generated wakefields with a long electron beam capable of sampling a full plasma wavelength [2].

A large part of the work involved in Run 1 is related to the operation and diagnostics of all the essential elements involved in the experiment, from the vapour cell and the laser system, to the beam transport; and their respective diagnostics systems. Especially the size and density uniformity of the plasma channel are essential parameters to control.

2.3.1.1 The Self-Modulation Instability in AWAKE

Run 1 of AWAKE has confirmed that seeded self-modulation of an SPS proton bunch indeed does occur in the AWAKE vapour stage when the laser is operating at high power. The results shown in Figure 2.5 were presented in the thesis work of M. Turner for the AWAKE experiment [111]. The left-most figure shows that no modulation occurs when the laser is at a low power setting and no plasma produced. When the laser is switched to high power in the middle figure, the SPS bunch is defocused starting from the region where the laser is positioned. The time scale of the vertical axis is too large to show if self-modulation does occur, but the right-most figure shows a region of the defocused bunch at a higher resolution, where the micro-bunch structure is clearly visible.

2.3.2 AWAKE Run 2

The electron bunch for Run 1 was designed to sample all phases of the accelerating field, and is therefore both long with respect to the optimal phase of the field (see Section 1.2.5), and wide compared to the matching condition with the plasma density (see Equation 1.28). It is expected

2. THE AWAKE EXPERIMENT

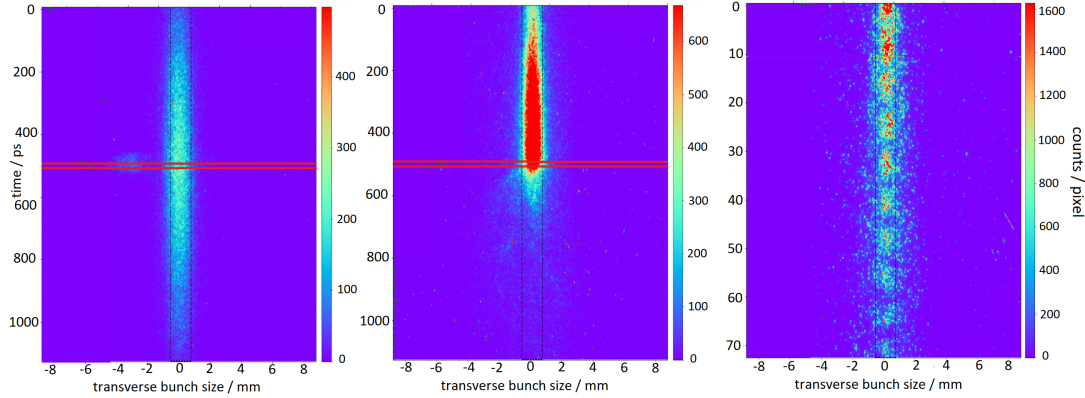


FIGURE 2.5: Resolved streak camera images of the SPS proton beam propagating through the Rb vapour in the AWAKE experiment. The read lines indicate the region of the laser pulse. **Left:** The laser on low power; that is, no plasma. **Centre:** The laser on high power, ionising the vapour and defocusing the beam. **Right:** A high resolution image of the defocused region, showing beam modulation. The image is borrowed from the thesis of M. Turner [111].

that for Run 1, only a small section of electron bunch will be accelerated, and energy spread and emittance will be large, but it will give a good impression of the performance of the different regions of the accelerating structure generated by the SPS drive bunch. This step is necessary to verify simulation results, and will help determine the experimental set-up for the next stage of AWAKE, Run 2.

The first target objective of Run 2 is the successful acceleration of a short electron beam, looking to maximise energy and charge while retaining a low emittance and energy spread in order to demonstrate that it is indeed possible to produce an accelerated beam with sufficient quality for further experimental applications. The results from Run 1 and simulations will dictate the parameters of the Run 2 electron bunch in order to achieve these goals.

The second target of Run 2 is to demonstrate scalability. Previous experiments have shown that high accelerating gradients can be achieved in short plasma stages, but using lasers or electron bunches as drivers puts constraints on the distances such gradients can be sustained over (see Section 1.2). As previously discussed, proton drive beams can propagate significantly longer in plasma, sustaining large accelerating fields over very long distances. However, producing long plasma channels with high enough quality to sustain such an accelerating structure may prove to be challenging. The Rubidium plasma stage currently uses a laser to ionise the vapour. How far the laser can propagate, as well as the availability of high power lasers, puts limits on how long such a plasma channel can be. This can be avoided by using multiple stages, but this requires additional beam optics which again increases the length of the accelerator at the expense of the average energy gradient.

There is also another reason why at least two stages may be necessary. The electron witness bunch needs to be injected into the accelerating structure when it has formed in order to produce a high quality accelerated bunch. This can be achieved by using two stages, where the first stage is used to let the proton bunch undergo self-modulation, and a second plasma stage that is used in its entirety for acceleration. In this scenario, the electron bunch will be injected between the

two stages. However, the optics required to steer the electron bunch onto the axis of the proton bunch implies a gap between these two stages would be required. Such a gap has a negative effect on the amplitude of the longitudinal field, reducing the maximum possible gradient for the second stage. This issue is in particular covered in Section 12 of the 2016 AWAKE Status Report [10].

An additional limitation to this solution, specifically for AWAKE, is that the experimental area itself has limited space for extending beam lines and adding multiple plasma stages. This is due to the highly radioactive target and shielding from the CNGS experiment is still present, and in the way of expanding the area [2]. To avoid the problems with staging, the ideal option would be to use a single plasma stage. This would require a different approach to the plasma source. Such alternatives are currently being looked into.

The simulation work presented in Chapters 4 and 5 in this thesis assumes option 1, in that the simulations assume that the available wakefield is reduced due to a gap between the two stages.

3 AWAKE Data Acquisition

Most of the work presented in this thesis is focused on determining the experiment parameters for Run 2 of AWAKE. However, during the final stages of construction and commissioning of Run 1, several month were designated to help integrate AWAKE instrumentation with the CERN Control System and data logging infrastructure. The key points of that work is presented here, and summarised in Publication III which was presented at IPAC in Copenhagen in 2017.

3.1 Experiment Measurements

AWAKE instrumentation involves many CERN standard instruments like analogue cameras (BTVs), sensors, etc. These are already supported by the CERN control system. Several instruments, however, are not CERN-standard, and a subset of these again only have driver software available for the Windows operating system. Since the CERN Control System run on a Scientific Linux or a CERN CentOS platform, some adaptations had to be made to make these instruments available to the existing infrastructure. They are as follows:

Vapour Density Measurement: The density of the Rubidium vapour is measured using a Mach-Zehnder type interferometers. The interferogram acquired by the interferometers is stored as a file which needs to be imported into the logging system for post-processing. In post-processing a fitting algorithm is applied to calculate the density to within $\pm 0.5\%$ accuracy [87].

Laser Diagnostics: The Rubidium vapour is ionised by a 4.5 TW, 100 – 120 fs laser [51]. The pulse length is measured by a single shot optical auto-correlator [100]. This device does not produce an automatic log file of the measurement, so a special tool was written to extract the information on a trigger. The digital camera data is post-processed with a fitting algorithm written by the instrument operator, and the pulse width is extracted. The data is written to a specially designed binary file format.

Oscilloscopes: Fast oscilloscopes are also used, for instance to measure real time signals from various Schottky diodes installed to measure Coherent Transition Radiation (CTR) emitted in the microwave band. Specifically, a 4-channel Tektronix oscilloscope which produces per-channel data files needed to be integrated into the data logging system.

Various Probes: In addition to the above specialised instruments, a number of simple probes needed to send single measurement values to the logging systems. these were treated with a flexible interface that could handle multiple data sources.

3.2 Data Acquisition

The benefit of integrating these instruments into the existing CERN Control System at the front end is that the experiment can take direct advantage of the existing infrastructure in the other layers; that is: short and long term data logging, fixed displays and standard control system graphical user interfaces (GUIs).

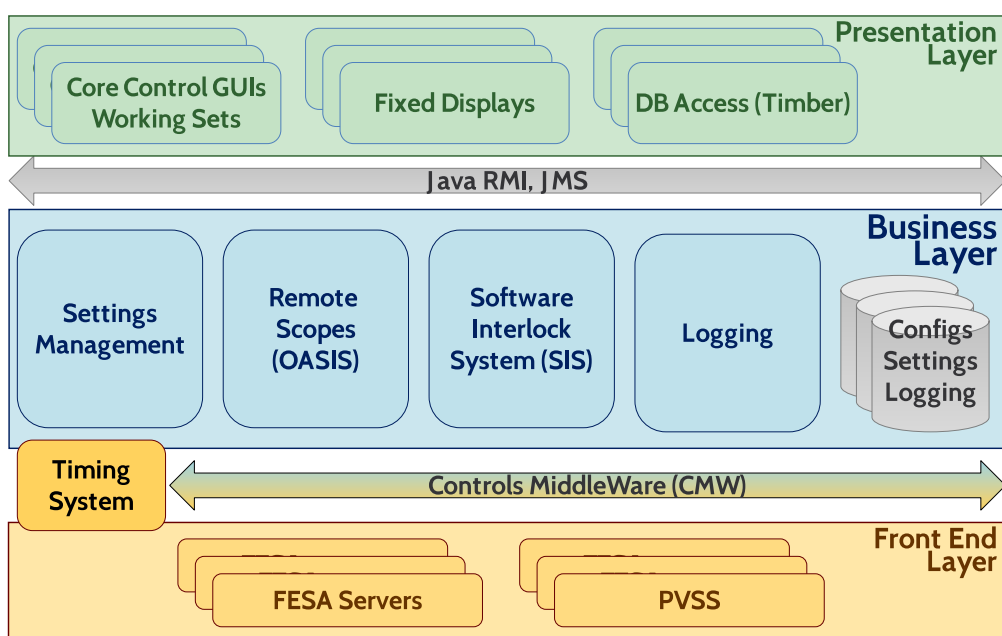


FIGURE 3.1: An overview of the CERN Control System structure. The system is layered and with standardised interfaces. The data acquisition happens on the Front End Layer where high performance PCs and PLCs provides real time processing of raw data, which is then fed up to the data logging layer, and then made available to the displays at the top layer. Illustration taken from Publication III, which is again recreated from [46].

The structure of the CERN Control System is presented in Figure 3.1. By integrating the new instruments at the lowest layer in the hierarchy, the standard application interfaces (APIs) between these are automatically available, significantly reducing the amount of custom code needed to be written. This still required the instruments to be integrated at the Front End Layer, and in addition a custom tool for collecting data on an event level was written to provide single event data packages for later analysis. This tool was named the *Event Builder*, and developed by J. Batkiewicz and R. Gorbonosov [44].

3.2.1 Front End Software Architecture (FESA)

The APIs of the Control System are standardised, and this is also the case on the Front End. The Front End Software Architecture (FESA), is a software framework originally developed at CERN. It provides a set of tools for developers to generate large portions of the code needed to control and read instruments and control infrastructure in the main accelerators at CERN, including the LHC. Collectively, the FESA classes provide a standard API towards the higher layers of the controls framework.

While originally developed by CERN, FESA was always intended to be usable for other experiments. The current iteration, FESA3, is developed in collaboration with GSI Helmholtz Centre for Heavy Ion Research in Germany, where it is used at the FAIR facility [104].

3.2.2 AWAKE Integration with FESA

As discussed above, several of the instruments used for AWAKE only have drivers for the Windows operating system. The straight forward solution in most of these cases were to use the file logging features available in the instrumentation software. These generated files could then be picked up by specially prepared FESA File Reader classes accessing the Windows servers through Samba file shares.

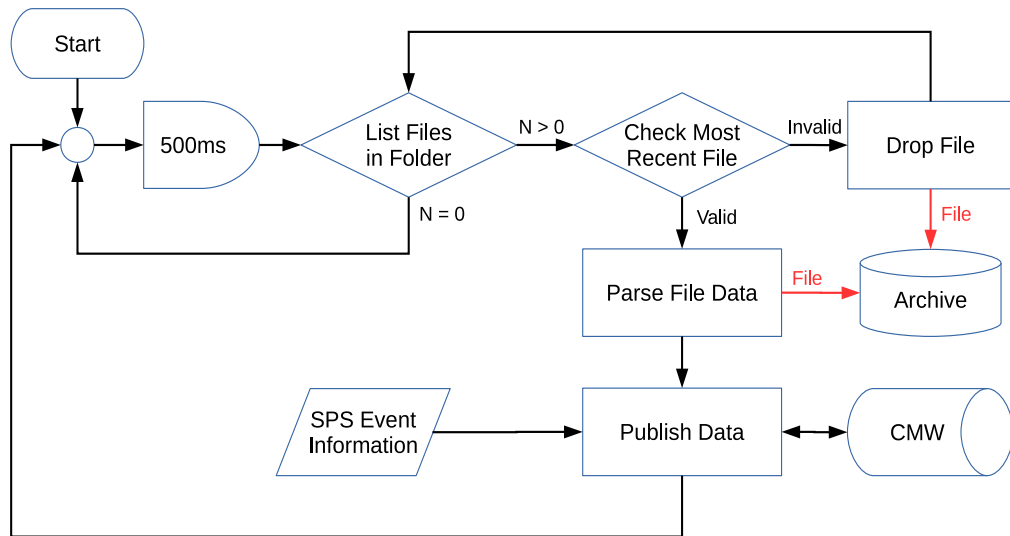


FIGURE 3.2: Flow chart of the internal logic in all the FESA File Reader classes developed for AWAKE. Illustration taken from Publication III, and was originally presented at an AWAKE Technical Board meeting in 2016 [15].

For the laser diagnostics instrument, however, the available software did not have an automatic logging feature, so we had to write our own. The solution was to extract data directly from the digital camera built into the instrument itself, and write a to binary file format specially designed for our purpose. This allowed the laser diagnostics to be treated in the same way as the other instruments: with a file reader class. Figure 3.2 illustrates the flow used for the development of these classes.

3. AWAKE DATA ACQUISITION

The class will probe for a new file every 500 ms, building a list of files. The list is then sorted, and the most recent file by file creation stamp, is read into a buffer and parsed. The parsing itself varies between the different classes depending on the format written by the respective instruments. If the file is deemed to be invalid, either because it does not conform to the expected format, or it is truncated for one reason or another, the file is dropped and moved into a special folder for discarded files. If the file is valid, the data is converted into the correct data type and published. The reader is designed such that no file is deleted, so a successfully parsed file is also moved to an archive folder.

The successfully acquired data is merged with the most recent information from the SPS accelerator, namely the information that identifies the specific proton bunch that was extracted and sent to the experiment at that given time. When the data is published, that is made available to upstream software, a notification is sent out alerting services that subscribe to the data that a new data set is available. If no one is listening and capturing the data, like the logging system or the Event Builder, the data is overwritten on the next successful acquisition. The raw data is, however, still available in the archive folders in case the data flow is interrupted.

A total of four of these special FESA File Reader classes were developed as part of this thesis work. These are all currently being used by the experiment, and being actively maintained by other members of the experiment.

4 Simulation Method

The work presented in this thesis has been performed using simulations with two particle-in-cell (PIC) codes: OSIRIS [43] and QuickPIC [6, 56]. OSIRIS is a proprietary full PIC code available in 1, 2 and 3 dimensions, with a choice between Cartesian and cylindrical coordinates. QuickPIC is a quasi-static 3D PIC code, that is available in an open source version [113]. In the simulations presented here, both OSIRIS and the open source version of QuickPIC has been used. For a more detailed description on PIC codes, see Appendix A.

Although PIC codes use macro particles – that is simulated particles represent more than one physical beam or plasma particle – these codes require a lot of CPU power. This is especially true when running 3D simulations. The preliminary studies presented in Publications I and II were done using OSIRIS with 2D cylindrical coordinates. The main study, Publication IV, was done using QuickPIC in 3D Cartesian coordinates. In order to perform the detailed parameter scans needed for these studies, the drive beam and accelerating structure had to be scaled down into a more manageable size than simulating the full SPS proton bunch would require. The full SPS proton bunch is orders of magnitude larger than both the electron bunch and the plasma wavelength, as can be seen in Table 2.1. This chapter will outline the simulation environment chosen for these studies, and the reasons behind these.

4.1 Simulating the Drive Bunch

An initial set of simulations were run to study the evolution of the self-modulation instability in the SPS proton bunch. These simulations assumed the plasma was ionised at the centre of the bunch (see Section 1.3.2), so only the back half of it was actually simulated. The beam profile function used took the form:

$$f(\xi, r) = \frac{A_q}{2} \left[1 + \cos \left(\xi \frac{\pi}{L} \right) \right] \exp \left(-\frac{r^2}{2\sigma_r^2} \right), \quad (4.1)$$

where $L = 2.5\sigma_{z,pb} = 30$ cm is the length of half an SPS proton bunch, R is the radius of the simulation box, and A_q is a charge scaling factor such that the total charge of the half bunch matches the charge outlined in Table 2.1. The charge of the simulated proton bunch in cylindrical

4. SIMULATION METHOD

coordinates is given by:

$$Q_{pb} = 2\pi \iint f(\xi, r) r dr d\xi, \quad (4.2)$$

A half period cosine function for the longitudinal density profile is more convenient for simulations than a Gaussian shape as the cosine goes to zero at a finite length [71]. Radially, the bunch is still Gaussian, and requires a cut-off to be added to prevent OSIRIS from generating macro particles with small weights. The CPU cost is proportional to the number of simulation particles, regardless of weight. An example of the SPS proton bunch before and after self-modulated has occurred, as simulated in OSIRIS 3.0, can be seen in Figure 4.1.

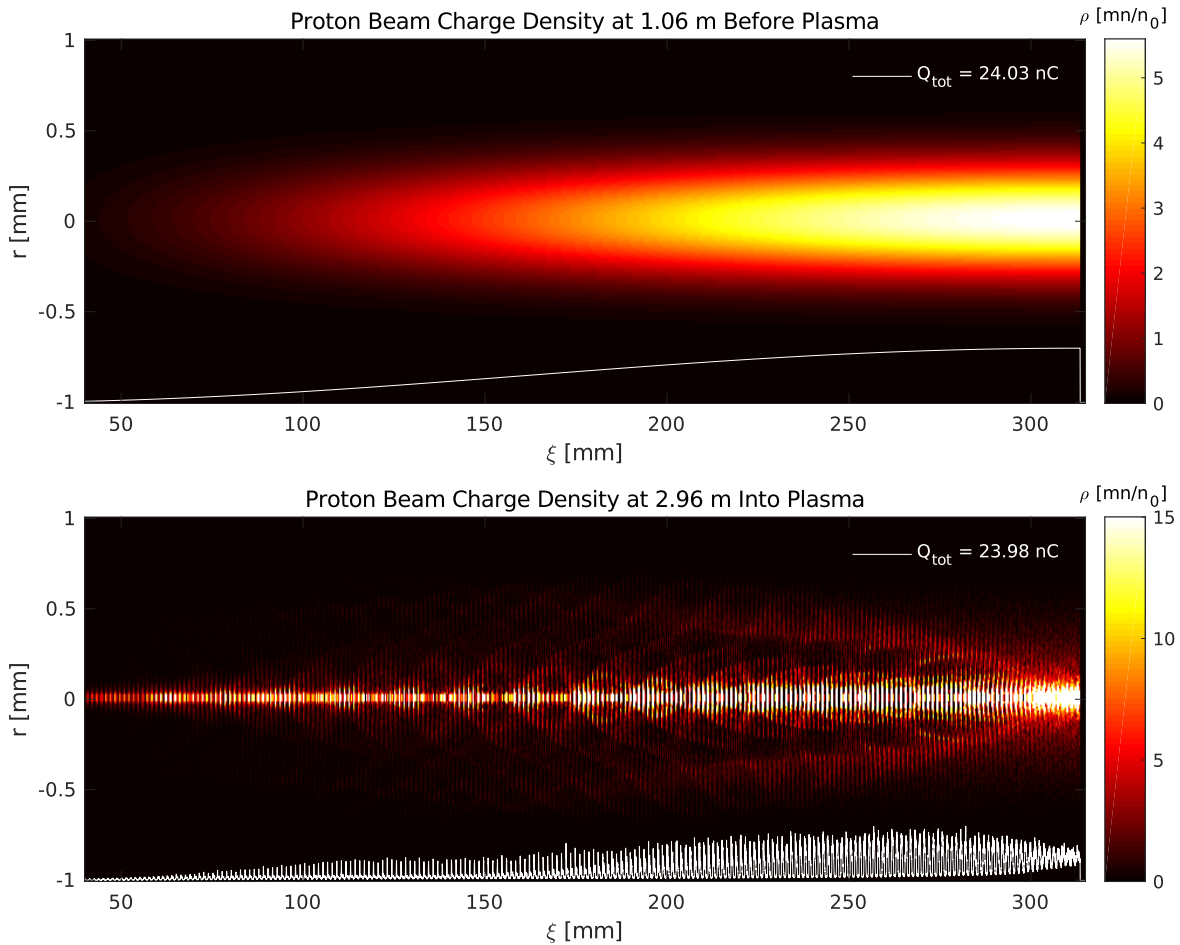


FIGURE 4.1: **Top:** An example of a simulation of half SPS proton bunch before reaching plasma. **Bottom:** The same bunch after having undergone self-modulation in about 3 m of plasma. The halo of protons ejected from the defocusing regions can be clearly seen, leaving a core of micro bunches on the beam axis.

4.1.1 With a Pre-Modulated Beam

The half SPS proton bunch is about 30 cm long, or $238\lambda_{pe}$, which requires a large number of grid cells to resolve. In order to make the simulations more manageable in size for the beam

loading studies, we decided to move to a sample proton bunch of 26 micro bunches – an order of magnitude smaller than the previous case.

These simulations were all done using OSIRIS 3.0. With this version it is necessary for the beams to drift in vacuum for a short distance for the electro-magnetic fields to develop properly, as they are initialised at zero (see further discussion in Section A.3). Since the evolution of the self-modulation instability was not of primary interest at this stage, we chose to modify the bunch profile to emulate a section of the modulated bunch. We refer to this as *pre-modulation*. This was done by shortening the period of the density envelope cosine function from Equation 4.1 to match that of the plasma wavelength.

$$f(\xi, r) = A\sqrt{2} \left[\frac{1}{2\sqrt{2}} + \cos(k_{pe}\xi - \mu) \right] \exp\left(-\frac{r^2}{2\sigma_r^2}\right), \quad (4.3)$$

where μ is the position of the first micro bunch, and k_{pe} is the plasma wave number [17]. The offset of the cosine function is chosen such that the width of the micro bunch matches the width of a bunch in the simulations done with a full SPS bunch, and there is a gap between the bunches that approximates the gaps we see between micro bunches in the simulated self-modulated case. Since OSIRIS ignores profile densities with negative values, the profile is automatically clipped at 0, requiring no further manipulation of the profile function to remove negative values.

Again, cosines are preferred over a series of Gaussian bunch profiles, although this time because the cosine is periodic, and because OSIRIS' mathematical functions cannot be longer than 256 characters.

Generating an equidistant bunch train in this manner causes the head of the second bunch to be partially defocused causing a decay of the micro bunches by the wakefield of the first bunch. This effect was not directly compensated for in Publication I. This can be avoided by increasing the separation between the first and second bunch from $2\pi c/\omega_p$ to $(2\pi + \pi/4)c/\omega_p$ [72].

The charge of the proton micro bunches were matched to that of a micro bunch generated by the self-modulation instability in the initial simulations. The charge density decreases towards the back end of the self-modulated bunch (see Figure 4.1), so for the pre-modulated set-up the densities of the micro bunches were fixed to a charge for the region where the injection of an electron bunch is reasonable – that is, around 100 plasma wavelengths behind the laser pulse. For the pre-modulated simulations, this charge was set to 100 pC such that the total charge of the sample proton beam was 2.6 nC. This corresponds to a peak current of 135 A. The electron witness bunch was injected between bunch 20 and 21.

4.1.2 With a Single Drive Bunch

Further approximations needed to be made to decrease the scale of the problem in order to study the beam loading and evolution of the electron witness beam more directly. Even the pre-modulated proton beam is somewhat costly to simulate – both because it still requires a multiple plasma-wavelength simulation box length, and because a large number of simulated particles are needed to populate the beam profile. These proved to be a challenge when doing larger parameter scans as the CPU cost would rise to levels beyond available resources. While

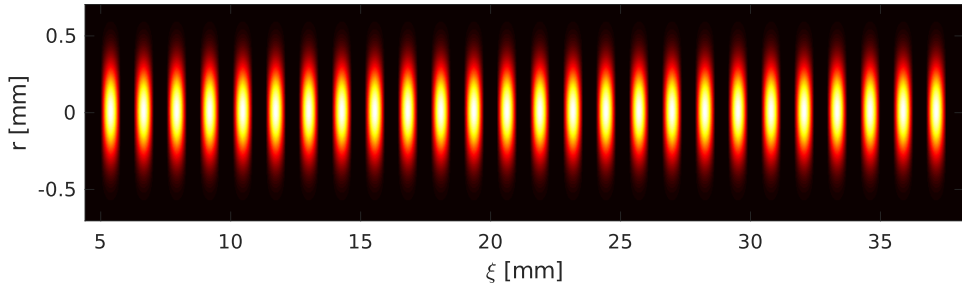


FIGURE 4.2: An example of a pre-modulated beam of 26 micro-bunches modulated at the plasma wavelength. This simulation set-up was used for Publication I. The density function (see Equation 4.3) is tuned to match the earlier self-modulation simulations shown in Figure 4.1.

additional resources could potentially have been requested, we considered the option to exclude the evolution of the proton bunch entirely from our studies and instead assume the region where the electron bunch was injected to have the properties laid out in the AWAKE status reports [10].

In these single bunch studies we therefore approximated the proton drive beam ahead of the witness bunch injection region as a single, ideal proton drive bunch generating the expected wakefields. To reproduce these conditions, we used a Gaussian bunch of 1.46×10^{10} protons corresponding to 2.34 nC, a length $\sigma_z = 40 \mu\text{m}$ corresponding to 7 kA, and a transverse size $\sigma_{x,y} = 200 \mu\text{m}$ [20]. To prevent the proton bunch from evolving at the time scale we were interested in for these studies – up to a 100 m of plasma – we also increased the mass of the bunch protons by a factor of 1×10^6 . This effectively froze the wakefields both longitudinally and transversely, and the only evolution of the wakefields was that which was caused by the electron witness bunch itself.

Figure 4.3 shows the simulation setup that was used for Publication IV, and shows both the proton bunch in blue, and the electron bunch in red. The plasma can be seen as a grey shaded area where the regions void of plasma electrons can be seen in white. This is mainly the bubble driven by the high charge density electron bunch, but also as ripples on the edge of the plasma channel. The density perturbation and longitudinal wakefield generated by the proton bunch falls in the quasi-linear regime, as illustrated in Figures 1.3 and 1.5.

4.2 Simulating the Witness Bunch

Simulating the witness bunch is generally straight forward as we have only considered a single bunch with a Gaussian shape both longitudinally and transversely. However, there are a few things to keep in mind when setting up the beam profile.

4.2.1 Witness Bunch Size and Resolution

For the early simulations, a transverse size of $\sigma_{x,y} = 105 \mu\text{m}$ was used, see Table 2.1. For later simulations, when the bunch transverse size was matched to its emittance and the plasma density (see Section 1.2.6), much narrower bunches were used – on the order of a few micrometres. The

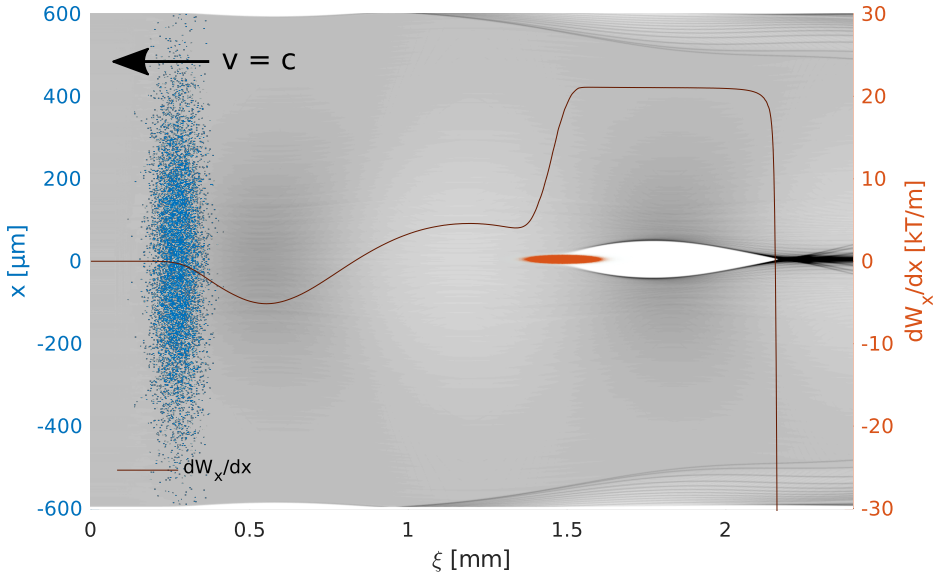


FIGURE 4.3: An example of the simulation set-up used for Publication IV. These simulations used a single, rigid proton bunch in blue, with a charge large enough to generate a wakefield equivalent to what we expect from the SPS proton bunch in AWAKE Run 2. The electron witness bunch is shown in red, and the plasma density is shown in grey where the white region is the plasma bubble void of plasma electrons. Note that in the QuickPIC simulations the simulation box travels towards the left, towards $\xi = 0$.

proton drive bunch size is tied to the plasma skin depth (see Section 1.3.2), which is $200 \mu\text{m}$. This, naturally, poses a resolution challenge when very narrow electron bunches need to be resolved, while at the same time, the simulation box needs to also be able to contain the proton drive bunch.

For the simulations with a pre-modulated proton beam, used for Publication I, the simulation box had a radius of 2.12 mm with 425 grid cells, resulting in a resolution of $5 \mu\text{m}$. This is more than sufficient to resolve and contain both the proton beam and the electron bunch, with a small buffer for the plasma (see Section 4.3). For the single drive bunch studies, Publications II and IV, the transverse grid resolution had to be increased. In most cases we tried to resolve the witness bunch with at least 5 grid cells per $\sigma_{x,y}$, although this was in some instances increased. It was also important to keep an eye on the distribution of macro particles on the simulation grid. This was especially important for the OSIRIS 3.0 based simulations, as OSIRIS creates macro particles of varying charge, with a fixed number of particles per cell defined by input parameters. Since most OSIRIS simulations were run with a 2D cylindrical geometry, a $1/r$ factor enters into the electromagnetic field equations. This results in numerical noise when $r \rightarrow 0$, which in return affects the evolution of the bunch itself. A sample of the 2D cylindrical simulations were re-run with 3D Cartesian coordinates in order to check that the results were not dominated by this noise. While the 3D simulations were much smoother along the beam axis, the actual results did not seem to differ to any significant degree.

QuickPIC uses 3D Cartesian coordinates, and thus, as OSIRIS 3D, does not have the $1/r$

problem. In addition, QuickPIC has a fixed charge per bunch macro particle, and instead varies the number of these per grid cell to create a charge distribution. A convergence scan of resolution dependency was performed for Publication IV to check that the results did not depend on resolution within the range we used for this study. The convergence scan is described in Section 5.5.3. QuickPIC defines resolution in exponents of 2, and thus are locked to a set of values that rapidly increase for each step. The simulations used for Publication IV were done with transverse grids of 2^9 and 2^{10} (512×512 and 1024×1024) cells, resolving a box size of 1.2 mm square. In the former case, the grid cell size was thus as large as $2 \mu\text{m}$ for the former case, and $1 \mu\text{m}$ for the latter. This did, however, not appear to have any significant impact on the results.

Further details on how QuickPIC and OSIRIS handle bunch particles is covered in Appendix A.

4.2.2 Witness Bunch Transverse Evolution

In OSIRIS 3.0, the electromagnetic fields are initialised at zero. It is therefore necessary to let the bunches drift a short distance before they enter the plasma region in order for the fields to develop. Due to this initial drift stage, it was technically challenging to inject an electron witness bunch while strictly controlling parameters like emittance, energy spread and transverse size during the drift phase. These parameters undergo evolution during this initial drift. It is, however, possible to prevent the beam from evolving by slowly ramping up the beam charge or the beam energy. During these ramping stages the macro particles are prevented from transverse evolution.

For the early studies, and for Publication I, only beam loading and acceleration were considered. For Publications II and IV it was, however, necessary to control the witness bunch emittance. While QuickPIC has input parameters defining beam emittance in each direction, OSIRIS 3.0 does not. OSIRIS 3.0 does let one define spatial and momentum distributions independently (see Appendix A). However, as correlation between σ_{p_i} and σ_i , for dimension i , cannot be controlled, the beam can only be initialised at waist (Twiss parameter $\alpha = 0$, see Appendix B).

For the OSIRIS simulations, the ramping parameters were tuned such that the bunch was unfrozen a few micrometres before it entered the plasma. This prevented betatron oscillations during the drift stage, ensuring that the bunch was still more or less at waist when it entered the plasma region.

While the need for a drift stage has been removed in OSIRIS 4.0, which was available when we started working on Publication IV, the need to study emittance evolution meant QuickPIC was a more suitable tool. Full PIC codes suffers from a numerical instability often referred to as the *Numerical Cherenkov effect*, which can partially be mitigated by improving the electromagnetic fields solver [69]. The quasi-static approximation avoids this issue entirely. This is discussed further in Appendix A.

4.3 Simulating the Plasma

For the simulations made with OSIRIS 3.0, where an initial drift stage is necessary, a decision had to be made on how to simulate the entry point into the plasma. Early tests showed that freezing the transverse evolution of the electron beam and releasing it immediately before the entry into plasma, posed a few challenges. The sudden change in conditions is itself un-physical, and the abrupt change from a frozen state to an evolving bunch while at the same time seeing an instant step in plasma density from 0 to $7 \times 10^{14} \text{ cm}^{-3}$, made it challenging to interpret the results. This was especially the case when the witness bunch was not matched to the plasma density (see Section 1.2.6). A rapid pinching of the bunch occurred immediately after entering the plasma region, causing a spike in the charge density that was within a region too narrow to resolve with the grid resolution we used. This is also a numerically noisy region, as discussed in Section 4.2.1. Eliminating the hard plasma edge by introducing a more realistic plasma ramp over 10 mm, using a cosine-shaped density function. was attempted. However, the effect on the witness bunch was not significant.

5 Simulation Analysis

A lot of work has been put into writing analysis tools to perform both initial and quick, as well as detailed, analyses of the many simulations run. This chapter outlines some of the key considerations and calculations performed on the data sets generated in these simulations. Analysis tools were developed in MATLAB for both OSIRIS and QuickPIC data sets. These are available online, and are described in more detail in Appendix B.

5.1 Extracting Twiss Parameters from Particle Arrays

Both OSIRIS and QuickPIC dump the macro particles as large arrays of six-dimensional data, providing each particle's position and momentum vector. QuickPIC uses equally weighted macro particles, greatly simplifying the analysis. OSIRIS 3, however, uses weighted macro particles, so the weights need to be considered when performing the statistical calculations. Additional statistical functions were added to MATLAB to perform these weighted calculations (see Appendix B).

To study the collective motion of particles it is useful to calculate the bunch total emittance in terms of the RMS value or standard deviation of its particles. Equation 1.8 from Section 1.2.1 can be rewritten in terms of the statistical distributions of its particles such that

$$\epsilon = \sqrt{\gamma\sigma_x^2 + 2\alpha\sigma_x\sigma_{x'} + \beta\sigma_{x'}^2}, \quad (5.1)$$

where the angle of the i -th particles can be taken from its momentum

$$x'_i = \frac{p_{i,x}}{p_{i,z}}. \quad (5.2)$$

For a set of macro particles, the geometric emittance can be calculated directly by taking the covariance matrix of the x and x' vectors

$$\mathbf{T} = \text{cov}(\mathbf{x}, \mathbf{x}'), \quad (5.3)$$

and then taking the square root of its determinant

$$\epsilon = \sqrt{\det(\mathbf{T})}. \quad (5.4)$$

The Twiss parameters can be extracted from the matrix \mathbf{T} as well:

$$\alpha = T_{12}/\epsilon, \quad \beta = T_{11}/\epsilon, \quad \gamma = T_{22}/\epsilon \quad (5.5)$$

5.2 A Measure for Beam Quality

For the emittance study in Publication IV, it was necessary to define a convenient unit for the quality of the accelerated bunch in terms of emittance evolution in regions along the bunch length. In the quasi-linear plus non-linear regime this publication investigates, emittance growth only occurs at the head of the bunch. However, the region of emittance growth varies when parameters such as charge and beam size changes. In the study, we defines the quantity

$$\tilde{Q} = \frac{1}{N} \sum_{m=0}^M \sum_{n=0}^N Q_{m+n} \chi(\xi_m, N), \quad (5.6)$$

where M is the number of longitudinal grid slices of length $\Delta\xi$ which contains macro particles for the witness bunch, and with corresponding coordinate ξ_m ; N is the number of such slices to average over; and $\chi(\xi_m, N)$ is the step function

$$\chi(\xi_i, N) = \begin{cases} 1, & \frac{\epsilon_i - \epsilon_0}{\epsilon_0} \leq 5\% \\ 0, & \frac{\epsilon_i - \epsilon_0}{\epsilon_0} > 5\% \end{cases} \quad \text{for } \epsilon_i \text{ over the interval } [\xi_i, \xi_i + N\Delta\xi], \quad (5.7)$$

where ϵ_i is the emittance as defined by Equations 5.3 and 5.4 for a set of macro particles within the interval ξ_i to $\xi_i + N\Delta\xi$, and ϵ_0 is the initial emittance defined in the simulation input file. For the studies included in Publication IV,

$$M = \left\lfloor \frac{10\sigma_z}{\Delta\xi} \right\rfloor, \quad N = 4. \quad (5.8)$$

The first slice coordinate for the iterator m is

$$\xi_{m=0} = \mu_{eb} - 5\sigma_{z,eb} - 0.5\Delta\xi, \quad (5.9)$$

where μ_{eb} is the longitudinal centre of the bunch.

Note: This method may yield a misleading result if the Twiss parameter α varies too much along the length of the bunch (the rotation of the ellipse, see Figure 1.2). That is, the emittance can be locally small, and qualify for the 5% criterion, even if the total emittance of the region included in \tilde{Q} is not. This can easily be checked after the seemingly optimal region of the bunch is known by verifying that its total emittance does not exceed the same criterion.

5.3 Full Scale Studies

A total of 38 simulations of a full AWAKE proton bunch, with and without an injected electron bunch, were run. As can be seen from Table 5.2, these simulations took an average of over 11 000 CPU hours each. The simulation parameters used for these studies are described in Section 4.1.

The purpose of the full scale studies were mainly to develop some familiarity with OSIRIS 3.0, but also to study the properties of the self-modulated beam in order to make a reasonable approximation of it for the later pre-modulated studies (see Section 4.1.1).

The modulation period of the self-modulated beam was checked with both Fast Fourier Transform (FFT) [115]. The FFT revealed that the core modulation frequency is indeed the characteristic frequency of the plasma as presented in Publication I.

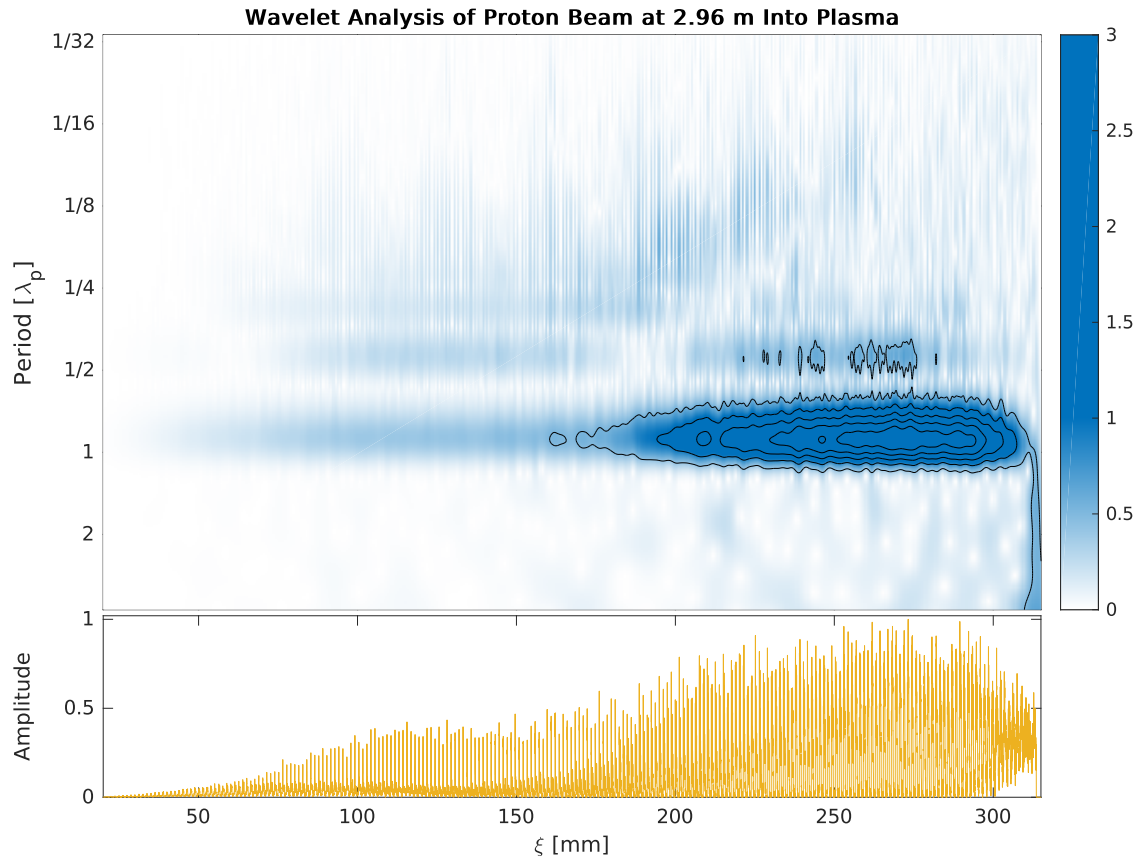


FIGURE 5.1: A wavelet analysis of the beam shown in Figure 4.1, at the same position in the plasma, using Morlet wavelet analysis [110]. The horizontal axis shows the position ξ in the simulation box. The vertical axis shows the Fourier period in units of the plasma wavelength λ_p . This density plot is the absolute value of the complex wavelet data, showing clearly the peak in frequency in the area around the plasma wavelength. The colour axis is saturated at amplitude 1 in order to show the fine structure of the harmonics. The contour plot overlay shows the full range of the density data in steps of 0.5.

A wavelet analysis was also performed using a Morlet Wavelet Analysis [22, 47]. The wavelet adds some additional information about the modulation frequency as a function of

position along the modulated beam of micro bunches. Such a plot is shown in Figure 5.1 where the proton bunch has propagated through about 3 m of plasma. The figure shows the magnitude of the wavelet analysis data [65], and the amplitude indicates that the density variation is the highest at the front of the bunch (compare with initial profile in Figure 4.1).

The frequency of the pre-modulated beam was slightly adjusted such that the FFT profiles matched that of the full scale SMI simulations [17].

Both of these analysis tools were implemented in the OsirisAnalysis package (see Section B.3).

5.4 Beam Loading and Energy Spread

When the parameters of the self-modulated bunch had been established, and the pre-modulated studies set up as laid out in Section 4.1.1, the evolution of the electron beam became the main focus. Of particular interest in the early studies was the beam loading of the electron witness beam on the longitudinal wakefields, as well as its energy spread as it propagated through the plasma section.

The transverse size of the beam was initially chosen to be $\sigma_{x,y} = 105 \mu\text{m}$, see Table 2.1. This is the size initially proposed for Run 1. The longitudinal size was chosen to be $\sigma_z = 40 \mu\text{m}$ for the studies included in Publication I, but several lengths were tested in simulations.

Tuning the longitudinal size is essential. On the one hand, a short bunch positioned at an optimal accelerating phase ensures a low energy spread as all electrons see close to the same accelerating field. On the other hand, a long bunch is capable of holding a larger charge without the charge density becoming critical.

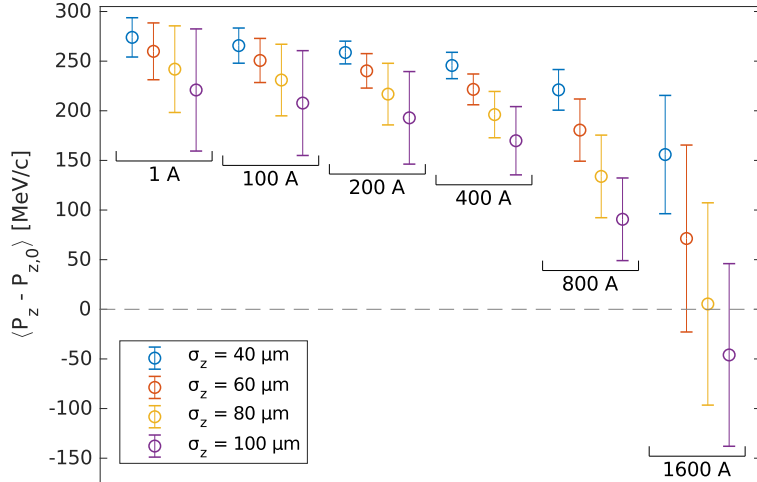


FIGURE 5.2: A parameter scan for the 26 bunch pre-modulated studies where six different beam currents and four different beam lengths were considered. The energy gain $P_z - P_{z,0}$ after 1.1 m of plasma is shown with the error bars representing the RMS energy spread. The figure is presented in Publication II and in Adli *et al.* [2].

The initial studies showed that $\sigma_z = 40 - 60 \mu\text{m}$ is a good compromise between having a short enough bunch to stay within the accelerating region of the accelerating wakefield, $\approx \lambda_{pe}/4$

(see Section 1.2.5), and a long enough bunch to contain a reasonable amount of electrons without overloading the wakefield. A larger parameter scan was done for Publication II presented as a contributing talk at North American Particle Accelerator Conference in Chicago in 2016, and was also included in [2]. The main results of this parameter scan is shown in Figure 5.2.

5.5 Emittance Evolution

Emittance is preserved in the linear regime

5.5.1 The Quasi-Linear Regime

Text

5.5.2 The Quasi-Linear + Non-Linear Case

Quasi-linear reference [98].

An electron beam matched to the typical AWAKE plasma density will be, as discussed in 1.2.6, very narrow. At a typical normalised emittance of $2.0 \mu\text{m}$ the beam is $5.25 \mu\text{m}$. Even at low beam charge and at the upper limit in terms of beam length, the wakefields of such a beam will quickly reach the non-linear regime. In the base case used in the beam loading study included in Publication IV [20] the peak density of the beam $n_b/n_0 > 35$, well beyond the saturation level of the bubble that occurs when $n_b/n_0 > 10$ [73].

The implication here is that there is an additional beneficial effect of loading the accelerating field with as much charge as it will allow without overloading it. The resulting non-linear wake driven by the head of the beam, which will see emittance growth due to the quasi-linear conditions of the proton wake, ensures that the rest of the beam sees a strong focusing force preventing further emittance growth. As the electron beam gains energy, its transverse size will decrease as its emittance is preserved as $\sigma_r = \sqrt{\epsilon_N \beta}$ [124].

5.5.3 Convergence Scan

For the large parameter scans performed for Publication IV, it was necessary to verify that the results were not dependant on grid resolution. The radial wakefields within the plasma bubble are linear, but so are the fields within one grid cell as they are interpolated on the grid. The effect of linear focusing could thus be an artefact of resolution. Especially in the case where the grid cells were only a factor 2.5 smaller than the bunch $\sigma_{x,y}$, and thus the bubble radius also small.

Verify and cite.

5.6 Optimising the Witness Beam

Bringing it all together.

5. SIMULATION ANALYSIS

TABLE 5.1: Convergence results for a reference simulations for Publication IV. The reference bunch has a charge of 250 pC, and the emittance tolerance criterion for the \tilde{Q} parameter is 5% (see Section 5.2).

	LENGTH	PARAM.	1024×1024		2048×2048		4096×4096	
40 μm		\tilde{Q}	213.9	pC	206.9	pC	213.1	pC
		MEAN(E)	2263	MeV	2233	MeV	2247	MeV
		STD(E)	267.4	MeV	250.4	MeV	261.5	MeV
60 μm		\tilde{Q}	221.6	pC	222.0	pC	222.1	pC
		MEAN(E)	2346	MeV	2336	MeV	2333	MeV
		STD(E)	166.8	MeV	165.0	MeV	165.5	MeV
80 μm		\tilde{Q}	229.9	pC	226.9	pC	224.8	pC
		MEAN(E)	2378	MeV	2379	MeV	2368	MeV
		STD(E)	120.0	MeV	117.6	MeV	119.1	MeV

5.7 Summary of Simulation Studies

TABLE 5.2: Overview of total simulation cost. 97% of the simulations were run on the supercomputer *Abel*, on Oct Core Intel Xeon E5-2670 CPUs. The remainder were run on older nodes with Quad Core AMD Opteron 2354 CPUs.

TOPIC OF STUDIES	CODE	COUNT	CPU TIME	AVERAGE
Preliminary studies (mostly testing)	OSIRIS	21	266 599 h	12 695 h
Full length AWAKE proton bunch studies	OSIRIS	38	440 583 h	11 594 h
Pre-modulated beam studies ¹	OSIRIS	144	319 093 h	2 216 h
3D reference studies	OSIRIS	23	245 974 h	10 695 h
Single drive bunch studies ²	OSIRIS	124	47 837 h	386 h
Beam loading and emittance studies ³	QuickPIC	293	369 887 h	1 262 h
Total		657	1 479 350 h	2 252 h

¹ Main studies for Publication I

² Main studies for Publication II

³ Main studies for Publication IV

6 Summary and Conclusion

Text

PUBLICATIONS

PUBLICATION I

Loading of a Plasma-Wakefield Accelerator Section Driven by a Self-Modulated Proton Bunch

Abstract: We investigate beam loading of a plasma wake driven by a self-modulated proton beam using particle-in-cell simulations for phase III of the AWAKE project. We address the case of injection after the proton beam has already experienced self-modulation in a previous plasma. Optimal parameters for the injected electron bunch in terms of initial beam energy and beam charge density are investigated and evaluated in terms of witness bunch energy and energy spread. An approximate modulated proton beam is emulated in order to reduce computation time in these simulations.

Authors: Veronica K. Berglyd Olsen, Erik Adli (University of Oslo, Oslo, Norway), Patric Muggli (Max Planck Institute for Physics, Munich, Germany), Ligia D. Amorim, Jorge M. Vieira (Instituto Superior Technico, Lisbon, Portugal)

Publication: Proceedings of IPAC 2015, Richmond, Virginia, USA [[17](#)]

Date: 3rd to 8th of May, 2015

LOADING OF A PLASMA-WAKEFIELD ACCELERATOR SECTION DRIVEN BY A SELF-MODULATED PROTON BUNCH

V. K. Berglyd Olsen*, E. Adli (University of Oslo, Norway)

P. Muggli (Max Planck Institute for Physics, Munich, Germany)

L. D. Amorim, J. M. Vieira (Instituto Superior Technico, Lisbon, Portugal)

Abstract

We investigate beam loading of a plasma wake driven by a self-modulated proton beam using particle-in-cell simulations for phase III of the AWAKE project. We address the case of injection after the proton beam has already experienced self-modulation in a previous plasma. Optimal parameters for the injected electron bunch in terms of initial beam energy and beam charge density are investigated and evaluated in terms of witness bunch energy and energy spread. An approximate modulated proton beam is emulated in order to reduce computation time in these simulations.

INTRODUCTION

The AWAKE experiment [1] is a proof-of-principle demonstration of acceleration of an electron bunch to the TeV energy range in a single plasma section, using a proton bunch driver [2].

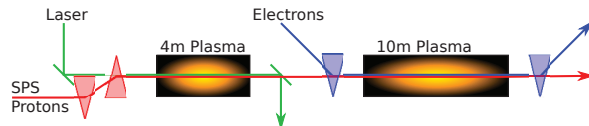


Figure 1: Simplified set-up of AWAKE Phase III. A long proton bunch experiences the SMI in a short plasma cell. The electron bunch is injected before the second plasma cell.

The AWAKE experiment proposes using a proton driver at 400 GeV, delivered by the SPS. The experiment is currently under construction at CERN, scheduled to start in late 2016. The SPS proton bunch is too long to generate a sufficiently strong wakefield [3]. A usable drive bunch needs to be close to the plasma wavelength λ_p in length; however, producing a short enough proton bunch is technically difficult.

The plasma wavelength and frequency are given by

$$\lambda_p = \frac{2\pi c}{\omega_p}, \quad \omega_p = \sqrt{\frac{N_p e^2}{m_e \epsilon_0}}, \quad (1)$$

where N_p is the plasma electron density, e is the elementary charge, m_e is the electron mass and ϵ_0 is the vacuum permittivity.

A proton bunch with $\sigma_{z,0} k_p \gg 1$, where $\sigma_{z,0}$ is the initial length of the bunch, will under certain conditions develop a self-modulation instability (SMI) when it travels through a plasma [4]. The proton bunch will then develop into a train of micro bunches with a period on the order of λ_p .

* v.k.olsen@fys.uio.no

3: Alternative Particle Sources and Acceleration Techniques

A22 - Plasma Wakefield Acceleration

In phase I of the AWAKE experiment the SMI of the proton bunch will be studied. In phase II, the proton wake will be studied using a long, externally injected electron bunch that will sample all phases of the wake. In phase III, acceleration of a short bunch in the wake of an already self-modulated proton beam will be studied, as illustrated in Fig. 1. In this paper we study the beam quality of a short electron bunch accelerated by an SMI proton wake in preparation for phase III of AWAKE.

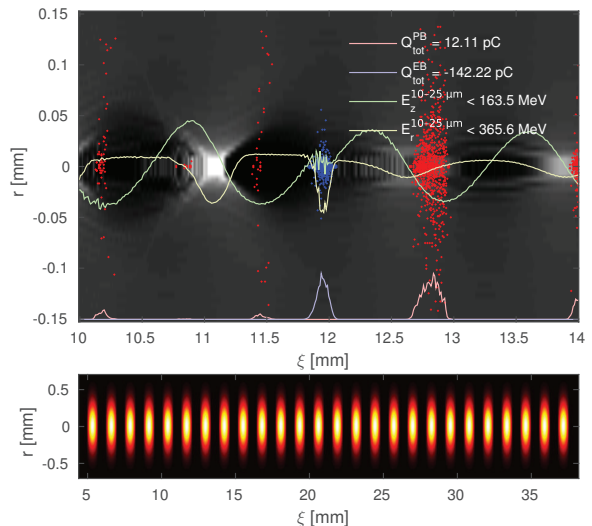


Figure 2: **Top:** An example showing the structure of the plasma electrons (grey) with a projection of the proton beam (red) and the electron bunch (blue) density on the bottom. The E_z (green) and E_r (yellow) fields have been overlaid on the plot. Shown is also a sample of electron (blue) and proton (red) macro particles. **Bottom:** An example of a pre-modulated proton drive beam at $t = 0$ plotted in terms of charge density.

SIMULATION SET-UP

All simulations in this paper have been performed using OSIRIS, a three-dimensional, relativistic, particle-in-cell code for modelling plasma based accelerators [5].

The parameter scans presented have all been run on a small scale test case with a shorter proton drive beam than AWAKE specifications. We simulate here only the second plasma stage in Fig. 1, assuming a pre-modulated proton beam profile with charge density function

$$\rho_{p^+}(\xi) = A \left[\frac{1}{2\sqrt{2}} + \cos(k_p \xi - \mu_1) \right] e^{-r^2/2\sigma_r}, \quad (2)$$

ISBN 978-3-95450-168-7

2551

where A is a charge scaling factor, μ_1 is the centre position of the first micro bunch, $k_p = 2\pi\lambda_p^{-1}$ is the wave number, and $\xi = z - ct$ is the coordinates in a frame moving at the speed of light.

The length of the beam is limited by a step function to 33 mm. Negative density values for the density profile is ignored by OSIRIS. This gives a beam of 26 micro bunches of protons, as seen in the bottom plot of Fig. 2. The beam has a total initial charge of 2.6 nC, with an initial peak current per micro bunch of 135 A. For the proton beam $\sigma_r = 200 \mu\text{m} = 1.00 \text{ c}/\omega_p$ in all simulations, where c/ω_p is the plasma skin depth.

The electron witness bunch is injected between micro bunches 20 and 21 of the drive beam, at $\xi \approx 12 \text{ mm}$, see Fig. 2. The charge density of the electron bunch is given by

$$\rho_{e^-}(\xi) = Ae^{-(\xi-\mu)^2/2\sigma_z^2}e^{-r^2/2\sigma_r^2}. \quad (3)$$

For the electron bunch $\sigma_r = 105 \mu\text{m} = 0.52 \text{ c}/\omega_p$, and $\sigma_z = 40 \mu\text{m} = 0.2 \text{ c}/\omega_p$ in the cases with a short electron bunch. The plasma density at the beginning of the plasma section for all these simulations is $N_p = 7 \times 10^{14} \text{ cm}^{-3}$.

BEAM INJECTION

While the peak-to-peak distance between micro bunches of the self-modulated proton beam corresponds closely to the plasma wavelength λ_p , it is not constant along the length of the beam [6]. A brief study of the SMI of both full scale and small scale proton beams, using Fourier transform and Wavelet analysis, revealed that the fundamental frequency was slightly lower than one k_p .

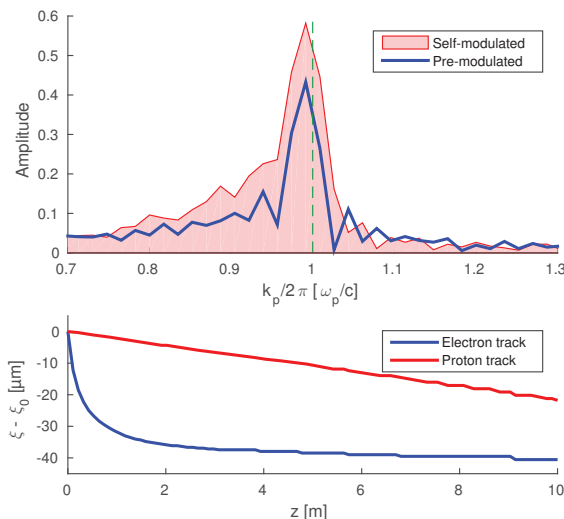


Figure 3: **Top:** The Fourier transform of the proton beam after 10 m of plasma for a self- and pre-modulated beam. The green line indicates $k_p = 2\pi/\lambda_p$. **Bottom:** Typical drift of a proton and electron macro particle through the plasma in respect to c .

To minimise further SMI development with a pre-modulated beam, the micro bunch distance was reduced

to $0.9939 k_p$, which produced a very good fit to the actual SMI for our test case, see Fig. 3.

An electron bunch of low MeV range initial energy will, due to its low gamma factor compared to the 400 GeV proton beam, slip backwards. In order to minimise this effect we set the initial energy of the electron bunch to 30 MeV, a little higher than AWAKE parameters. Typical slip for the beams through 10 m of plasma is illustrated in Fig. 3.

Staying in phase with the drive beam is essential to optimise energy transfer. Establishing an optimal injection point of the electron bunch was achieved by using bunches with length in the order of one λ_p , and tracking a selection of the electrons with optimal energy gain back to $z = 0$.

BEAM LOADING AND ENERGY SPREAD

In a plasma wakefield accelerator, the witness bunch should be accelerated at high efficiency while preserving a low energy spread. Beam loading in the linear regime can be calculated by the linear addition of fields. Only very narrow electron bunches, with $\sigma_r \ll c/\omega_p$, can maintain low energy spread and emittance [7, 8].

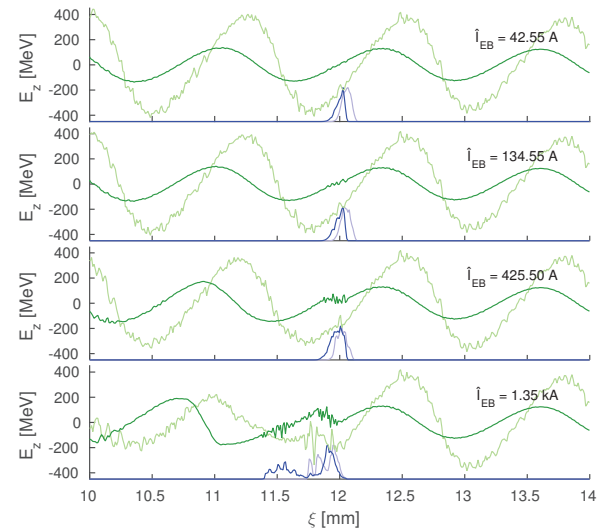


Figure 4: Comparison between the E_z field at 1 m (light green) and 10 m (dark green) of plasma for four different electron bunch currents. The fields are averages over a region $10 - 25 \mu\text{m}$ from the axis. A dimensionless plot of the charge density of the electron bunch is added in blue.

In the non-linear blowout regime, the plasma electrons are blown out by the drive beam, leaving behind a uniform region of plasma ions. The ions pull the electrons back towards the axis, forming a bubble with length on the order of the plasma wavelength [8, 9]. In this regime, the charge and current profile required to optimally load the wake can be estimated analytically. Optimal loading results in a flat E_z field across the bunch with high wake to beam energy transfer efficiency. There is a trade-off between the number of particles that can be accelerated and the accelerating gradient, as discussed in detail by Tzoufras et. al [10].

The beam-plasma interaction studied in this paper has similarities with the above blowout regime, but the train of micro bunches produces a more complex wakefield [4]. We have studied the beam loading through simulations. Based on beam loading in the blowout regime, we use as starting point for the studies a witness bunch with the same peak current as the initial peak current of one proton micro bunch, 135 A. We then performed a scan with logarithmic steps of current from 13.46 A to 13.46 kA. A selection of these are shown in Fig. 4, significant loading of the E_z field does occur when the witness bunch has significantly higher current than the proton beam. An approximate flattening of the field is observed when the witness bunch current is about 3 times higher than the initial micro bunch current, as shown in Fig. 4c. For higher witness bunch currents, we observe that the field from the witness bunch itself starts to dominate the wake it experiences, as expected. The trailing part of the electron bunch is therefore decelerated, as shown for example in Fig. 4d.

We notice that constant loading as the drive and witness bunch propagate in the plasma is not possible, as protons keep being ejected radially throughout the plasma, eating up the micro bunches from the front. This leads to the energy gain levelling off after approximately 4 m of plasma, turning into energy loss as the dephasing between the electron bunch and the E_z fields becomes too large. The phase difference of E_z at 1 m and 10 m is shown in Fig. 4. The mean energy gain (816.2 MeV) and relative energy spread (12%) of the electron bunch, as it travels through the plasma, is visible in blue in Fig. 5, showing a case with peak electron current of 425.5 A. The peak current of a micro bunch after 10 m of plasma, within one skin depth of the axis, is only 45 A.

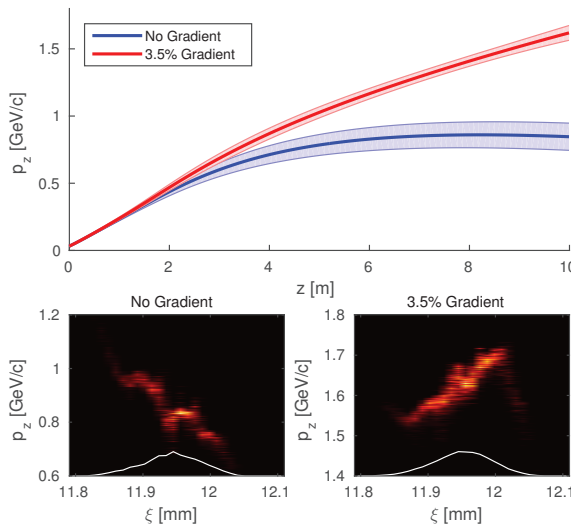


Figure 5: **Top:** Energy gain through 10 m of plasma for a short electron witness bunch with $\sigma_z = 40 \mu\text{m}$ and $\hat{I} = 425.5 \text{ A}$, for the case of no plasma gradient and 3.5% plasma gradient. **Bottom:** $\xi - p_z$ phase plot for both simulations at the end of the plasma.

3: Alternative Particle Sources and Acceleration Techniques

A22 - Plasma Wakefield Acceleration

PLASMA GRADIENT

Due to the backwards drift of the E_z field, the electron bunch falls out of optimal phase after a few metres of plasma. It is possible to stabilise the accelerating bucket by gradually increasing the plasma density. We performed a scan of plasma gradients ranging from 0% to 10% along 10 m of plasma, with a square bunch of length λ_p . We found that a gradient of $0.2 - 0.3 \times 10^{14} \text{ cm}^{-3}$ (3 – 4%) per metre plasma for our initial density of $7 \times 10^{14} \text{ cm}^{-3}$, produced the highest energy gain for the electrons with optimal phase. By tracking some of these electrons back to their injection point, we could move the centre of the short bunch and do a new simulation comparing no gradient to a 3.5% gradient. The best result was for a gradient with a density at 10 m of $7.245 \times 10^{14} \text{ cm}^{-3}$ (3.5%), see Fig. 5 and Table 1.

Table 1: Electron Bunch Energy After 10 m of Plasma

Energy	No Gradient	3.5% Gradient
Mean	846.20 MeV	1618.77 MeV
RMS	101.23 MeV	54.93 MeV
RMS/Mean	11.96 %	3.39 %

CONCLUSION

We have studied beam loading of a SMI proton wake. A scan of electron witness bunch charges over three orders of magnitude revealed that a witness bunch peak current of about a factor 3 higher than the initial peak current of one proton micro bunch was optimal for flattening the wakefield. It is important to note that protons keep getting ejected radially, resulting in a loss of proton charge close to the axis, as the beam travels through the plasma. This decreases the current of a micro bunch by a factor of ~ 3 in the no gradient case.

The electron bunch does not stay in optimal phase for very long as the E_z field starts to drift significantly after 2 – 4 m of plasma. In most simulations the bunch ends up around the zero point of the E_z field, and the energy gradient flattens, and in some cases turns negative. For our optimal case of phase and charge, this effect could to a large degree be counteracted by a 3.5% gradient of the plasma, which forces a positive phase shift of the E_z field, keeping the electron bunch synchronous with the accelerating phase of the wake.

ACKNOWLEDGEMENT

The authors would like to acknowledge the OSIRIS Consortium, consisting of UCLA and IST (Lisbon, Portugal) for the use of OSIRIS, for providing access to the OSIRIS framework.

REFERENCES

- [1] AWAKE Collaboration et al., *Plasma Phys. Control. Fusion* **56**, 084013 (2014).

ISBN 978-3-95450-168-7

2553

- [2] E. Gschwendtner et al., in Proceedings of IPAC2014 (2014), pp. 582–585.
- [3] N. Kumar et al., Phys. Rev. Lett. **104**, 255003 (2010).
- [4] A. Caldwell et al., Phys. Plasmas **18**, 103101 (2011).
- [5] R. A. Fonseca et al., in *Computational science — ICCS 2002*, edited by P. M. A. Sloot et al., Lecture Notes in Computer Science 2331 (Springer Berlin Heidelberg, 2002), pp. 342–351.
- [6] J. Vieira et al., Phys. Plasmas **19**, 063105 (2012).
- [7] T. Katsouleas et al., Part. Acc. **22**, 81–99 (1987).
- [8] M. Tzoufras et al., Phys. Rev. Lett. **101**, 145002 (2008).
- [9] W. Lu et al., Phys. Plasmas **13**, 056709 (2006).
- [10] M. Tzoufras et al., Phys. Plasmas **16**, 056705 (2009).

PUBLICATION II

Loading of Wakefields in a Plasma Accelerator Section Driven by a Self-Modulated Proton Beam

Abstract: Using parameters from the AWAKE project and particle-in-cell simulations we investigate beam loading of a plasma wake driven by a self-modulated proton beam. Addressing the case of injection of an electron witness bunch after the drive beam has already experienced self-modulation in a previous plasma, we optimise witness bunch parameters of size, charge and injection phase to maximise energy gain and minimise relative energy spread and emittance of the accelerated bunch.

Authors: Veronica K. Berglyd Olsen, Erik Adli (University of Oslo, Oslo, Norway), Patric Muggli (Max Planck Institute for Physics, Munich, Germany and CERN, Geneva, Switzerland), Jorge M. Vieira (Instituto Superior Technico, Lisbon, Portugal)

Publication: Proceedings of NAPAC 2016, Chicago, Illinois, USA [18]

Date: 9th to 14th of October, 2016

LOADING OF WAKEFIELDS IN A PLASMA ACCELERATOR SECTION DRIVEN BY A SELF-MODULATED PROTON BEAM

V. K. Berglyd Olsen*, E. Adli (University of Oslo, Oslo, Norway)

P. Muggli (Max Planck Institute for Physics, Munich, Germany and CERN, Geneva, Switzerland)

J. M. Vieira (Instituto Superior Technico, Lisbon, Portugal)

Abstract

Using parameters from the AWAKE project and particle-in-cell simulations we investigate beam loading of a plasma wake driven by a self-modulated proton beam. Addressing the case of injection of an electron witness bunch after the drive beam has already experienced self-modulation in a previous plasma, we optimise witness bunch parameters of size, charge and injection phase to maximise energy gain and minimise relative energy spread and emittance of the accelerated bunch.

INTRODUCTION

The AWAKE experiment at CERN proposes to use a proton beam to drive a plasma wakefield accelerator with a gradient on the order of 1 GeV/m to accelerate an electron witness beam [1, 2].

In this paper we present two simulation configurations with a modified proton drive beam based on the baseline parameters for the AWAKE experiment. The drive beam is delivered from the SPS accelerator at CERN at an energy of 400 GeV/c , a bunch length $\sigma_z = 12 \text{ cm}$, and $\sigma_{x,y} = 200 \mu\text{m}$. [3].

The baseline plasma electron density n_{pe} for AWAKE is $7 \times 10^{14} \text{ cm}^{-3}$. The corresponding plasma wavelength $\lambda_{pe} = 2\pi c/\omega_{pe} = 1.26 \text{ mm}$, where $c/\omega_{pe} = 200 \mu\text{m}$ is the plasma skin depth, and ω_{pe} is the plasma frequency given as $[n_{pe} e^2/m_e \epsilon_0]^{1/2}$.

In order to generate a suitable wakefield, the drive beam must be shorter than λ_{pe} . This is not achievable for the SPS proton beam. In order to use such a beam to drive a wakefield we exploit the self-modulation instability (SMI) that can occur when the beam travels through a plasma and $\sigma_z \gg \lambda_{pe}$. The SMI modulates the beam at a period of $\approx \lambda_{pe}$ [4], allowing us to inject the witness beam in an optimal bucket between two such proton micro bunches.

BEAM LOADING

A particle beam at high energy travelling through a plasma will excite a plasma wave in its wake, and the plasma can sustain a very high accelerating gradient [5]. It is possible to accelerate a secondary beam by extracting energy from this wakefield, thus transferring energy from a drive beam to a trailing witness beam. Such an accelerator design was first proposed by Chen in 1985 [6]. However, there are some challenges in this transfer of energy from drive to witness beam.

* v.k.olsen@fys.uio.no

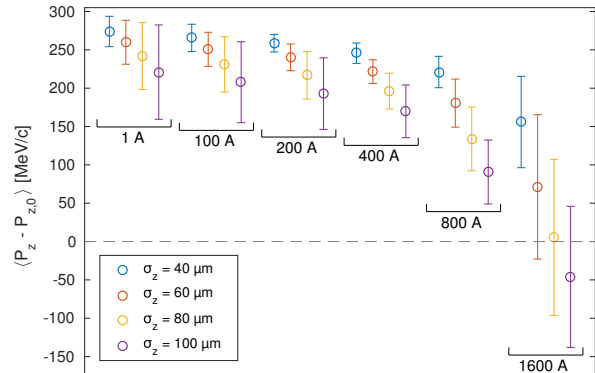


Figure 1: Energy gain and spread for a series of witness beams after $\approx 1.1 \text{ m}$ of plasma. The initial momentum of the witness beam is 217.8 MeV/c . Mean momentum and RMS spread is calculated for all macro particles in the PIC simulation.

One such challenge stems from the witness beam generating its own field, modifying the E_z -field behind it such that the particles in the tail will be accelerated less than those in the front. This causes an increase in energy spread in the beam [7]. This effect can in theory be corrected for by shaping the witness beam. An optimally shaped and positioned beam, such as a triangular beam, can flatten the wakefield such that change in energy spread is effectively zero [8]. However, this requires beam shapes that are difficult to produce experimentally.

BEAM LOADING OF SMI WAKEFIELDS

For AWAKE, most of the SMI evolves during the first stage of $z < 4 \text{ m}$ [2]. This evolution results in a phase change of the wakefields that causes the optimal point for acceleration to drift backwards relative to the witness beam [9, 10].

In our current study we have restricted ourselves to Gaussian witness beams, and seek to demonstrate through simulations how small energy spread can still be achieved by optimally loading the field. The first set of simulations presented uses a subset of 26 micro bunches resulting from the self-modulation that occurs in the previous plasma stage. The pre-modulated beam does undergo further evolution as the envelope function does not fully match the SMI beam, but we only look at the first $\leq 3 \text{ m}$ of this stage, before the phase change starts to dominate [11]. All simulations have been done using OSIRIS 3.0 [12].

A second set of proposed simulations for the second plasma stage will use a single drive beam scaled to produce an accelerating field of 500 MV/m, but with its transverse evolution inhibited in order to study the loading of the field produced by the witness beam alone. The drive beam is short, $\sigma_z = 40 \mu\text{m} \ll \lambda_{pe}$, which is well below the SMI limit.

MULTI DRIVE BUNCH SIMULATIONS

In the multiple drive bunch simulations we assume self-modulation has occurred in a previous stage, and approximate the resulting proton beam in the second stage where acceleration of the witness beam occurs. In this first series of studies we have used a short series of 26 proton bunches with a clipped cosine envelope. This setup is about 10 times shorter than full scale AWAKE simulations, allowing us to run more detailed parameter scans. The setup is described in more detail in our IPAC'15 proceedings, where we looked at beam loading as well as the evolution of the proton beam in a 10 m plasma section [11].

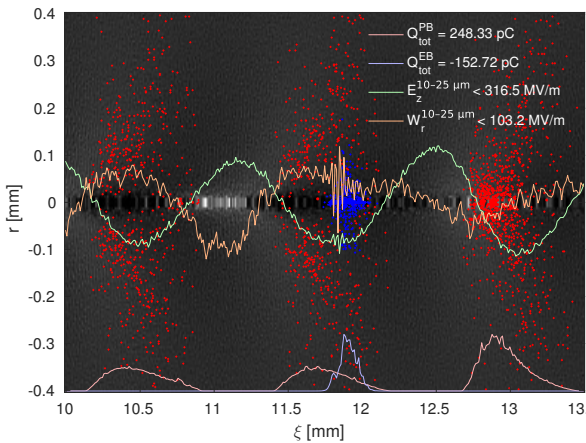


Figure 2: Loading of the field after ≈ 1.1 m of plasma for a 400 A/60 μm electron beam. A sample of electrons (blue) and protons (red) are plotted with their respective projection at the bottom. The total charge within the region of the plot is given as the first two lines of the legend. The longitudinal e-field E_z is shown in green. The transverse wakefield $W_r = E_r - v_z B_\theta$ is shown in orange, where $v_z = c$ is the moving frame of the simulation. The fields are averages over 15 μm near the axis.

The quality and energy of the accelerated witness beam depends on both its position in relation to the field as well as how uniform the field is in the region where the beam is located. We have matched the initial γ of both witness and drive beam in order to avoid initial slipping of the witness beam with relation to the wakefield. The accelerating phase of the field is in the order of $\lambda_{pe}/4 \approx 300 \mu\text{m}$ in length, which puts a constraint on the longitudinal size of the witness beam. The transverse size $\sigma_r = 100 \mu\text{m}$, however we observe in simulations that the beam shrinks by a factor of 4 – 6 as it enters the plasma section. This again results in a sharp

increase in charge density. A scan of different beam sizes and initial beam current and their corresponding energy gain and spread is shown in Fig. 1.

The best result in terms of total energy spread is for the 40 μm beam of an initial current of 200 A, and for the 60 μm beam of an initial current of 400 A. The former beam carries 67 pC and the latter beam 200 pC. As we want to load the field as close to its maximum as possible, this comes at a cost as the tail of the beam will extend beyond the optimal point into the defocusing region of the wakefields. Fig. 2 shows a snapshot of the 60 $\mu\text{m}/400$ A simulation from Fig. 1. The longitudinal field is nearly flat as a result of the loading.

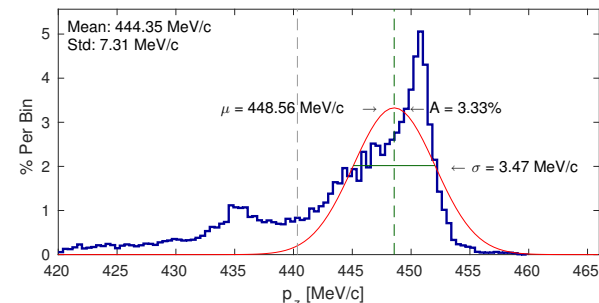


Figure 3: Electron beam momentum spread after ≈ 1.1 m of plasma for the 400 A/60 μm beam. 75 % of the beam charge is accelerated to more than 440 MeV/c, the vertical grey line. The fit is applied to the data above this line, $R^2 = 0.755$.

A closer look at the energy spread in Fig. 3 reveals that ≈ 75 % of the beam is accelerated in this region, with a long tail in energy. This case is not only optimal in terms of beam loading, but also in energy spread of the bulk of the beam of 150 pC. For that part of the beam in front of the grey line we get a relative energy spread $\sigma_{P_z}/[P_z - P_{z,0}] = 1.5$ %. The tail of the beam in terms of energy is lagging behind as it is experiencing defocusing and being pushed outwards and eventually lost from the plasma channel. This loss of beam in the tail can be counteracted by shaping the beam, and making the backwards half $\sigma_z = 20 \mu\text{m}$ and keeping the forward half at $\sigma_z = 60 \mu\text{m}$. In simulations this has reduced this loss to 4 – 5 %. However, such shaping of the beam is technically difficult.

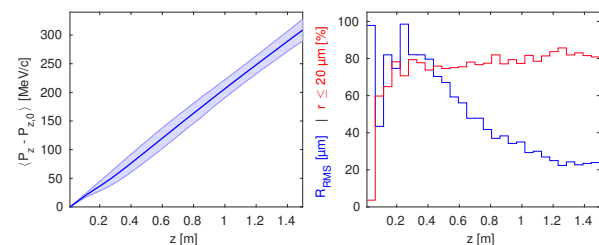


Figure 4: The 400 A/60 μm electron beam as it travels through plasma. The left plot shows the mean energy of the beam with the RMS energy spread as a shaded bar. The right plot shows the RMS radius in blue, and the percentage of macro particles the are within 20 μm of the axis in red.

The relative energy spread of 1.5 % is still undesired. The witness beam in these simulations is initiated with no energy spread in the longitudinal direction. Fig. 4 shows that for our best case the energy spread we see mainly develops in the first 20 cm of plasma. As the right plot illustrates, the transverse RMS size of the beam shrinks by a factor of 5 over the first metres of plasma, but already after a few centimetres about 80 % of the charge is found near the axis. It is this more compact beam that optimally loads the field, and for the first 20 cm the field is under-loaded, probably causing the increase in energy spread. This, however, needs to be studied further.

SINGLE DRIVE BUNCH SIMULATIONS

In order to study the loading of the accelerating e-field in more detail, a second set of simulations have been set up where we have a single proton drive bunch driving a wakefield on the order of 500 MV/m, which is the magnitude of the field we expect to see in the second plasma stage of AWAKE Run 2, based on simulations [13, 14].

This series of simulations is set up in such a way that the accelerating field is as static as possible in order to eliminate other factors than the beam loading by the witness bunch. To achieve this, the proton bunch is prevented from evolving transversely by setting the proton mass to a much higher value than its real value. The gamma of the drive and witness bunches are again matched to prevent dephasing.

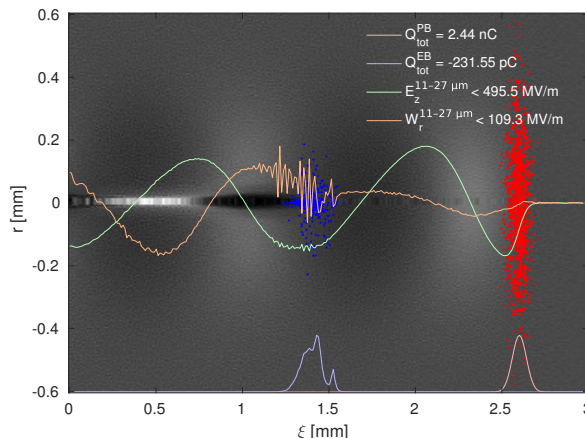


Figure 5: Loading of the field after ≈ 28 cm of plasma for a 500 A/60 μm electron beam. As in Fig. 2 a sample of electrons (blue) and protons (red) are plotted with their respective projections, and the E_z and W_r wakefields are shown.

This provides a much cleaner environment to study the effects of beam loading from the electron beam alone without any evolution caused by the proton beam. Fig. 5 shows an example of this setup. It reproduces the transverse wakefields we saw in our 26 bunch simulations. We also see a shrinking of the witness beam in the first few centimetres, which, together with emittance evolution, is the focus of this next stage of on-going simulation studies.

3: Advanced Acceleration Techniques and Alternative Particle Sources

A22 - Plasma Wakefield Acceleration

CONCLUSION AND CONTINUATION

There are a number of challenges with accelerating an electron beam by a self-modulated proton beam in plasma. Not only does the continued evolution of the proton beam affect the wakefield and thus the acceleration of the witness beam, but the evolution of the witness beam itself affects the wakefields, causing among other things, energy spread. However, by tuning the charge density of the beam, this loading of the field can be used to prevent continuing growth in energy spread provided the phase of the wakefield does not evolve too much.

This is an on-going study, and we are currently looking into the cause of the growth of energy spread. It is worth noting that we have so far run these simulations with an unmatched witness beam. We do see emittance growth in this same region where energy spread increases, but further studies are needed to properly understand the numerical contribution to both these effects.

ACKNOWLEDGEMENTS

The authors would like to acknowledge the OSIRIS Consortium, consisting of UCLA and IST (Lisbon, Portugal), for providing access to the OSIRIS framework.

The numerical simulations have been possible through access to the Abel supercomputer maintained by UNINETT Sigma2 AS, and financed by the Research Council of Norway, the University of Bergen, the University of Oslo, the University of Tromsø and the Norwegian University of Science and Technology. Project code: nn9303k.

REFERENCES

- [1] A. Collaboration, *et al.*, *Plasma Phys. Control. Fusion* 56, 084013 (2014).
- [2] A. Caldwell, *et al.*, *Nucl. Instr. Meth. Phys. Res. A* 829, 3–16 (2016).
- [3] E. Gschwendtner, *et al.*, *Nucl. Instr. Meth. Phys. Res. A* 829, 76–82 (2016).
- [4] N. Kumar, *et al.*, *Phys. Rev. Lett.* 104, 255003 (2010).
- [5] E. Esarey, *et al.*, *IEEE Transactions on Plasma Science* 24, 252–288 (1996).
- [6] P. Chen, *et al.*, *Phys. Rev. Lett.* 54, 693–696 (1985).
- [7] S. Van der Meer, tech. rep. CERN/PS/85-65 (AA), CLIC Note No. 3 (1985).
- [8] T. Katsouleas, *et al.*, *Part. Acc.* 22, 81–99 (1987).
- [9] A. Pukhov, *et al.*, *Phys. Rev. Lett.* 107, 145003 (2011).
- [10] C. B. Schroeder, *et al.*, *Phys. Rev. Lett.* 107, 145002 (2011).
- [11] V. K. B. Olsen, *et al.*, in *Proceedings of IPAC2015* (2015), pp. 2551–2554.
- [12] R. A. Fonseca, *et al.*, in *Computational Science — ICCS 2002*, 2331 (Springer Berlin Heidelberg, 2002), pp. 342–351.
- [13] A. Collaboration, *et al.*, tech. rep. CERN-SPSC-2016-033 (2016).
- [14] E. Adli, *et al.*, in *Proceedings of IPAC2016* (2016), pp. 2557–2560.

PUBLICATION III

Data Acquisition and Controls Integration of the AWAKE Experiment at CERN

Abstract: The AWAKE experiment has been successfully installed in the CNGS facility at CERN, and is currently in its first stage of operation. The experiment seeks to demonstrate self-modulation of an SPS proton beam in a rubidium plasma, driving a wakefield of several gigavolt per meter. We describe the data acquisition and control system of the AWAKE experiment, its integration into the CERN control system and new control developments specifically required for AWAKE.

Authors: Veronica K. Berglyd Olsen (University of Oslo, Oslo), Spencer J. Gessner, Jozef J. Batkiewicz, Stephane Deghaye, Edda Gschwendtner (CERN, Geneva, Switzerland), Patric Muggli (Max Planck Institute for Physics, Munich, Germany and CERN, Geneva, Switzerland)

Publication: Proceedings of IPAC 2017, Copenhagen, Denmark [[19](#)]

Date: 14th to 19th of May, 2017

DATA ACQUISITION AND CONTROLS INTEGRATION OF THE AWAKE EXPERIMENT AT CERN

Veronica K. Berglyd Olsen*, University of Oslo, Oslo, Norway
 Jozef J. Batkiewicz, Stephane Deghaye, Spencer J. Gessner, Edda Gschwendtner,
 CERN, Geneva, Switzerland
 Patric Muggli, Max Planck Institute for Physics, Munich, Germany and
 CERN, Geneva, Switzerland

Abstract

The AWAKE experiment has been successfully installed in the CNGS facility at CERN, and is currently in its first stage of operation. The experiment seeks to demonstrate self-modulation of an SPS proton beam in a rubidium plasma, driving a wakefield of several gigavolt per meter. We describe the data acquisition and control system of the AWAKE experiment, its integration into the CERN control system, and new control developments specifically required for AWAKE.

INTRODUCTION

AWAKE is an Advanced Wakefield Experiment designed to demonstrate proton driven plasma wakefield acceleration utilising a 400 GeV proton drive beam from the Super Proton Synchrotron at CERN [1]. The first phase of the experiment has been successfully installed in the former CNGS facility, and was commissioned in October and November 2016.

The first phase of AWAKE is intended to demonstrate the self-modulation instability in the proton drive beam [2], and we had a first short 48 hour run with rubidium plasma and protons in December 2016. Further three weeks of beam time are scheduled at the end of May and in August 2017. The installation of the electron beam phase is scheduled to be completed in September 2017, with first physics expected in November.

CERN CONTROL SYSTEM

Located at CERN, AWAKE is taking advantage of the extensive support infrastructure that already exists for experiments. This also includes integration into the CERN control system.

The Large Hadron Collider is controlled through the Front End Software Architecture (FESA), developed at CERN. This software framework has been extended and generalised in FESA3 to be usable by other experiments as well. FESA device classes are developed based on standardised and modular code tailored for each specific device. These classes are split into a real time and a server process. The real time process is intended to access the hardware directly, and in addition provides access to internal and external timing as well as information from other device classes. The server process provides an interface for get and set operations for

device settings and acquired data, as well as subscription to any further data updates [3].

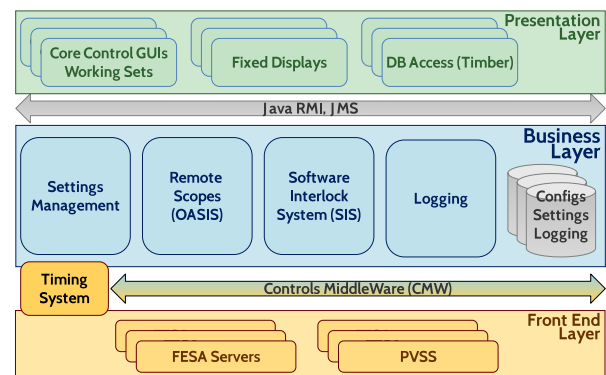


Figure 1: The CERN Control System is structured in three main layers. The Front End Layer consists of VME crates, PCs and PLCs dealing with high performance data acquisition and real time processing. These communicate with application, database and file servers as well as central timing on the Business Layer via the Controls Middleware. Graphical user interfaces and database access are found on the Presentation Layer, and interact with the Business Layer via Java APIs [4].

FESA classes run on Front End Computers (FEC), which run on the Linux operating system. The data from these classes are fed to both data logging systems and control room displays and interfaces as outlined in Fig. 1.

DATA ACQUISITION FOR WINDOWS BASED INSTRUMENTS

The AWAKE experiment has largely been integrated into this infrastructure through direct hardware access between the instruments and the FESA framework. However, some of the instruments depend on proprietary software that is not supported by the standard Front End Computer platform running on Scientific Linux. In order to get around this, and to avoid writing new software, data from three of the instruments currently have to be written to files on shared folders on Windows computers. These files are then imported by designated FESA file reader classes running on CERN supported FECs.

Three instruments currently require software or drivers only available for the Windows operating system:

* v.k.olsen@cern.ch

AWAKE uses Mach-Zehnder type interferometers to measure and calculate the vapour density at either end of the 10 m rubidium plasma cell. The acquired interferogram is stored as a file from the instruments software, and a fitting algorithm is applied to calculate the density to within at least $\pm 0.5\%$ relative accuracy [5]. As the fitting is too computationally heavy to run in real time, the fitting is not currently done by the file reader, but will be performed by a separate FESA class running on a dedicated computer.

The rubidium plasma is ionised by a 780 nm, 4.5 TW peak power laser with a pulse length of 100–120 fs [6]. The pulse length is measured by a single shot optical autocorrelator [7]. The autocorrelator itself is a commercial product, and we extract the data directly from its camera through its Windows drivers. On the local computer we compute the projection and fit it with a sech^2 function using Levenberg-Marquardt. We then write the projection, fit, pulse width and the full image to a binary file.

In addition, we have a 4-channel Tektronix oscilloscope with 23 GHz analogue bandwidth and a 50 GSa sampling rate per channel. The oscilloscope is used to measure real time signals from various Schottky diodes installed in a proton beam diagnostic setup downstream of the plasma cell. They measure Coherent Transition Radiation (CTR) emitted in the microwave band. We use proprietary Windows software to automatically save all channel data files at each event trigger.

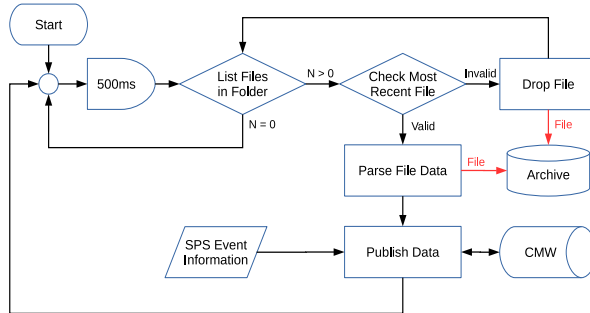


Figure 2: The FESA file reader classes written specifically for AWAKE all operate in the same way. A process polls a dedicated watch folder every 500 ms for new files. The file content is verified according to the instruments' expected format, and either imported and archived, or moved to a dropped folder for later manual control. Imported data is immediately made available on the CMW interface to subscribed services [8].

These instruments require their own FESA class to handle their respective file formats. However, each of these classes operates in the same way, and therefore only requires individual data parsing code. A flow chart illustrating their operation is shown in Fig. 2. The beam cycle time for the experiment itself is around 30 seconds [6], but some of the instruments may be required to run at a higher frequency. The 500 ms delay is both chosen to allow for a ≤ 1 Hz data acquisition frequency with some margin allowed for file system response time, as well as to ensure there is no significant

delay between the time the file is written and when the data is available to the data logging layer. The class polls a dedicated watch folder and attempts to import all files present in reverse chronological order. This is to ensure all data is imported in case of for instance a network interruption. Valid files are then parsed, the data forwarded, and the file itself moved to an archive folder. The original file name of the imported file, as well as its creation time, is stored with the imported data. In the event of an invalid file, a warning is raised and the file is moved to a dropped files folder for later manual verification.

PXI DIGITAL CAMERA SYSTEM

AWAKE uses the analogue camera system provided by the CERN BI group to monitor the proton beam at BTV stations along the beam line. The analogue camera system is radiation hard and requires minimal mechanical upkeep. However, the system is asynchronous to beam extractions. It acquires frames at a fixed rate of 50 FPS and records the frame corresponding to beam extraction. This method of acquisition is not ideal for AWAKE, because AWAKE uses scintillating Chromox screens to image the beam. The scintillation has a long decay time of 140 ms, which is longer than the frame exposure time of 20 ms. This means that under identical experimental conditions, the recorded beam intensity on the screen will vary, simply because the analogue frame is not synced with the beam arrival time.

In addition to this issue, the analogue cameras cannot acquire data at 10 Hz, which is the repetition rate of the laser. For purposes of feedback and stability, it is critical to monitor the laser at this frequency. A digital camera system was implemented to monitor the laser. The camera server is a PXI crate made by National Instruments, and it comprises a trigger and timing system as well as GigE framegrabbers. The digital cameras are made by Basler Ace, and the system supports both CCD and CMOS sensors in a variety of sizes. The image data and camera power are both delivered by a GigE connection using the Power-over-Ethernet (PoE) standard.

The digital camera system was implemented at the laser merging point of the beamline and survived the radiation received during operations in 2016. Because of this success, the digital cameras are being implemented along the beamline to measure both the particle and laser beams. The cameras will be monitored for radiation exposure at areas where high doses are expected in order to understand the total integrated dose (TID) and the single event upset rate (SEU).

EVENT BUILDER

Devices at AWAKE can be read synchronously with SPS beam extractions or asynchronously between extractions. The synchronous/asynchronous distinction depends on the device. For instance, BPMs are read out only when the proton beam is present, but the temperature probes for the Rubidium cell are read out continuously in one second inter-

vals. All of the data from the AWAKE and SPS diagnostics are recorded by the logging system and it is possible to reconstruct the experiment after the fact. It is also desirable to have fast event reconstruction. In order to facilitate this process, the Event Builder was developed to take a “snapshot” of the experiment at the time of the SPS extraction. The Event Builder is subscribed to the key experimental diagnostics, and records their values at the time of extraction, thus providing an instantly correlated dataset comprising both the synchronous and asynchronous variables.

The Event Builder is a JAVA client that is able to subscribe to any variable exposed by the CMW. The Event Builder includes a time-out feature that waits for devices to return data following an extraction. Once the time-out ends, the Event Builder collects the data from all devices and writes them to an HDF5 file, which can be analysed instantly. This data is also copied to the CERN EOS system once per day.

SUMMARY

The integration of the AWAKE experiment into the CERN control system posed a number of challenges. CERN Front End Computers run on Scientific Linux, a platform not supported by all of our instruments. The straight forward solution was to let the Windows based instruments write data dump files on their respective computers, and then use the standard CERN Front End Software Architecture framework to develop file reader classes that can import these via shared network folders.

Due to the relatively large time interval between events, roughly 30 s, the data can be gathered based on time stamps

and collected per event in HDF5 files by an Event Builder. These event files are available immediately after an event, as well as backed up and stored for later analysis.

AWAKE uses many of CERN’s standard analogue and radiation hard cameras. However, these cameras pose synchronisation issues as they have a fixed frame rate of 50 FPS. At critical points, AWAKE uses digital cameras with a trigger and timing system instead.

ACKNOWLEDGEMENTS

The authors would like to thank the AWAKE team at CERN, as well as the CERN Beams, Engineering and Technical Departments for all their assistance in getting the experiment up and running.

REFERENCES

- [1] E. Gschwendtner, et al., in Proceedings of IPAC 2014 (2014), pp. 582–585.
- [2] A. Caldwell, et al., Nucl. Instr. Meth. Phys. Res. A **829**, 3–16 (2016).
- [3] A. Schwinn, et al., in Proceedings of PCaPAC 2010 (2010), pp. 22–26.
- [4] R. Gorbonosov, AWAKE Collaboration Meeting, Apr. 2013.
- [5] E. Öz, F. Batsch, and P. Muggli, Nucl. Instr. Meth. Phys. Res. A **829**, 321–325 (2016).
- [6] E. Gschwendtner, et al., Nucl. Instr. Meth. Phys. Res. A **829**, 76–82 (2016).
- [7] F. Salin, et al., Appl. Opt., AO **26**, 4528–4531 (1987).
- [8] V. K. Berglyd Olsen, 17th AWAKE Technical Board, Feb. 2016.

PUBLICATION IV

Emittance Preservation of an Electron Beam in a Loaded Quasilinear Plasma Wakefield

Abstract: We investigate beam loading and emittance preservation for a high-charge electron beam being accelerated in quasilinear plasma wakefields driven by a short proton beam. The structure of the studied wakefields are similar to those of a long, modulated proton beam, such as the AWAKE proton driver. We show that by properly choosing the electron beam parameters and exploiting two well known effects, beam loading of the wakefield and full blow out of plasma electrons by the accelerated beam, the electron beam can gain large amounts of energy with a narrow final energy spread (%-level) and without significant emittance growth.

Authors: Veronica K. Berglyd Olsen, Erik Adli (University of Oslo, Oslo, Norway), Patric Muggli (Max Planck Institute for Physics, Munich, Germany and CERN, Geneva, Switzerland)

Publication: Physical Review Accelerators and Beams [20]

Date: 16th of January, 2018

Emittance preservation of an electron beam in a loaded quasilinear plasma wakefield

Veronica K. Berglyd Olsen^{*} and Erik Adli
University of Oslo, 0316 Oslo, Norway

Patric Muggli

Max Planck Institute for Physics, D-80805 Munich, Germany and CERN, CH-1211 Geneva, Switzerland



(Received 13 October 2017; published 16 January 2018)

We investigate beam loading and emittance preservation for a high-charge electron beam being accelerated in quasilinear plasma wakefields driven by a short proton beam. The structure of the studied wakefields are similar to those of a long, modulated proton beam, such as the AWAKE proton driver. We show that by properly choosing the electron beam parameters and exploiting two well known effects, beam loading of the wakefield and full blow out of plasma electrons by the accelerated beam, the electron beam can gain large amounts of energy with a narrow final energy spread (%-level) and without significant emittance growth.

DOI: [10.1103/PhysRevAccelBeams.21.011301](https://doi.org/10.1103/PhysRevAccelBeams.21.011301)

I. INTRODUCTION

Beam driven plasma wakefield accelerators [1] have the potential to offer compact linear accelerators with high energy gradients, and have been of interest for several decades. With a relativistic charged particle drive beam travelling through a plasma, a strong wakefield is excited that can be loaded by a trailing witness beam. When the witness beam optimally loads the wakefield, an increase in absolute energy spread can be kept small. The concept has been demonstrated experimentally in the past using electron drive beams accelerating electron witness beams [2–5].

A major challenge with plasma wakefield accelerators is, however, to accelerate a beam while keeping both energy spread and emittance growth small. In the well-described linear regime, valid when the beam density n_b is much smaller than the plasma density n_0 , a nonlinear transverse focusing force causes emittance growth of the witness beam. The beam also sees a transversely and longitudinally varying accelerating field causing a spread in energy after the beam has been accelerated [6]. In the nonlinear regime, where $n_b > n_0$, a bubble is formed by the transverse oscillations of the plasma electrons, gathering in a sheath around an evacuated area filled with only ions. The ions, assumed stationary, form a uniform density ion channel

creating a focusing force that varies linearly with radius. This focusing force preserves emittance [7].

In this paper we present simulation results showing how emittance preservation of a high charge density witness beam can be ensured when accelerated by a proton drive beam producing quasilinear wakefields [8]. By quasilinear wakefields we here mean wakefields with only partial blow out of the plasma electrons in the accelerating structure (bubble). The key idea is to have enough charge in the witness beam to at the same time load the wakefield to produce low relative energy spread, and completely blow out the electrons left in the accelerating structure after the beam to reach conditions that preserves emittance. The results have importance for the preparation of AWAKE Run 2 [9], and possibly other applications in the quasilinear regime.

A. AWAKE Run 2

The energy carried by electron drive beams used in previous plasma wakefield experiments have been on the order of 100 J and the propagation length typically no more than 1 m [3,10]. For high-energy physics application a higher total beam energy is often desired. For instance, the energy of a high-charge electron beam accelerated to 1 TeV with 1×10^{10} electrons, similar to the beam that could be produced by the International Linear Collider, is 1.6 kJ. Using electron beams as drivers, a large number of plasma stages is required to reach an energy of a kJ for the accelerated beam. However, staging plasma accelerators without reducing the effective gradient and spoiling the beam quality is challenging [11,12].

Proton beams available at CERN carry significantly more energy than available electron beams, 19 kJ for the

^{*}v.k.b.olsen@cern.ch

Published by the American Physical Society under the terms of the [Creative Commons Attribution 4.0 International license](#). Further distribution of this work must maintain attribution to the author(s) and the published article's title, journal citation, and DOI.

SPS beam [13], allowing for much longer plasma wakefield accelerator stages. The SPS beam is orders of magnitude longer than the plasma wavelengths needed for such applications, and it does not drive a strong wake [13]. By letting the proton beam undergo self-modulation before injecting the witness beam into the accelerating structure, stronger wakefields are excited. The self-modulation is produced by the transverse fields generated by the beam acting upon itself, causing regions of the beam to rapidly defocus [14]. The modulation frequency is close to that of the plasma electrons, and produces a train of short proton bunches along the beam axis with a surrounding halo of defocused particles. This train of bunches resonantly drives wakefields to large amplitudes.

AWAKE at CERN is a proof of concept proton beam driven plasma wakefield accelerator experiment [15], currently in its first phase of operation. The experiment uses a 400 GeV proton beam delivered by the SPS as its driver, and a single 10 m plasma stage with a nominal plasma density of $7 \times 10^{14} \text{ cm}^{-3}$ [13]. This plasma density corresponds to $\lambda_{pe} = 1.26 \text{ mm}$ and is matched to the transverse size of the proton beam such that $k_{pe}\sigma_{x,y,pb} = 1$ [16], where $k_{pe} = 2\pi/\lambda_{pe}$ is the plasma wave number, $\lambda_{pe} = 2\pi c/\omega_{pe}$, and $\omega_{pe} = (n_0 e^2/m_e \epsilon_0)^{1/2}$ is the plasma electron angular frequency.

The aim of the first phase of the experiment is to demonstrate self-modulation of the proton beam. The aim of the second phase, in 2018, is to sample the wakefield with a long electron beam ($\approx \lambda_{pe}$). The study presented here has relevance for Run 2 [9], starting in 2021 after the LHC long shutdown 2, and aims to demonstrate acceleration of a short electron beam ($\ll \lambda_{pe}$) to high energy and with a minimal increase in emittance and absolute energy spread.

The plans for AWAKE Run 2 propose to use two plasma sections, as illustrated in Fig. 1. The first section of about 4 m is the self-modulation stage where the proton beam undergoes self-modulation without the electron beam present. The electron witness beam is then injected into the modulated proton beam before section two where it undergoes acceleration. The self-modulated proton beam does not produce a fully non-linear wakefield, and therefore not all plasma electrons are evacuated from the plasma bubble. The result is that the focusing force does not increase linearly with radius and the accelerated beam emittance is not preserved.

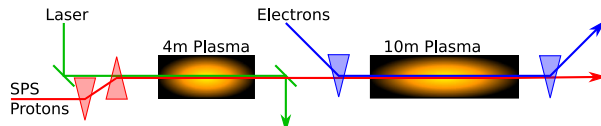


FIG. 1. A simplified illustration of the experimental setup for AWAKE Run 2. The SPS proton beam undergoes self-modulation in the first plasma section. The electron witness beam is injected into the accelerating structure, and undergoes acceleration in the second plasma section [9,17].

II. METHOD

The focus in this study is on the beam loading of the wakefields driven by the proton beam. Studies of self-modulated proton beams show that the beam evolves as it propagates through a uniform plasma [18], but small variations in the plasma profile the modulation, and thus the wakefields, may be stabilized over long distances [18–20]. To study the witness beam evolution in a stable wake, independent of the dynamics of the self-modulation, we use a single, nonevolving proton bunch as driver. The proton beam parameters are chosen so that key features of the wake—the plasma electron density in the wake and the longitudinal electric field—are the same as in the wake of a self-modulated proton beam with AWAKE baseline parameters [13]. Both the proton beam and the witness beam have Gaussian longitudinal charge distribution and bi-Gaussian transverse charge distributions.

We have previously studied the beam loading in a proton beam wake using the full particle-in-cell (PIC) code OSIRIS [21] with 2D cylindrical-symmetric simulations. The studies [17,22] primarily looked at beam loading, energy gain and energy spread, as well as different approaches to creating a stable drive beam structure based on previous self-modulation studies. In order to study the witness beam emittance evolution we use the recently released open-source version of QUICKPIC [23,24]. QUICKPIC is a fully relativistic 3D quasi-static PIC code. It does not suffer from the numerical Cherenkov effect that full PIC codes do [25,26], making it a well suited tool to study emittance preservation. All simulation results in this paper were obtained using QUICKPIC open-source [27].

A. Drive beam parameters

The modulation process used in AWAKE does not reach the fully nonlinear regime and thus does not produce a bubble void of plasma electrons. When the SPS beam, containing 3×10^{11} protons [13], enters the second plasma section (Fig. 1), the peak electric field is expected to be about 500 MV/m. The plasma electron density is only depleted to around 65% of nominal value at the point where we inject the electron beam [28]. The plasma electron density depletion and the peak field are replicated using a single bunch with 1.46×10^{10} protons (2.34 nC), a length $\sigma_z = 40 \mu\text{m}$ (7 kA), and a transverse size $\sigma_{x,y,pb} = 200 \mu\text{m}$. The beam peak density is $0.83 \cdot n_0$ and results in a quasi-linear wake. To avoid transverse evolution of the proton driver, emulating the stable propagation of the self-modulated beam [18–20], we freeze the transverse evolution of the equivalent proton bunch by increasing the particles mass by six orders of magnitude.

B. Witness beam parameters

In order to prevent large amplitude oscillations of the witness beam particles, which may cause additional energy

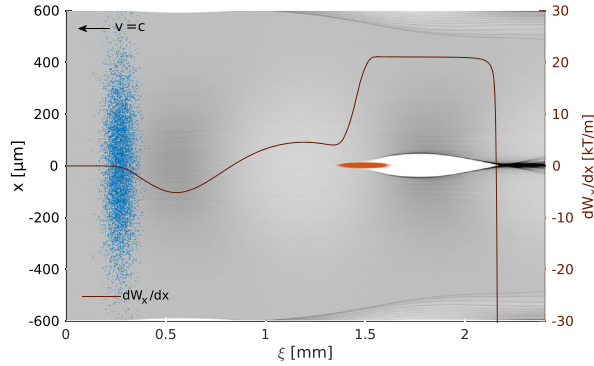


FIG. 2. QuickPIC simulation results showing the initial time step for the single proton drive beam and witness beam setup. Plasma electron density is shown in grey with the drive beam (blue) and the witness beam (red) superimposed. The line plot indicates the transverse wakefield gradient dW_x/dx where $W_x = E_x - v_b B_y$, evaluated along the beam axis. Beams move to the left.

spread as well as emittance growth, we consider a witness beam matched to the plasma density. The matched beam transverse size [29] is

$$\sigma_{x,y,eb} = \left(\frac{2c^2 e_N^2 m_e \epsilon_0}{n_{pe} e^2 \gamma} \right)^{1/4}. \quad (1)$$

We assume an initial normalized emittance of $\epsilon_N = 2 \mu\text{m}$. This emittance is possible to produce with a standard rf-injector, while at the same time yielding a sufficiently narrow beam.

Beam loading by a short witness beam is sensitive to its position relative to the electric field [30] as well as, at low energy, to its dephasing with respect to the wakefields. To eliminate dephasing of the witness beam, the initial beam energy is set such that $\gamma_{eb} = \gamma_{pb} = 426.3$, giving an energy of 217 MeV. A lower initial energy is likely to be sufficient for AWAKE Run 2 injection.

Equation (1) yields a transverse size $\sigma_{x,y,eb}$ of 5.25 μm , which is narrow compared to the drive beam $\sigma_{x,y,pb} = 200 \mu\text{m}$. The bunch length was set to $\sigma_z = 60 \mu\text{m}$ based on earlier beam loading studies [22]. The charge is adjusted to 100 pC for optimal beam loading, as discussed in the next section. We refer to the defined drive beam and witness beam parameter set as the *base case*. Figure 2 shows the two beams—the proton beam in blue, the trailing electron beam in red, and the plasma electron density in grey—from a QUICKPIC simulation of the initial time step, for the base case parameters.

C. Simulation parameters

The relatively small size of the witness beam puts constraints on the transverse grid cell size and number in the simulations. We need a small size to resolve the

narrow electron beam, and a large number of grid cells to resolve the much wider proton beam and its wakefields. We use a transverse grid cell size of 1.17 μm , and of 2.34 μm for the longitudinal grid cells for the simulations presented in Sec. III. The witness beam was simulated with 16.8×10^6 and the drive beam with 2.1×10^6 nonweighted particles, and the plasma electrons with 1024×1024 weighted particles per transverse slice. Convergence checks of the simulations were done with a grid size down to 0.51 μm and with up to 4096×4096 plasma electrons per slice.

III. BEAM LOADING

Figure 3 shows the results of QUICKPIC simulations of the initial time step for the base case parameters. The E_z -field generated by the proton drive beam is seen as the blue line, shown with and without the electron beam present. With a proton beam density $n_{pb} \simeq n_0$, the wakefields are in the quasilinear regime [8]. The dashed green line in the lower part of Fig. 3 shows that the on-axis plasma density has a depletion to 67%, close to what we see in full scale reference simulations for AWAKE Run 2 [28].

The witness beam generates its own wakefield that loads the E_z -field generated by the drive beam. With an ideally shaped electron beam charge profile it is possible to optimally load the field in such a way that the accelerating field is constant along the beam [6,30]. Gaussian beams, as assumed in these studies, cannot completely flatten the electric field in the tails of the charge distribution, and our base case beam therefore has a tail in energy both at the

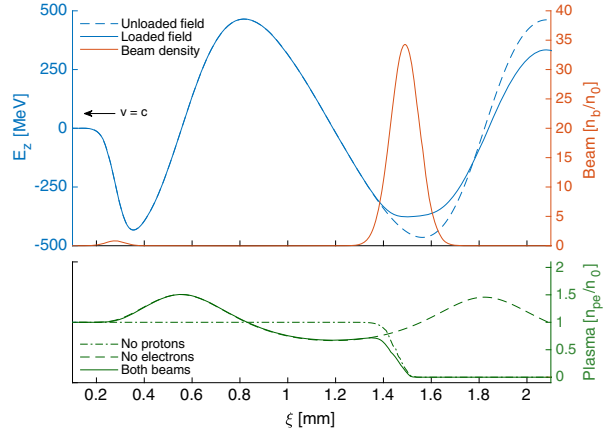


FIG. 3. Top plot: Unloaded longitudinal electric field with no witness beam (dashed blue line) and loaded field (whole blue line) along the beam axis. The beam density along the axis for both beams are shown in red. Bottom plot: Plasma densities along the beam axis for a drive beam with no witness beam (dashed green line), witness beam with no drive beam (dash-dotted green line), and both beams present (continuous green line). The position in the simulation box $\xi = z - tc$, moving toward the left. The plots show the initial time step.

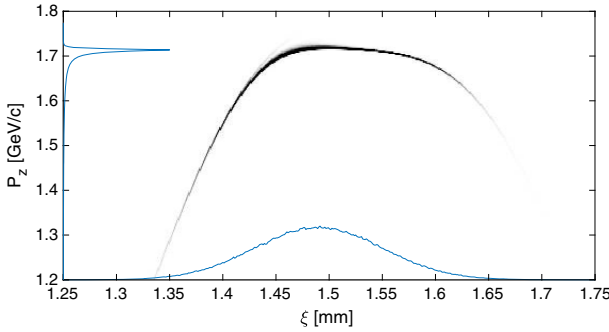


FIG. 4. Longitudinal phase space charge distribution of a 100 pC, 60 μm long witness beam after 4 m of plasma. The mean momentum is 1.67 GeV/c with an RMS energy spread of 87 MeV/c (5.2%) for the full beam.

front and the back of the beam, as illustrated in Fig. 4. The bulk of the beam, however, sees a relatively flat field.

The initial electron beam density is $n_{eb} \approx 35 \cdot n_0$. This means that the witness beam's own wakefield is in the fully nonlinear regime, where the space charge force is sufficient to blow out all plasma electrons, resulting in the formation of a pure ion column (see Fig. 3, bottom). This ion column, as is well known [7], provides a linear focusing force on the part of the electron beam within the column, and therefore prevents emittance growth for this part of the beam. This bubble and the focusing force is shown for our base case in Fig. 2. The focusing field has a gradient of 20 kT/m near the beam axis, corresponding to the matched field gradient.

Figure 5 shows the slice emittance along the beam for the base case, sampled after propagating through 0, 4, 40 and 100 m of plasma. We define emittance of a slice as preserved if the growth is less than 5%, and \tilde{Q} as the sum charge of the slices for which the emittance is preserved. Simulation results show that $\tilde{Q}/Q = 73\%$ of the electron beam longitudinal slices retain their initial

emittance after the propagation in the plasma. The total (projected) emittance of these slices combined is also preserved. Emittance growth mainly occurs in the first few metres, and no significant emittance growth is observed after this for propagation lengths up to 100 m. The head of the beam does not benefit from the full ion column focusing, but since the proton beam creates a quasilinear wake, the emittance of the head of the beam still stabilizes after some time. For the 100 m simulation, the drive beam energy was increased to 7 TeV (LHC energy) to prevent dephasing, as dephasing starts to become a significant effect for the SPS beam of 400 GeV after about 50 m.

So far we have considered a witness beam injected on the axis of the proton beam. We now briefly examine the case of injection of a witness beam with an offset with respect to the proton beam axis. Since the witness beam creates its own plasma bubble, the emittance of the part of the beam inside that bubble is not affected by small transverse offsets of the witness beam with respect to the proton beam axis. This is illustrated in Fig. 5, right, for an electron beam offset of one $\sigma_{x,eb}$. Emittance preservation for small offsets is an added benefit of this accelerating regime, and may ease transverse injection tolerances. The head of the beam experiences a larger initial emittance growth than for the on-axis case (compare Fig. 5, left, to Fig. 5, right). However, also for the head of the beam the emittance growth ends after the first few metres. Figure 6(a)–6(c) show the phase space of the head of the electron beam after 0, 1.0 and 2.5 m, while Fig. 6(d)–6(f) show the phase space of the trailing part of the beam. The centroid oscillations of the head and the trailing part are shown in Fig. 6(g). This effect of a transverse offset is greater for larger offsets as the beam oscillates around the axis of the drive beam wakefield.

The transverse beam size within the bubble, where normalized emittance is preserved, follows the evolution given by Eq. (1); that is, evolves to stay matched.

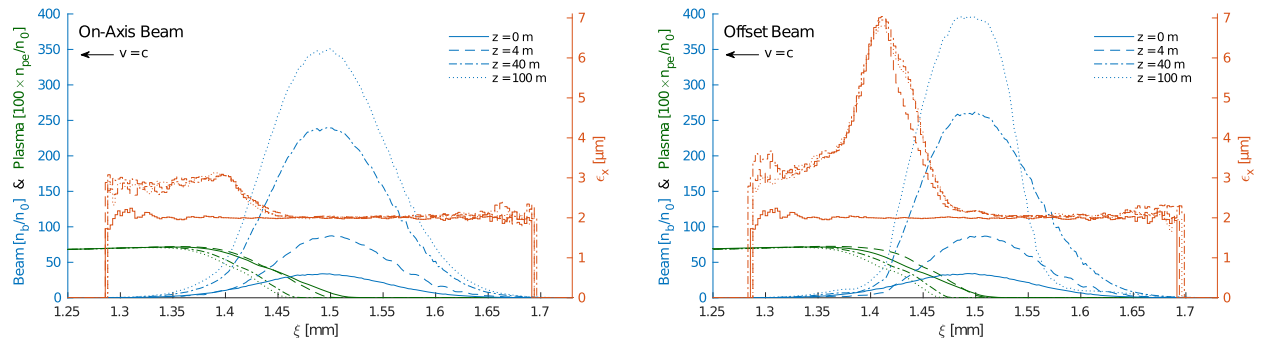


FIG. 5. Beam density in blue along the beam axis for an on-axis beam with respect to the drive beam axis (left), and an offset beam (right) with an offset of one $\sigma_{x,eb} = 5.24 \mu\text{m}$ in the x-plane—at four different positions z in the plasma stage. The red lines show a moving window calculation of transverse normalised emittance. The moving window calculation uses longitudinal slices of $l = 4 \cdot \Delta\xi = 9.38 \mu\text{m}$ with a step of $\Delta\xi$. Only slices with more than 100 macro particles have been included. The plasma density profile is included in green, and scaled up by a factor of 100 to be visible. These simulations were run with an LHC energy drive beam of 7 TeV.

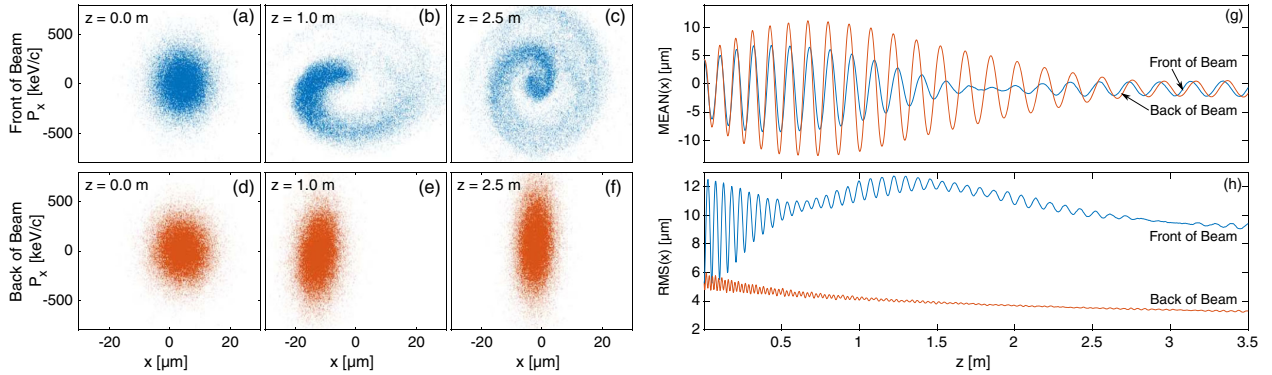


FIG. 6. Plots **a** to **f** show the transverse phase space of the offset electron beam at different plasma positions. Plot **g** shows the macro particle mean position, and plot **h** their RMS spread. Plots **a**, **b** and **c**, as well as the blue lines in plots **g** and **h** represent particles not in the ion column (see Fig. 5), with position $1.40 \mu\text{m} < \xi < 1.42 \mu\text{m}$. Plots **d**, **e**, and **f**, and the red lines in plots **g** and **h** represent particles in the ion column with position $1.55 \mu\text{m} < \xi < 1.57 \mu\text{m}$.

The on-axis density of the electron beam, as a result, increases as its gamma factor increases and its transverse size decreases. This effect can be seen in Fig. 6(h). This has the potential to cause overloading of the field. However, for the base case no significant overloading is observed. Parameters can also be chosen in order to minimize this effect by slightly underloading the wakefield at first, and let the high energy beam overload the wakefield at the end.

IV. PARAMETER OPTIMIZATION

The beam loading and blow out properties of the electron beam depend on a large number of parameters, including longitudinal profile, transverse profile, as well as relative phasing of the proton and the electron beams. We present a limited parameter study aimed to guide beam parameter choices for AWAKE Run 2. For an electron beam to be externally injected in AWAKE Run 2 (see Fig. 1) it is desired to maximize the energy gain, minimize the energy spread, maximize the charge to be accelerated, and minimize the emittance growth [9]. In addition, the beam length should be such that it is possible to generate and transport the beam using a compact electron injector [9]. We investigate the interdependence of these parameters in simulation by varying the electron beam length, its charge, and initial emittance. The results are quantified in terms of how much of the beam retains its initial emittance. For these parameter scans we used a transverse grid cell size of $2.34 \mu\text{m}$, and let the beams propagate through 4 m of plasma.

Figure 7 shows the dependence of charge and energy spread on witness beam length and incoming charge. An initial beam emittance of $2 \mu\text{m}$ was used. Therefore, we define the fractional charge \tilde{Q} as the charge whose emittance remains smaller than $2.1 \mu\text{m}$. The beam charge ranges from 10 pC to 300 pC, and σ_z ranges from $40 \mu\text{m}$ to $100 \mu\text{m}$. As can be seen from Fig. 7 (red curves), both

the $40 \mu\text{m}$ and the $60 \mu\text{m}$ beams have a well defined minimum energy spread with an initial beam charge $\approx 50 \text{ pC}$ and $\approx 100 \text{ pC}$, respectively. Lower beam charges tend to underload the electric field, while higher beam charges tend to overload it. It is also clear that longer beams with respect to the accelerating phase of the field, $\approx \lambda_{pe}/4$, do not optimally load the wake, thus producing a larger spread in energy. The blue curves show the fraction of charge whose initial emittance is preserved (the slice emittance for the base case is shown in Fig. 5). As the witness beam charge increases, the fraction of slices with preserved emittance increases—as expected from an earlier onset of the bubble formation—and also increases in the bubble size [31,32]. We note here that operation with 100 pC leads to a significantly larger charge (factor ~ 4)

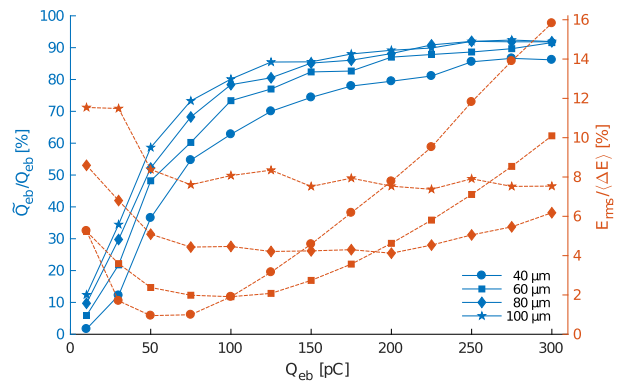


FIG. 7. Ratio of witness beam charge with emittance preserved, \tilde{Q}/Q (blue symbols, lines), as a function of initial beam charge, and relative energy spread of the accepted charge (red symbols, dashed lines), after 4 m of plasma and with an initial emittance $\epsilon_{N,0} = 2 \mu\text{m}$. These are shown for four different σ_z from $40 \mu\text{m}$ to $100 \mu\text{m}$. The detailed studies presented in beam loading section correspond to the square marked lines at 100 pC.

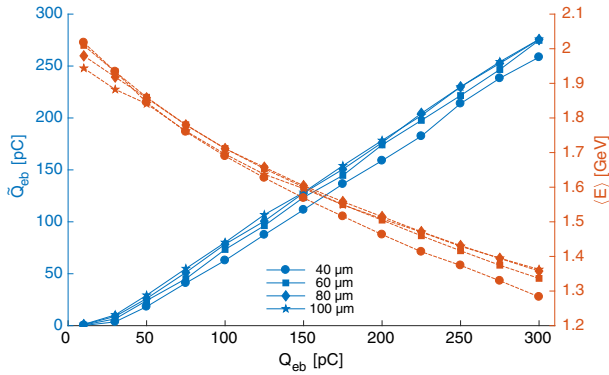


FIG. 8. Witness beam charge with emittance preserved, \tilde{Q} (blue symbols, lines), as a function of initial beam charge, and final energy (red symbols, dashed lines), after 4 m of plasma and with an initial emittance $\epsilon_{N,0} = 2 \mu\text{m}$.

with emittance preserved, at the expense of an increase of relative energy spread by a factor of two.

Figure 8 shows the dependence of mean energy gain on beam length and beam charge (red curves). The blue curves show the amount of charge in the longitudinal slices where the emittance has been preserved, as a function of beam length and beam charge. The results are weakly dependent on the electron beam length. As expected, a larger value of \tilde{Q} corresponds to a lesser energy gain. No optimum is observed.

Figure 9 shows how the growth in emittance and energy spread varies with initial electron beam emittance. In these simulations we adjusted the witness beam radius to maintain the matching condition at each emittance. The smaller the initial emittance is, the better the emittance is preserved. There are two effects that lead to emittance growth for high initial emittance beams: the transverse beam size may increase beyond the size of the bubble, and the beam

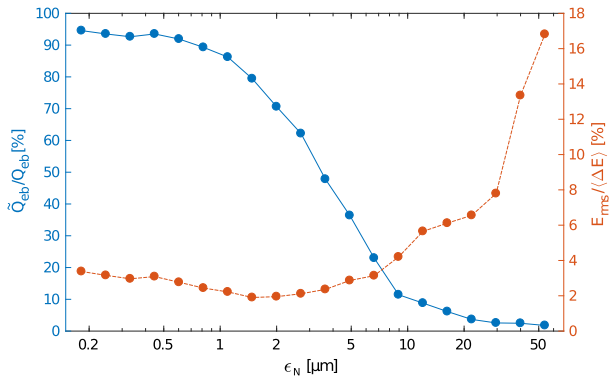


FIG. 9. Ratio of witness beam charge with emittance preserved, \tilde{Q}/Q (blue symbols, line), as a function of beam initial emittance (right), with relative energy spread of the accepted charge (red symbols, dashed line), after 4 m of plasma.

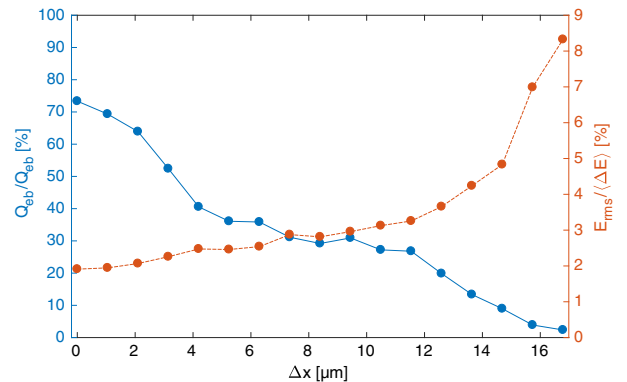


FIG. 10. Ratio of witness beam charge with emittance preserved, \tilde{Q}/Q (blue symbols, line), as a function of beam offset, with relative energy spread of the accepted charge (red symbols, dashed line), after 4 m of plasma.

density may be reduced so much that the plasma electrons are no longer fully evacuated from the bubble. Emittance values higher than a few micrometres lead to a significant increase in both emittance and energy spread.

Our base case showed some robustness to a small offset from the proton beam axis on the order of one $\sigma_{x,eb}$, but with a reduction of the fraction of the beam which retains its initial emittance. Figure 10 shows the correlation between this ratio for a range of offsets up to 16.8 μm, corresponding to $3.2 \cdot \sigma_{x,eb}$. The effect on the head of the beam, shown in Figs. 5 and 6, increases with larger offsets causing the part of the beam being defocused to extend backwards to the point where the witness beam wakefields are no longer in the blow-out regime. At around $3 \cdot \sigma_{x,eb}$ emittance is no longer preserved at all.

The optimal working point will depend on the application and must be studied for each case and is, as illustrated in this section, a trade off between beam length, beam charge, and emittance preservation, as well as other parameters like the plasma density.

V. CONCLUSION

We have devised a method to accelerate an electron witness beam to high energy with a low relative energy spread while maintaining its incoming emittance in wakefields such that the accelerating structure is not void of plasma electrons. This is the case for the AWAKE experiment in which the wakefields are driven by a train of proton bunches produced by self-modulation of a long proton beam. This method is in principle applicable to all experiments operating in the quasi-linear regime. Low relative energy spread and emittance preservation are achieved by choosing the electron beam parameters to load the wakefields and evacuate the remaining plasma electrons from the accelerating structure.

Parameter studies indicate that for up to a few 100 pC, about 70% of the incoming beam charge is accelerated for beam of lengths of 40–60 μm . Such electron beams may be generated by an injector based on a standard rf photo-emission gun [33].

In order to use manageable computer time for simulations, this study assumes a simplified case with respect to a self-modulated proton beam, where the wake is driven by a single, short proton bunch producing similar wakefields. However, the wakefields driven by a train of bunches evolve with the ramp of a real plasma and when entering the plasma. Therefore, to be fully applicable to an experiment such as AWAKE, the study will have to be redone with more realistic parameters. However, using loading of the wakefields and the pure plasma ion column fields to produce an accelerated beam with low relative energy spread and emittance remains applicable.

ACKNOWLEDGMENTS

The simulations for this study have been performed using the open source version of QuickPIC released in early 2017 and owned by UCLA. This work was performed on the Abel Cluster, owned by the University of Oslo and the Norwegian metacenter for High Performance Computing (NOTUR), and operated by the Department for Research Computing at USIT, the University of Oslo IT-department. Project code: nn9303k. Some of the simulations were also run on the student-maintained computing cluster *Smaug* at the University of Oslo, Department of Physics. We gratefully acknowledge helpful discussions with Jorge Vieira from IST, Lisbon.

- [1] P. Chen, J. M. Dawson, R. W. Huff, and T. Katsouleas, Acceleration of Electrons by the Interaction of a Bunched Electron Beam with a Plasma, *Phys. Rev. Lett.* **54**, 693 (1985).
- [2] J. B. Rosenzweig, D. B. Cline, B. Cole, H. Figueroa, W. Gai, R. Konecny, J. Norem, P. Schoessow, and J. Simpson, Experimental Observation of Plasma Wake-Field Acceleration, *Phys. Rev. Lett.* **61**, 98 (1988).
- [3] I. Blumenfeld, C. E. Clayton, F.-J. Decker, M. J. Hogan, C. Huang, R. Ischebeck, R. Iverson, C. Joshi, T. Katsouleas, N. Kirby, W. Lu, K. A. Marsh, W. B. Mori, P. Muggli, E. Oz, R. H. Siemann, D. Walz, and M. Zhou, Energy doubling of 42 GeV electrons in a metre-scale plasma wakefield accelerator, *Nature (London)* **445**, 741 (2007).
- [4] E. Kallos, T. Katsouleas, W. D. Kimura, K. Kusche, P. Muggli, I. Pavlyshin, I. Pogorelsky, D. Stolyarov, and V. Yakimenko, High-Gradient Plasma-Wakefield Acceleration with Two Subpicosecond Electron Bunches, *Phys. Rev. Lett.* **100**, 074802 (2008).
- [5] M. Litos, E. Adli, W. An, C. I. Clarke, C. E. Clayton, S. Corde, J. P. Delahaye, R. J. England, A. S. Fisher, J. Frederico, S. Gessner, S. Z. Green, M. J. Hogan, C. Joshi, W. Lu, K. A. Marsh, W. B. Mori, P. Muggli,
- [6] T. Katsouleas, S. Wilks, P. Chen, J. M. Dawson, and J. J. Su, Beam loading in plasma accelerators, Part. Accel. **22**, 81 (1987).
- [7] J. B. Rosenzweig, B. Breizman, T. Katsouleas, and J. J. Su, Acceleration and focusing of electrons in two-dimensional nonlinear plasma wake fields, *Phys. Rev. A* **44**, R6189 (1991).
- [8] J. B. Rosenzweig, G. Andonian, M. Ferrario, P. Muggli, O. Williams, V. Yakimenko, and K. Xuan, Plasma Wakefields in the Quasi-Nonlinear Regime, *AIP Conf. Proc.* **1299**, 500 (2010).
- [9] E. Adli (AWAKE Collaboration), in *Proceedings of IPAC2016* (JAoCoW, Busan, Korea, 2016), p. 2557.
- [10] A. Caldwell, K. Lotov, A. Pukhov, and F. Simon, Proton-driven plasma-wakefield acceleration, *Nat. Phys.* **5**, 363 (2009).
- [11] S. Steinke, J. van Tilborg, C. Benedetti, C. G. R. Geddes, C. B. Schroeder, J. Daniels, K. K. Swanson, A. J. Gonsalves, K. Nakamura, N. H. Matis, B. H. Shaw, E. Esarey, and W. P. Leemans, Multistage coupling of independent laser-plasma accelerators, *Nature (London)* **530**, 190 (2016).
- [12] C. A. Lindstrøm, E. Adli, J. M. Allen, J. P. Delahaye, M. J. Hogan, C. Joshi, P. Muggli, T. O. Raubenheimer, and V. Yakimenko, Staging optics considerations for a plasma wakefield acceleration linear collider, *Nucl. Instrum. Methods Phys. Res., Sect. A* **829**, 224 (2016).
- [13] E. Gschwendtner, AWAKE, The Advanced Proton Driven Plasma Wakefield Acceleration Experiment at CERN, *Nucl. Instrum. Methods Phys. Res., Sect. A* **829**, 76 (2016).
- [14] N. Kumar, A. Pukhov, and K. Lotov, Self-Modulation Instability of a Long Proton Bunch in Plasmas, *Phys. Rev. Lett.* **104**, 255003 (2010).
- [15] R. Assmann (AWAKE Collaboration), Proton-driven plasma wakefield acceleration: a path to the future of high-energy particle physics, *Plasma Phys. Controlled Fusion* **56**, 084013 (2014).
- [16] W. Lu, C. Huang, M. M. Zhou, W. B. Mori, and T. Katsouleas, Limits of linear plasma wakefield theory for electron or positron beams, *Phys. Plasmas* **12**, 063101 (2005).
- [17] V. K. Berglyd Olsen, E. Adli, P. Muggli, L. D. Amorim, and J. Vieira, in *Proceedings of IPAC 2015* (Richmond, VA, USA, 2015), p. 2551.
- [18] K. V. Lotov, Controlled self-modulation of high energy beams in a plasma, *Phys. Plasmas* **18**, 024501 (2011).
- [19] K. V. Lotov, Physics of beam self-modulation in plasma wakefield accelerators, *Phys. Plasmas* **22**, 103110 (2015).
- [20] A. Caldwell and K. V. Lotov, Plasma wakefield acceleration with a modulated proton bunch, *Phys. Plasmas* **18**, 103101 (2011).
- [21] R. A. Fonseca, L. O. Silva, F. S. Tsung, V. K. Decyk, W. Lu, C. Ren, W. B. Mori, S. Deng, S. Lee, T. Katsouleas, and J. C. Adam, in *Computational Science—ICCS 2002*, Lecture Notes in Computer Science No. 2331, edited by

- P. M. A. Sloot, A. G. Hoekstra, C. J. K. Tan, and J. J. Dongarra (Springer Berlin Heidelberg, 2002), p. 342.
- [22] V. K. Berglyd Olsen, E. Adli, P. Muggli, and J. Vieira, in *Proceedings of NAPAC 2016* (JACoW, Chicago, IL, USA, 2016).
- [23] C. Huang, V. K. Decyk, C. Ren, M. Zhou, W. Lu, W. B. Mori, J. H. Cooley, T. M. Antonsen, and T. Katsouleas, QUICKPIC: A highly efficient particle-in-cell code for modeling wakefield acceleration in plasmas, *J. Comput. Phys.* **217**, 658 (2006).
- [24] W. An, V. K. Decyk, W. B. Mori, and T. M. Antonsen, An improved iteration loop for the three dimensional quasi-static particle-in-cell algorithm: QuickPIC, *J. Comput. Phys.* **250**, 165 (2013).
- [25] B. B. Godfrey, Numerical Cherenkov instabilities in electromagnetic particle codes, *J. Comput. Phys.* **15**, 504 (1974).
- [26] R. Lehe, A. Lifschitz, C. Thaury, V. Malka, and X. Davoine, Numerical growth of emittance in simulations of laser-wakefield acceleration, *Phys. Rev. ST Accel. Beams* **16**, 021301 (2013).
- [27] UCLA Plasma Simulation Group, QuickPIC-OpenSource, GitHub repository (2017).
- [28] A. Caldwell (AWAKE Collaboration), CERN Technical Report No. CERN-SPSC-2016-033, 2016.
- [29] E. Esarey, P. Sprangle, J. Krall, and A. Ting, Overview of plasma-based accelerator concepts, *IEEE Trans. Plasma Sci.* **24**, 252 (1996).
- [30] M. Tzoufras, W. Lu, F. S. Tsung, C. Huang, W. B. Mori, T. Katsouleas, J. Vieira, R. A. Fonseca, and L. O. Silva, Beam loading by electrons in nonlinear plasma wakes, *Phys. Plasmas* **16**, 056705 (2009).
- [31] W. Lu, C. Huang, M. Zhou, W. B. Mori, and T. Katsouleas, Nonlinear Theory for Relativistic Plasma Wakefields in the Blowout Regime, *Phys. Rev. Lett.* **96**, 165002 (2006).
- [32] W. Lu, C. Huang, M. Zhou, M. Tzoufras, F. S. Tsung, W. B. Mori, and T. Katsouleas, A nonlinear theory for multidimensional relativistic plasma wave wakefields, *Phys. Plasmas* **13**, 056709 (2006).
- [33] S. Doeberl (private communication).

APPENDICES

APPENDIX A

Particle in Cell (PIC)

The Particle in Cell method (PIC) is a numerical technique to solve a certain class of partial differential equations. Particles are usually represented by macro particles, that is, one virtual particle in the simulation represents multiple real particles. The particles are tracked in continuous phase space, and they interact only through average fields. Moments of the distribution function are computed simultaneously on a Eulerian mesh to solve the self-consistent field equations [52]. PIC codes can be electrostatic or electromagnetic. Both PIC codes used in this work are electromagnetic, so we will only cover that approach.

Most of the work presented in this thesis was done using OSIRIS [42, 43]. OSIRIS is a fully relativistic and parallelised 3D PIC code. It is written in an object-oriented style with Fortran 90.

For the concluding paper, we opted to instead use QuickPIC [6, 56] as the main simulation tool, although preliminary simulations were done using OSIRIS. QuickPIC is a quasi-static PIC code, which was better suited for emittance studies as the full PIC method suffers from instabilities that proved to be significant for that study.

This Appendix will briefly outline some of the properties of the PIC method, but limited to what is relevant for the work presented and the simulation codes used.

A.1 The Full Electromagnetic PIC Method

The main steps involved in the Electromagnetic PIC method are outlined in Figure A.1. This method is solved on a grid using Maxwell's equations

$$\nabla \cdot \vec{E} = \frac{\rho}{\epsilon_0} \quad (\text{A.1})$$

$$\nabla \cdot \vec{B} = 0 \quad (\text{A.2})$$

$$\nabla \times \vec{E} = -\frac{\partial \vec{B}}{\partial t} \quad (\text{A.3})$$

$$\nabla \times \vec{B} = \mu_0 \left(\vec{J} + \epsilon_0 \frac{\partial \vec{E}}{\partial t} \right), \quad (\text{A.4})$$

A. PARTICLE IN CELL (PIC)

while the particles are advanced in time using the Newton-Lorentz equations

$$\frac{dx}{dx} = \vec{v} \quad (\text{A.5})$$

$$\frac{d(\gamma x)}{dx} = \frac{q}{m} (\vec{E} + \vec{v} \times \vec{B}). \quad (\text{A.6})$$

The charge density ρ and current density \vec{J} are interpolated onto the grid from the particle positions and velocity respectively, while the electric and magnetic fields are interpolated onto the particles when updating their position and velocity [117].

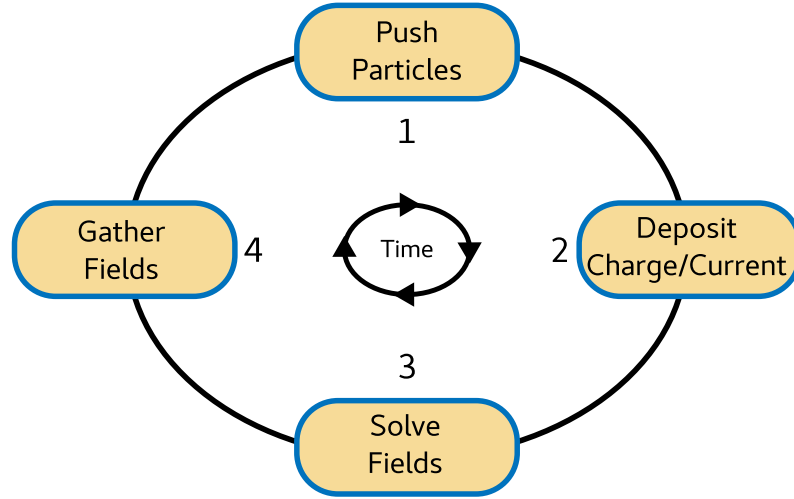


FIGURE A.1: The four main steps of the PIC algorithm. 1: Evolve the velocity and position of the particles using the Newton-Lorentz equations. 2: Interpolate and deposit the charge/current densities onto the grid. 3: Evolve the Maxwell's equations, or Poisson's equation if electrostatic. 4: Interpolate the fields from the grid onto the particles for the next push. Recreated from Vay *et al.* [117].

Step 1 – Particle Push: The Newton-Lorentz equations can be discretised with a centred finite difference discretisation, such that

$$\frac{\vec{x}^{i+1} - \vec{X}^i}{\Delta t} = \vec{v}^{i+1/2} \quad (\text{A.7})$$

$$\frac{\gamma^{i+1/2} \vec{v}^{i+1/2} - \gamma^{i-1/2} \vec{v}^{i-1/2}}{\Delta t} = \frac{q}{m} (\vec{E}^1 + \vec{v}^i \times \vec{B}^1). \quad (\text{A.8})$$

This requires that \vec{v}^i can be represented by the known quantities, to which the Boris' method provides a very efficient second-order accurate and time reversible solution outlined in a 1970 paper [25]. However, this method is not Lorentz-invariant [116] making it unsuitable for ultra-relativistic applications. Lorentz-invariance can be achieved by substituting a velocity average in place of a single-step velocity calculation. This, however,

comes with a performance penalty. For further details and derivations of the different methods, see [117] and therein cited references.

Step 2 – Charge and Current Deposition: The charge and current can be deposited on the grid using various interpolation methods [1]. The densities are deposited from the particle position and velocities using an interpolation S ,

$$\rho = \frac{1}{\Delta x \Delta y \Delta z} \sum_n q_n S_n \quad (\text{A.9})$$

$$\vec{J} = \frac{1}{\Delta x \Delta y \Delta z} \sum_n q_n \vec{v}_n S_n. \quad (\text{A.10})$$

Accumulation of errors resulting from violation of Gauss' law by the discretisation need to be prevented. This can be achieved by either modifying the deposition to prevent such violations, or by using methods that are exact when combined with the field solver in step 3 [117]. OSIRIS makes several interpolation methods available to the user, with varying level of performance and accuracy.

Step 3 – Field Solver There are many implementations of field solvers for PIC codes, and OSIRIS supports multiple such methods. The most relevant here, and the OSIRIS default, is the Yee solver [125]. The Yee solver uses a staggered grid where the electric field components are located between nodes, while the magnetic field components are located at the centre of the grid cell faces. This is illustrated in Figure A.2. The time integration of the fields is done using alternate half time-step leaps, also known as the *Leapfrog* integration scheme. Other solvers not covered here are outlined in [117], some of which are also available in OSIRIS.

Step 4 – Gather Fields: The fields are gathered from the grid and onto the macro particles, usually through the same interpolation S as used in Step 2. This is generally done through a scheme tuned to conserve either energy or momentum.

This method is computationally heavy as all the particle species that make up the plasma accelerator need to be simulated. This includes the electrons and possibly ions that makes up the plasma. In most cases the ions can be assumed to be stationary, and can thus be replaced by a static background charge density. However, OSIRIS does have the ability to simulate ions as well as ionisation of a neutral gas if necessary.

A common way to reduce the computational cost is to only simulate the region populated by the propagating beams using both a moving window in a Lorentz-boosted frame. The latter significantly reduces the number of time steps needed by up to $\approx (i + \beta_r) \gamma_r^2$ [118].

A.1.1 Numerical Cherenkov

The effect [45, 48] Lehe solver [69]

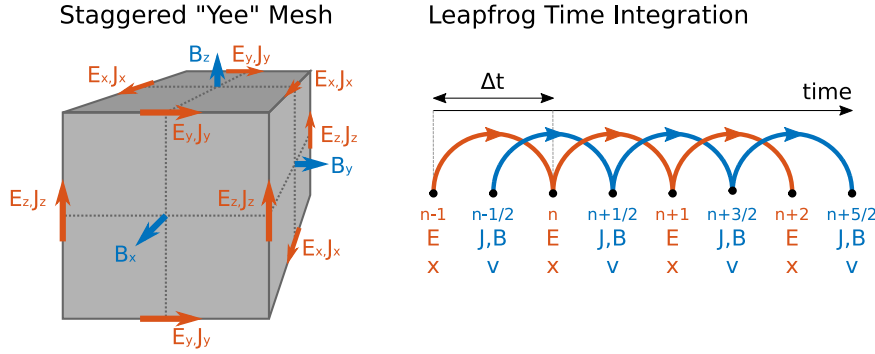


FIGURE A.2: **Left:** The staggered Yee grid. Current densities and electric fields are defined on the edges of the cells, and magnetic fields on the faces. **Right:** Leapfrog time integration uses alternating half time steps for electric and magnetic fields. Recreated from Vay *et al.* [117].

A.2 The Quasi-Static Electromagnetic Method

The quasi-static approximation takes advantage of the fact that a beam travelling close to the speed of light is very rigid, and therefore responds slowly, while the plasma response is very fast in comparison. This separation of response in time scale allows a separation in how these components of the simulation are treated.

While the particle bunches are simulated in 3D, the plasma is simulated in 2D slices. The response of the plasma can then be computed slice by slice as the particle bunches pass through them. This can in fact be done in parallel very efficiently. The longitudinal and transverse structure of the wake can then be constructed from the slices of plasma, and a complete electromagnetic field map computed. This can then be applied to the macro particles to evolve their position and velocity.

There are several ways to perform the necessary calculations, and each implementation of the method may have different solutions. Some key details are outlined in [117].

For example:

In QuickPIC, the plasma particle trajectories are parametrised with $[x(\xi), y(\xi), s(\xi)]$, while the beam particles are parametrised with $[x(s), y(s), \xi(s)]$, where $\xi = ct - z$ is the simulation window coordinate and $s = z$ is the position along the simulation. The variables ξ and s have the same unit, but correspond to the two different time scales, fast and slow respectively [56]. This approximation implies that for short bunches, s is the same for all plasma particles, reducing the plasma particle motion to movement in the x, y -plane. At the same time the beam evolves very slowly and with respect to s , compared to the fast plasma response on the plasma wavelength scale of the coordinate ξ . When solving the field equations it is thus assumed that $\partial/\partial s = 0$, meaning the corresponding first and second derivative terms can be dropped [6]. The charge and current densities for the beam are deposited onto the grid in the same way as with the full PIC method.

The flow of the QuickPIC algorithm is slightly different than presented for full PIC in Figure A.1. While the main loop is 3D, a 2D loop is embedded inside it. After initialisation, the 3D loop hands the token over to the 2D loop which initialises new slices of plasma, runs its field solver, pushes the plasma particles, and deposits onto the grid. The token is then passed back to the 3D routine which pushes the beam particles, and deposits the charge and current of these onto the grid, before returning to the start of the 3D loop again. For a full review of the flow and the numerical implementation of each of the steps, see Huang *et al.* [56].

A.3 Considerations

Mention how OSIRIS needs a ramp-up for fields to be valid
Describe how macro particles are defined
Describe how emittance can be described in OSIRIS

APPENDIX B

Data Analysis Tools

The simulation codes used in these studies produce large amounts of data. It has been very useful to develop a tool for effective analysis of both input and output files. Most of the initial studies were done using OSIRIS 3 (for Publication I and II), and the final emittance study was done using QuickPIC (Publication IV).

The analysis tools written for these studies are publicly available on GitHub. The toolbox for OSIRIS 3 is named OsirisAnalysis [14], and the corresponding toolbox for QuickPIC is named QuickPICAAnalysis [16]. Both toolboxes are written for MATLAB.

This appendix briefly outlines the structure and basic function of these tools.

B.1 The Osiris Analysis Toolbox

The OsirisAnalysis toolbox is a modular and object oriented data analysis toolbox written in MATLAB. It was designed as a three layer tool to wrap a single data set of OSIRIS simulation data:

Layer 1 consists of the core data wrapper class *OsirisData* with its subclass *OsirisConfig*. The *OsirisData* class provides an interface for accessing the raw data files, while the *OsirisConfig* class parses the simulation input file. *OsirisData* provides a uniform set of calls for extracting the data, and gives through *OsirisConfig* access to all the simulation parameters and conversion factors for converting OSIRIS' normalised units into SI units.

Layer 2 consists of a set of classes that takes an *OsirisData* object as input, and returns standardised structs of data that can be scaled and converted to preferred units. They perform often needed tools and methods to parse data and extract more detailed information from the larger raw datasets.

Layer 3 consist of a number of useful standardised plots, and a GUI tool to quickly do a preliminary analysis of simulation data.

The idea behind this layering of the analysis tool is to allow the user to choose how many of these they will use. Only using the first layer will give the user access to all the simulation parameters as well as a method to extract data in a standardised manner, and return a simple matrix of its content. Adding the second layer gives additional access to automatic unit conversion

and other data conversion tools like slicing and line-outs, as well as various properties extracted from the macro particle arrays. The third layer provides a quick way to browse through the datasets and display density plots, phase space plots, Twiss parameters, time evolution, etc.

B.1.1 Core Objects

The innermost layer consists of two classes:

OsirisData: This class wraps the simulation data folder and is the core interface through which data is extracted. The class also provides some simple methods for extracting information about the dataset like physical dimensions of the beam and the distribution of the plasma.

OsirisConfig: This class is a wrapper for the input file itself, and contains a parser for this file which extracts all the relevant information for both analysis and provides lists of available diagnostics for the graphical user interface (GUI). All conversion factors to SI units are calculated on the fly when the input file is loaded. The *OsirisConfig* class is not intended to be called by the user, but is found as a child object of the *OsirisData* data object.

B.1.2 Data Types

The secondary layer of the OsirisAnalysis framework is a set of subclasses under a parent class named *OsirisType*. The subclasses will give access to specific types of data more or less directly related to the diagnostics types produced by the OSIRIS simulation code.

The classes provided are:

Density and Field: These are classes that produce grid diagnostics data for the particle density data dumps or the field diagnostics data. They support all the different density diagnostics outputs of OSIRIS, and will in addition calculate the wakefields from the magnetic and electric fields given by $W = F/q = E - v \times B$.

Momentum: This class consists of a set of methods that will calculate the evolution of the beams energy and momentum over several time dumps.

Phase: This class provides several tools for phase space diagnostics, including calculations of Twiss parameters.

UDist: This class is similar to the *Density* and *Field* classes, and provides methods to process velocity and thermal distribution data.

Species: This class provides a few additional specialised tools for calculating energy deposition and gain into and from the plasma by the beams, and is also the class where particle tracking data is parsed.

In addition to these data parsing classes, there is also a *Variables* class that will translate OSIRIS diagnostics variables into readable forms, and into strings usable for plot labels. There is also a *MathFunc* class that provides a math parser that emulates the one used by OSIRIS to parse mathematical functions from the input files. This class is mainly used to extract geometric information about beam density based on the function provided in the input file without the need to first run the code to provide raw particle data.

B.1.3 Graphical Interface and Plots

The final layer of the OsirisAnalysis framework is a set of very flexible plotting tools. Most of these have a long list of optional input argument that will change the way data is aggregated and presented. To make these plots easier to use, most of these optional arguments are available through a graphical interface, also written in MATLAB, named *AnalysisGUI*.

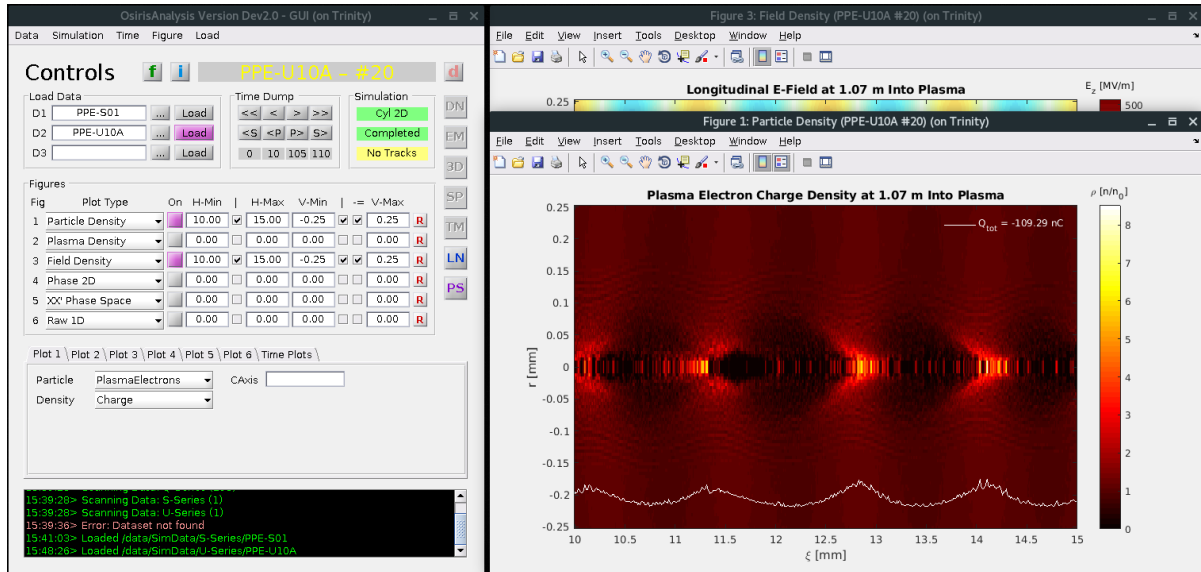


FIGURE B.1: A screen shot of the OsirisAnalysis GUI tool.

B.2 QuickPIC Analysis Framework

The toolbox developed for OSIRIS was also partially rewritten to work with QuickPIC simulations. As QuickPIC uses more or less the same normalised units, the code required little modification to work with these output files. The conversion was also made easier by QuickPIC having a simpler and more consistent set out output files and formats.

As QuickPIC was only used for the final set of studies, only the core objects and input file wrapper classes, and the data type classes were converted. No graphical user Interface was developed for this toolbox, and only a few standardised plots were added. The analysis toolbox is available on GitHub [16].

B.3 Additional Tools Extending MATLAB Functionality

A number of additional statistics and analysis tools were added due to the lack of MATLAB support, or because alternative methods were beneficial.

Weighted Statistics: Additional functions for weighted mean, percentile and standard deviation used by various parts of both analysis tools were added.

Weighted Covariance: The MATLAB `cov` function does support weighted datasets, but for the OsirisAnalysis tool an exponentially weighted covariance function was used instead [91]. This was an attempt to reduce effect of noise in the datasets as this method reduces the impact of statistical outliers. For the QuickPIC implementation, the regular MATLAB `cov` method was used.

Wavelets: The Wavelet implementation used in OsirisAnalysis is provided by two script acquired from the websites of The Department of Atmospheric and Oceanic Sciences at The University of Colorado Boulder [110].

Bibliography

- [1] H. Abe, N. Sakairi, R. Itatani, and H. Okuda. [High-order spline interpolations in the particle simulation](#). *Journal of Computational Physics*, 63(2):247–267, Apr. 1986. ISSN 0021-9991. doi:[10.1016/0021-9991\(86\)90193-2](https://doi.org/10.1016/0021-9991(86)90193-2).
- [2] E. Adli and AWAKE Collaboration. [Towards Awake Applications: Electron Beam Acceleration in a Proton Driven Plasma Wake](#). In *Proceedings of IPAC 2016*, International Particle Accelerator Conference, pages 2557–2560, Busan, Korea, June 2016. JACoW. ISBN 978-3-95450-147-2. doi:[doi:10.18429/JACoW-IPAC2016-WEPMY008](https://doi.org/10.18429/JACoW-IPAC2016-WEPMY008).
- [3] E. Adli and P. Muggli. [Proton-Beam-Driven Plasma Acceleration](#). *Reviews of Accelerator Science and Technology*, 09:85–104, Jan. 2016. ISSN 1793-6268. doi:[10.1142/S1793626816300048](https://doi.org/10.1142/S1793626816300048).
- [4] M. Aicheler, P. Burrows, M. Draper, T. Garvey, P. Lebrun, K. Peach, N. Phinney, H. Schmickler, D. Schulte, and N. Toge. [A Multi-TeV Linear Collider Based on CLIC Technology](#). Technical Report CERN-2012/007, CERN, Geneva, Switzerland, 2012.
- [5] B. Allen, V. Yakimenko, M. Babzien, M. Fedurin, K. Kusche, and P. Muggli. [Experimental Study of Current Filamentation Instability](#). *Physical Review Letters*, 109(18):185007, Nov. 2012. doi:[10.1103/PhysRevLett.109.185007](https://doi.org/10.1103/PhysRevLett.109.185007).
- [6] W. An, V. K. Decyk, W. B. Mori, and T. M. Antonsen. [An improved iteration loop for the three dimensional quasi-static particle-in-cell algorithm: Quick-PIC](#). *Journal of Computational Physics*, 250:165–177, Oct. 2013. ISSN 0021-9991. doi:[10.1016/j.jcp.2013.05.020](https://doi.org/10.1016/j.jcp.2013.05.020).
- [7] G. Apollinari, I. Béjar Alonso, O. Brüning, P. Fessia, M. Lamont, L. Rossi, and L. Tavian. [High-Luminosity Large Hadron Collider \(HL-LHC\) Technical Design Report V. 0.1](#). Technical Design Report CERN-2017-007-M, CERN, Geneva, Switzerland, Sept. 2017. DOI: 10.23731/CYRM-2017-004.
- [8] R. Assmann, Y. Papaphilippou, M. Giovannozzi, G. Xia, F. Zimmermann, and A. Caldwell. [Generation of short Proton bunches in the CERN Accelerator Complex](#). In *Proceedings of PAC09*, pages 4542–4544, Vancouver, BC, Canada, Sept. 2009. FR5RFP004.

- [9] S. Augst, D. Strickland, D. D. Meyerhofer, S. L. Chin, and J. H. Eberly. [Tunneling ionization of noble gases in a high-intensity laser field](#). *Physical Review Letters*, 63(20): 2212–2215, Nov. 1989. doi:[10.1103/PhysRevLett.63.2212](https://doi.org/10.1103/PhysRevLett.63.2212).
- [10] AWAKE Collaboration and A. Caldwell. [AWAKE Status Report, 2016](#). Technical Report CERN-SPSC-2016-033, CERN, Geneva, Switzerland, Oct. 2016.
- [11] AWAKE Collaboration and A. Caldwell. [AWAKE Status Report, 2017](#). Technical Report CERN-SPSC-2017-039, CERN, Geneva, Switzerland, Oct. 2017.
- [12] AWAKE Collaboration, R. Assmann, R. Bingham, T. Bohl, C. Bracco, B. Buttenschön, A. Butterworth, A. Caldwell, S. Chattopadhyay, S. Cipiccia, E. Feldbaumer, R. A. Fonseca, B. Goddard, M. Gross, O. Grulke, E. Gschwendtner, J. Holloway, C. Huang, D. Jaroszynski, S. Jolly, P. Kempkes, N. Lopes, K. Lotov, J. Machacek, S. R. Mandry, J. W. McKenzie, M. Meddahi, B. L. Militsyn, N. Moschuering, P. Muggli, Z. Namjuidin, T. C. Q. Noakes, P. A. Norreys, E. Öz, A. Pardons, A. Petrenko, A. Pukhov, K. Rieger, O. Reimann, H. Ruhl, E. Shaposhnikova, L. O. Silva, A. Sosedkin, R. Tarkeishian, R. M. G. N. Trines, T. Tückmantel, J. Vieira, H. Vincke, M. Wing, and G. Xia. [Proton-driven plasma wakefield acceleration: a path to the future of high-energy particle physics](#). *Plasma Physics and Controlled Fusion*, 56(8):084013, Aug. 2014. ISSN 0741-3335. doi:[10.1088/0741-3335/56/8/084013](https://doi.org/10.1088/0741-3335/56/8/084013).
- [13] K. L. F. Bane, P. Chen, and P. B. Wilson. [On collinear wake field acceleration](#). volume NS-32, pages 3524–3526. IEEE Transaktions on Nuclear Science,, May 1985.
- [14] V. K. Berglyd Olsen. [OsirisAnalysis: Matlab Analysis Code for Osiris Simulations](#). GitHub Repository, 2013. <https://github.com/vkbo/OsirisAnalysis>.
- [15] V. K. Berglyd Olsen. [FESA File Reader Progress](#). 17th AWAKE Technical Board, Feb. 2016. <https://indico.cern.ch/event/523605>.
- [16] V. K. Berglyd Olsen. [QuickPICAnalysis: Matlab Analysis Code for QuickPIC Simulations](#). GitHub Repository, 2017. <https://github.com/vkbo/QuickPICAnalysis>.
- [17] V. K. Berglyd Olsen, E. Adli, P. Muggli, L. D. Amorim, and J. Vieira. [Loading of a Plasma-Wakefield Accelerator Section Driven by a Self-Modulated Proton Bunch](#). In *Proceedings of IPAC 2015*, pages 2551–2554, Richmond, VA, USA, May 2015. ISBN 978-3-95450-168-7. WEPWA026.
- [18] V. K. Berglyd Olsen, E. Adli, P. Muggli, and J. Vieira. [Loading of Wakefields in a Plasma Accelerator Section Driven by a Self-Modulated Proton Beam](#). In *Proceedings of NAPAC 2016*, North American Particle Accelerator Conference, Chicago, IL, USA, Oct. 2016. JACoW. ISBN 978-3-95450-180-9. doi:[10.18429/JACoW-NAPAC2016-TUA4CO03](https://doi.org/10.18429/JACoW-NAPAC2016-TUA4CO03). TUA4CO03.

- [19] V. K. Berglyd Olsen, J. J. Batkiewicz, S. Deghaye, S. J. Gessner, E. Gschwendtner, and P. Muggli. [Data Acquisition and Controls Integration of the AWAKE Experiment at CERN](#). In *Proceedings of IPAC 2017*, Copenhagen, Denmark, May 2017. JACoW. ISBN 978-3-95450-182-3. doi:[10.18429/JACoW-IPAC2017-TUPIK061](https://doi.org/10.18429/JACoW-IPAC2017-TUPIK061). TUPIK061.
- [20] V. K. Berglyd Olsen, E. Adli, and P. Muggli. [Emittance preservation of an electron beam in a loaded quasilinear plasma wakefield](#). *Physical Review Accelerators and Beams*, 21(1):011301, Jan. 2018. doi:[10.1103/PhysRevAccelBeams.21.011301](https://doi.org/10.1103/PhysRevAccelBeams.21.011301).
- [21] M. Bernardini and K. Foraz. [Long Shutdown 2 @ LHC](#). *CERN Yellow Reports*, 2(00):290, Feb. 2016. ISSN 0007-8328. doi:[10.5170/CERN-2015-002.290](https://doi.org/10.5170/CERN-2015-002.290).
- [22] A. Bernardino and J. Santos-Victor. [A Real-Time Gabor Primal Sketch for Visual Attention](#). In *Pattern Recognition and Image Analysis*, Lecture Notes in Computer Science, pages 335–342. Springer, Berlin, Heidelberg, June 2005. ISBN 978-3-540-26153-7 978-3-540-32237-5. https://link.springer.com/chapter/10.1007/11492429_41. DOI: 10.1007/11492429_41.
- [23] B. E. Blue, C. E. Clayton, C. L. O’Connell, F.-J. Decker, M. J. Hogan, C. Huang, R. Iverson, C. Joshi, T. C. Katsouleas, W. Lu, K. A. Marsh, W. B. Mori, P. Muggli, R. Siemann, and D. Walz. [Plasma-Wakefield Acceleration of an Intense Positron Beam](#). *Physical Review Letters*, 90(21):214801, May 2003. doi:[10.1103/PhysRevLett.90.214801](https://doi.org/10.1103/PhysRevLett.90.214801).
- [24] I. Blumenfeld, C. E. Clayton, F.-J. Decker, M. J. Hogan, C. Huang, R. Ischebeck, R. Iverson, C. Joshi, T. Katsouleas, N. Kirby, W. Lu, K. A. Marsh, W. B. Mori, P. Muggli, E. Oz, R. H. Siemann, D. Walz, and M. Zhou. [Energy doubling of 42 GeV electrons in a metre-scale plasma wakefield accelerator](#). *Nature*, 445(7129):741–744, Feb. 2007. ISSN 0028-0836. doi:[10.1038/nature05538](https://doi.org/10.1038/nature05538).
- [25] J. P. Boris. [Relativistic plasma simulation-optimization of a hybrid code](#). *Proceeding of Fourth Conference on Numerical Simulations of Plasmas*, Nov. 1970.
- [26] H. H. Braun, S. Döbert, I. Wilson, and W. Wuensch. [Frequency and Temperature Dependence of Electrical Breakdown at 21, 30, and 39 GHz](#). *Physical Review Letters*, 90(22):224801, June 2003. doi:[10.1103/PhysRevLett.90.224801](https://doi.org/10.1103/PhysRevLett.90.224801).
- [27] A. Caldwell, K. Lotov, A. Pukhov, and F. Simon. [Proton-driven plasma-wakefield acceleration](#). *Nature Physics*, 5(5):363–367, May 2009. ISSN 1745-2473. doi:[10.1038/nphys1248](https://doi.org/10.1038/nphys1248).
- [28] A. Caldwell, E. Gschwendtner, K. Lotov, P. Muggli, and M. Wing. [AWAKE Status Report, 2015](#). Technical Report CERN-SPSC-2015-032. SPSC-SR-169, CERN, Geneva, Switzerland, Oct. 2015.
- [29] Y. W. Chan. [Ultra-intense laser radiation as a possible energy booster for relativistic charged particle](#). *Physics Letters A*, 35(4):305–306, June 1971. ISSN 0375-9601. doi:[10.1016/0375-9601\(71\)90397-5](https://doi.org/10.1016/0375-9601(71)90397-5).

BIBLIOGRAPHY

- [30] F. F. Chen. *Introduction to Plasma Physics*. Springer, Boston, MA, 1974. ISBN 978-1-4757-0459-4. <https://doi.org/10.1007/978-1-4757-0459-4>.
- [31] P. Chen, J. M. Dawson, R. W. Huff, and T. Katsouleas. **Acceleration of Electrons by the Interaction of a Bunched Electron Beam with a Plasma**. *Physical Review Letters*, 54(7): 693–696, Feb. 1985. doi:[10.1103/PhysRevLett.54.693](https://doi.org/10.1103/PhysRevLett.54.693).
- [32] P. Chen, J. J. Su, T. Katsouleas, S. Wilks, and J. M. Dawson. Plasma Focusing for High-Energy Beams. *IEEE Transactions on Plasma Science*, 15(2):218–225, Apr. 1987. ISSN 0093-3813. doi:[10.1109/TPS.1987.4316688](https://doi.org/10.1109/TPS.1987.4316688).
- [33] E. Chevallay, M. Csatari, A. Dabrowski, S. Doebert, D. Egger, V. Fedosseev, Oznur Mete, M. Olvegaard, and M. Petrarca. **PHIN photo-injector as the CLIC drive beam source**. *Journal of Physics: Conference Series*, 347(1):012036, 2012. ISSN 1742-6596. doi:[10.1088/1742-6596/347/1/012036](https://doi.org/10.1088/1742-6596/347/1/012036).
- [34] E. D. Courant and H. S. Snyder. **Theory of the alternating-gradient synchrotron**. *Annals of Physics*, 3(1):1–48, Jan. 1958. ISSN 0003-4916. doi:[10.1016/0003-4916\(58\)90012-5](https://doi.org/10.1016/0003-4916(58)90012-5).
- [35] J. M. Dawson. **Nonlinear Electron Oscillations in a Cold Plasma**. *Physical Review*, 113 (2):383–387, Jan. 1959. doi:[10.1103/PhysRev.113.383](https://doi.org/10.1103/PhysRev.113.383).
- [36] G. P. Djotyan, J. S. Bakos, M. Á. Kedves, B. Ráczkevi, D. Dzsotjan, K. Varga-Umbrich, Z. Sörlei, J. Szigeti, P. Ignácz, P. Lévai, A. Czitrovszky, A. Nagy, P. Dombi, and P. Rácz. **Real-time interferometric diagnostics of rubidium plasma**. *Nuclear Instruments and Methods in Physics Research Section A: Accelerators, Spectrometers, Detectors and Associated Equipment*, 884:25–30, Mar. 2018. ISSN 0168-9002. doi:[10.1016/j.nima.2017.12.004](https://doi.org/10.1016/j.nima.2017.12.004).
- [37] B. J. Duda and W. B. Mori. **Variational principle approach to short-pulse laser-plasma interactions in three dimensions**. *Physical Review E*, 61(2):1925–1939, Feb. 2000. doi:[10.1103/PhysRevE.61.1925](https://doi.org/10.1103/PhysRevE.61.1925).
- [38] B. J. Duda, R. G. Hemker, K. C. Tzeng, and W. B. Mori. **A Long-Wavelength Hosing Instability in Laser-Plasma Interactions**. *Physical Review Letters*, 83(10):1978–1981, Sept. 1999. doi:[10.1103/PhysRevLett.83.1978](https://doi.org/10.1103/PhysRevLett.83.1978).
- [39] E. Esarey, J. Krall, and P. Sprangle. **Envelope analysis of intense laser pulse self-modulation in plasmas**. *Physical Review Letters*, 72(18):2887–2890, May 1994. doi:[10.1103/PhysRevLett.72.2887](https://doi.org/10.1103/PhysRevLett.72.2887).
- [40] E. Esarey, P. Sprangle, J. Krall, and A. Ting. **Overview of plasma-based accelerator concepts**. *IEEE Transactions on Plasma Science*, 24(2):252–288, Apr. 1996. ISSN 0093-3813. doi:[10.1109/27.509991](https://doi.org/10.1109/27.509991).

- [41] Y. Fang, V. E. Yakimenko, M. Babzien, M. Fedurin, K. P. Kusche, R. Malone, J. Vieira, W. B. Mori, and P. Muggli. [Seeding of Self-Modulation Instability of a Long Electron Bunch in a Plasma](#). *Physical Review Letters*, 112(4):045001, Jan. 2014. doi:[10.1103/PhysRevLett.112.045001](https://doi.org/10.1103/PhysRevLett.112.045001).
- [42] R. A. Fonseca. Introduction to OSIRIS 4.0 for developers (and users). Presentation. OSIRIS Workshop 2017, 2017.
- [43] R. A. Fonseca, L. O. Silva, F. S. Tsung, V. K. Decyk, W. Lu, C. Ren, W. B. Mori, S. Deng, S. Lee, T. Katsouleas, and J. C. Adam. OSIRIS: A Three-Dimensional, Fully Relativistic Particle in Cell Code for Modeling Plasma Based Accelerators. In P. M. A. Sloot, A. G. Hoekstra, C. J. K. Tan, and J. J. Dongarra, editors, *Computational Science — ICCS 2002*, number 2331 in Lecture Notes in Computer Science, pages 342–351. Springer Berlin Heidelberg, 2002. ISBN 978-3-540-43594-5 978-3-540-47789-1. http://link.springer.com/chapter/10.1007/3-540-47789-6_36.
- [44] S. Gessner. [AWAKE: The proton beam-driven plasma wakefield experiment](#). BE-CO technical meeting, Mar. 2018. <https://indico.cern.ch/event/704904>.
- [45] B. B. Godfrey. [Numerical Cherenkov instabilities in electromagnetic particle codes](#). *Journal of Computational Physics*, 15(4):504–521, Aug. 1974. ISSN 0021-9991. doi:[10.1016/0021-9991\(74\)90076-X](https://doi.org/10.1016/0021-9991(74)90076-X).
- [46] R. Gorbonosov. [Control Systems at CERN](#). AWAKE Collaboration Meeting, Apr. 2013. <https://indico.cern.ch/event/282031>.
- [47] P. Goupillaud, A. Grossmann, and J. Morlet. [Cycle-octave and related transforms in seismic signal analysis](#). *Geoexploration*, 23(1):85–102, Oct. 1984. ISSN 0016-7142. doi:[10.1016/0016-7142\(84\)90025-5](https://doi.org/10.1016/0016-7142(84)90025-5).
- [48] A. D. Greenwood, K. L. Cartwright, J. W. Luginsland, and E. A. Baca. [On the elimination of numerical Cerenkov radiation in PIC simulations](#). *Journal of Computational Physics*, 201(2):665–684, Dec. 2004. ISSN 0021-9991. doi:[10.1016/j.jcp.2004.06.021](https://doi.org/10.1016/j.jcp.2004.06.021).
- [49] E. Gschwendtner, K. Cornelis, I. Efthymiopoulos, A. Ferrari, A. Pardons, W. Treberspurg, H. Vincke, J. Wenninger, D. Autiero, A. Guglielmi, and P. Sala. [Performance and Operational Experience of the CNGS Facility](#). In *Proceedings of IPAC 2010*, pages 4164–4166, Kyoto, Japan, May 2010. JACoW. ISBN 978-92-9083-352-9. THPEC046.
- [50] E. Gschwendtner, T. Bohl, C. Bracco, A. Butterworth, S. Cipiccia, S. Doebert, V. Fedossev, E. Feldbaumer, C. Hessler, W. Hofle, M. Martyanov, M. Meddahi, J. Osborne, A. Pardons, A. Petrenko, and H. Vincke. [The AWAKE Experimental Facility at CERN](#). In *Proceedings of IPAC 2014*, pages 582–585, Dresden, Germany, 2014. JACoW. ISBN 978-3-95450-132-8. MOPRI005.

- [51] E. Gschwendtner, E. Adli, L. Amorim, R. Apsimon, R. Assmann, A. M. Bachmann, F. Batsch, J. Bauche, V. K. Berglyd Olsen, M. Bernardini, R. Bingham, B. Biskup, T. Bohl, C. Bracco, P. N. Burrows, G. Burt, B. Buttenschön, A. Butterworth, A. Caldwell, M. Cassella, E. Chevallay, S. Cipiccia, H. Damerau, L. Deacon, P. Dirksen, S. Doeberl, U. Dorda, J. Farmer, V. Fedosseev, E. Feldbaumer, R. Fiorito, R. Fonseca, F. Friebel, A. A. Gorn, O. Grulke, J. Hansen, C. Hessler, W. Hofle, J. Holloway, M. Hüther, D. Jaroszynski, L. Jensen, S. Jolly, A. Joulaei, M. Kasim, F. Keeble, Y. Li, S. Liu, N. Lopes, K. V. Lotov, S. Mandry, R. Martorelli, M. Martyanov, S. Mazzoni, O. Mete, V. A. Minakov, J. Mitchell, J. Moody, P. Muggli, Z. Najmudin, P. Norreys, E. Öz, A. Pardons, K. Pepitone, A. Petrenko, G. Plyushchev, A. Pukhov, K. Rieger, H. Ruhl, F. Salveter, N. Savard, J. Schmidt, A. Seryi, E. Shaposhnikova, Z. M. Sheng, P. Sherwood, L. Silva, L. Soby, A. P. Sosedkin, R. I. Spitsyn, R. Trines, P. V. Tuev, M. Turner, V. Verzilov, J. Vieira, H. Vincke, Y. Wei, C. P. Welsch, M. Wing, G. Xia, and H. Zhang. [AWAKE, The Advanced Proton Driven Plasma Wakefield Acceleration Experiment at CERN](#). *Nuclear Instruments and Methods in Physics Research Section A*, 829:76–82, Sept. 2016. ISSN 0168-9002. doi:[10.1016/j.nima.2016.02.026](https://doi.org/10.1016/j.nima.2016.02.026).
- [52] R. Hatzky and A. Bottino. Particle-in-Cell methods in plasma physics. Presentation, Oct. 2010.
- [53] M. J. Hogan. [Electron and Positron Beam–Driven Plasma Acceleration](#). *Reviews of Accelerator Science and Technology*, 09:63–83, Jan. 2016. ISSN 1793-6268. doi:[10.1142/S1793626816300036](https://doi.org/10.1142/S1793626816300036).
- [54] M. J. Hogan, C. E. Clayton, C. Huang, P. Muggli, S. Wang, B. E. Blue, D. Walz, K. A. Marsh, C. L. O’Connell, S. Lee, R. Iverson, F.-J. Decker, P. Raimondi, W. B. Mori, T. C. Katsouleas, C. Joshi, and R. H. Siemann. [Ultrarelativistic-Positron-Beam Transport through Meter-Scale Plasmas](#). *Physical Review Letters*, 90(20):205002, May 2003. doi:[10.1103/PhysRevLett.90.205002](https://doi.org/10.1103/PhysRevLett.90.205002).
- [55] H. Hotchi, H. Harada, N. Hayashi, M. Kinsho, P. Saha, Y. Shobuda, F. Tamura, K. Yamamoto, M. Yamamoto, M. Yoshimoto, S. Kato, Y. Irie, T. Koseki, Y. Sato, K. Satou, and M. Shirakata. [Beam commissioning and operation of the Japan Proton Accelerator Research Complex 3-GeV rapid cycling synchrotron](#). *Progress of Theoretical and Experimental Physics*, 2012(1), Jan. 2012. doi:[10.1093/ptep/pts021](https://doi.org/10.1093/ptep/pts021).
- [56] C. Huang, V. K. Decyk, C. Ren, M. Zhou, W. Lu, W. B. Mori, J. H. Cooley, T. M. Antonsen, and T. Katsouleas. [QUICKPIC: A highly efficient particle-in-cell code for modeling wakefield acceleration in plasmas](#). *Journal of Computational Physics*, 217(2): 658–679, Sept. 2006. ISSN 0021-9991. doi:[10.1016/j.jcp.2006.01.039](https://doi.org/10.1016/j.jcp.2006.01.039).
- [57] S. Ivanov. [Accelerator Complex U70 of IHEP: Status and Upgrades](#). In *Proceedings of RuPAC2014*, Obninsk, Russia, 2014. JACoW. ISBN 978-3-95450-170-0. TUX02.

- [58] C. Jing, A. Kanareykin, J. Power, M. Conde, Z. Yusof, and W. Gai. [Observation of Enhanced Transformer Ratio in Collinear Wakefield Acceleration](#). *AIP Conference Proceedings*, 877(1):511–519, Nov. 2006. ISSN 0094-243X. doi:[10.1063/1.2409177](https://doi.org/10.1063/1.2409177).
- [59] C. Jing, A. Kanareykin, J. G. Power, M. Conde, Z. Yusof, P. Schoessow, and W. Gai. [Observation of Enhanced Transformer Ratio in Collinear Wakefield Acceleration](#). *Physical Review Letters*, 98(14):144801, Apr. 2007. doi:[10.1103/PhysRevLett.98.144801](https://doi.org/10.1103/PhysRevLett.98.144801).
- [60] E. Kallos, T. Katsouleas, P. Muggli, I. Pavlishin, I. Pogorelsky, D. Stolyarov, V. Yakinenko, and W. D. Kimura. Plasma wakefield acceleration utilizing multiple electron bunches. In *2007 IEEE Particle Accelerator Conference (PAC)*, pages 3070–3072, June 2007. doi:[10.1109/PAC.2007.4440671](https://doi.org/10.1109/PAC.2007.4440671).
- [61] T. Katsouleas, S. Wilks, P. Chen, J. M. Dawson, and J. J. Su. [Beam loading in plasma accelerators](#). *Particle Accelerators*, 22(18):81–99, 1987.
- [62] R. Keinigs and M. E. Jones. [Two-dimensional dynamics of the plasma wakefield accelerator](#). *The Physics of Fluids*, 30(1):252–263, Jan. 1987. ISSN 0031-9171. doi:[10.1063/1.866183](https://doi.org/10.1063/1.866183).
- [63] J. Krall and G. Joyce. [Transverse equilibrium and stability of the primary beam in the plasma wake-field accelerator](#). *Physics of Plasmas*, 2(4):1326–1331, Apr. 1995. ISSN 1070-664X. doi:[10.1063/1.871344](https://doi.org/10.1063/1.871344).
- [64] N. Kumar, A. Pukhov, and K. Lotov. [Self-Modulation Instability of a Long Proton Bunch in Plasmas](#). *Physical Review Letters*, 104(25):255003, June 2010. doi:[10.1103/PhysRevLett.104.255003](https://doi.org/10.1103/PhysRevLett.104.255003).
- [65] D. T. Lee and A. Yamamoto. [Wavelet analysis: theory and applications](#). *Hewlett-Packard Journal*, 45:44–54, Dec. 1994.
- [66] E. P. Lee and R. K. Cooper. [General envelope equation for cylindrically symmetric charged-particle beams](#). *Particle Accelerators*, 7(2):83–95, 1976.
- [67] S. Lee, T. Katsouleas, R. Hemker, and W. B. Mori. [Simulations of a meter-long plasma wakefield accelerator](#). *Physical Review E*, 61(6):7014–7021, June 2000. doi:[10.1103/PhysRevE.61.7014](https://doi.org/10.1103/PhysRevE.61.7014).
- [68] S. Lee, T. Katsouleas, R. G. Hemker, E. S. Dodd, and W. B. Mori. [Plasma-wakefield acceleration of a positron beam](#). *Physical Review E*, 64(4):045501, Sept. 2001. doi:[10.1103/PhysRevE.64.045501](https://doi.org/10.1103/PhysRevE.64.045501).
- [69] R. Lehe, A. Lifschitz, C. Thaury, V. Malka, and X. Davoine. [Numerical growth of emittance in simulations of laser-wakefield acceleration](#). *Physical Review Special Topics - Accelerators and Beams*, 16(2):021301, Feb. 2013. doi:[10.1103/PhysRevSTAB.16.021301](https://doi.org/10.1103/PhysRevSTAB.16.021301).

- [70] M. Litos, E. Adli, W. An, C. I. Clarke, C. E. Clayton, S. Corde, J. P. Delahaye, R. J. England, A. S. Fisher, J. Frederico, S. Gessner, S. Z. Green, M. J. Hogan, C. Joshi, W. Lu, K. A. Marsh, W. B. Mori, P. Muggli, N. Vafaei-Najafabadi, D. Walz, G. White, Z. Wu, V. Yakimenko, and G. Yocky. [High-efficiency acceleration of an electron beam in a plasma wakefield accelerator](#). *Nature*, 515(7525):92–95, Nov. 2014. ISSN 0028-0836. doi:[10.1038/nature13882](https://doi.org/10.1038/nature13882).
- [71] K. V. Lotov. [Simulation of proton driven plasma wakefield acceleration](#). *Physical Review Special Topics - Accelerators and Beams*, 13(4):041301, Apr. 2010. doi:[10.1103/PhysRevSTAB.13.041301](https://doi.org/10.1103/PhysRevSTAB.13.041301).
- [72] K. V. Lotov. [Stable bunch trains for plasma wakefield acceleration](#). *Plasma Physics and Controlled Fusion*, 60(2):024002, 2018. ISSN 0741-3335. doi:[10.1088/1361-6587/aa9f97](https://doi.org/10.1088/1361-6587/aa9f97).
- [73] W. Lu, C. Huang, M. M. Zhou, W. B. Mori, and T. Katsouleas. [Limits of linear plasma wakefield theory for electron or positron beams](#). *Physics of Plasmas*, 12(6):063101, May 2005. ISSN 1070-664X. doi:[10.1063/1.1905587](https://doi.org/10.1063/1.1905587).
- [74] W. Lu, C. Huang, M. Zhou, W. B. Mori, and T. Katsouleas. [Nonlinear Theory for Relativistic Plasma Wakefields in the Blowout Regime](#). *Physical Review Letters*, 96(16):165002, Apr. 2006. doi:[10.1103/PhysRevLett.96.165002](https://doi.org/10.1103/PhysRevLett.96.165002).
- [75] W. Lu, C. Huang, M. Zhou, M. Tzoufras, F. S. Tsung, W. B. Mori, and T. Katsouleas. [A nonlinear theory for multidimensional relativistic plasma wave wakefieldsa\)](#). *Physics of Plasmas (1994-present)*, 13(5):056709, May 2006. ISSN 1070-664X, 1089-7674. doi:[10.1063/1.2203364](https://doi.org/10.1063/1.2203364).
- [76] V. Malka and P. Mora. [Principles of laser–plasma accelerators](#). *Comptes Rendus Physique*, 10(2):106–115, Mar. 2009. ISSN 1631-0705. doi:[10.1016/j.crhy.2009.03.008](https://doi.org/10.1016/j.crhy.2009.03.008).
- [77] E. Mobs. [The CERN accelerator complex. Complexe des accélérateurs du CERN](#). Illustration. OPEN-PHO-ACCEL-2016-009, July 2016. <https://cds.cern.ch/record/2197559>.
- [78] A. Modena, Z. Najmudin, A. E. Dangor, C. E. Clayton, K. A. Marsh, C. Joshi, V. Malka, C. B. Darrow, C. Danson, D. Neely, and F. N. Walsh. [Electron acceleration from the breaking of relativistic plasma waves](#). *Nature*, 377(6550):377606a0, Oct. 1995. ISSN 1476-4687. doi:[10.1038/377606a0](https://doi.org/10.1038/377606a0).
- [79] P. Muggli. [Beam-driven, Plasma-based Particle Accelerators](#). In *CAS - CERN Accelerator School: Plasma Wake Acceleration*, pages 119–142, CERN, Geneva, Switzerland, May 2017. ISBN 978-92-9083-424-3. doi:[10.5170/CERN-2016-001.119](https://doi.org/10.5170/CERN-2016-001.119). arXiv: 1705.10537.
- [80] P. Muggli and M. J. Hogan. [Review of high-energy plasma wakefield experiments](#). *Comptes Rendus Physique*, 10(2):116–129, Mar. 2009. ISSN 1631-0705. doi:[10.1016/j.crhy.2009.03.004](https://doi.org/10.1016/j.crhy.2009.03.004).

- [81] P. Muggli, B. E. Blue, C. E. Clayton, F. J. Decker, M. J. Hogan, C. Huang, C. Joshi, T. C. Katsouleas, W. Lu, W. B. Mori, C. L. O’Connell, R. H. Siemann, D. Walz, and M. Zhou. [Halo Formation and Emittance Growth of Positron Beams in Plasmas](#). *Physical Review Letters*, 101(5):055001, July 2008. doi:[10.1103/PhysRevLett.101.055001](https://doi.org/10.1103/PhysRevLett.101.055001).
- [82] P. Muggli, O. Reimann, E. Adli, V. Olsen, L. Amorim, S. Gessner, M. Hogan, S. Li, M. Litos, C. Joshi, K. Marsh, W. Mori, N. Vafaei-Najafabadi, N. Lopes, and J. Vieira. [Electron Bunch Self-modulation in Long Plasmas at SLAC FACET](#). In *Proceedings of IPAC 2014*, pages 1476–1478, Dresden, Germany, 2014. JACoW. ISBN 978-3-95450-132-8.
- [83] P. Muggli, O. Reimann, L. D. Amorim, N. C. Lopes, L. O. Silva, J. M. Vieira, J. Allen, S. J. Gessner, M. Hogan, S. Z. Green, M. D. Litos, B. D. O’Shea, V. Yakimenko, G. Andonian, C. Joshi, K. Marsh, W. Mori, N. Vafaei-Najafabadi, O. Williams, E. Adli, C. A. Lindstrom, and V. B. Olsen. [Measuring the Self-Modulation Instability of Electron and Positron Bunches in Plasmas](#). In *Proceedings of IPAC 2015*, pages 2506–2508, Richmond, VA, USA, 2015. JACoW. ISBN 978-3-95450-168-7. WEPWA008.
- [84] P. Muggli, E. Adli, R. Apsimon, F. Asmus, R. Baartman, A.-M. Bachmann, M. B. Marin, F. Batsch, J. Bauche, V. K. B. Olsen, M. Bernardini, B. Biskup, E. B. Vinuela, A. Boccardi, T. Bogey, T. Bohl, C. Bracco, F. Braunmuller, S. Burger, G. Burt, S. Bustamante, B. Buttenschön, A. Butterworth, A. Caldwell, M. Cascella, E. Chevallay, M. Chung, H. Damerau, L. Deacon, A. Dexter, P. Dirksen, S. Doeberl, J. Farmer, V. Fedosseev, T. Feniet, G. Fior, R. Fiorito, R. Fonseca, F. Friebel, P. Gander, S. Gessner, I. Gorgisyan, A. A. Gorn, O. Grulke, E. Gschwendtner, A. Guerrero, J. Hansen, C. Hessler, W. Hofle, J. Holloway, M. Hüther, M. Ibison, M. R. Islam, L. Jensen, S. Jolly, M. Kasim, F. Keeble, S.-Y. Kim, F. Kraus, A. Lasheen, T. Lefevre, G. LeGodec, Y. Li, S. Liu, N. Lopes, K. V. Lotov, M. Martyanov, S. Mazzoni, D. M. Godoy, O. Mete, V. A. Minakov, R. Mompo, J. Moody, M. T. Moreira, J. Mitchell, C. Mutin, P. Norreys, E. Öz, E. Ozturk, W. Pauw, A. Pardons, C. Pasquino, K. Pepitone, A. Petrenko, S. Pitmann, G. Plyushchev, A. Pukhov, K. Rieger, H. Ruhl, J. Schmidt, I. A. Shalimova, E. Shaposhnikova, P. Sherwood, L. Silva, A. P. Sosedkin, R. Speroni, R. I. Spitsyn, K. Szczurek, J. Thomas, P. V. Tuev, M. Turner, V. Verzilov, J. Vieira, H. Vincke, C. P. Welsch, B. Williamson, M. Wing, G. Xia, H. Zhang, and T. A. collaboration. [AWAKE readiness for the study of the seeded self-modulation of a 400 GeV proton bunch](#). *Plasma Physics and Controlled Fusion*, 60(1):014046, Nov. 2017. ISSN 0741-3335. doi:[10.1088/1361-6587/aa941c](https://doi.org/10.1088/1361-6587/aa941c).
- [85] S. Nagaitsev. [Fermilab Antiproton Source, Recycler Ring, and Main Injector](#). arXiv:1408.0759 [hep-ex, physics:physics], Aug. 2014. arXiv: 1408.0759.
- [86] K. Nakajima, A. Enomoto, H. Kobayashi, H. Nakanishi, Y. Nishida, A. Ogata, S. Ohsawa, T. Oogoe, T. Shoji, and T. Urano. [Plasma wake-field accelerator experiments at KEK](#). *Nuclear Instruments and Methods in Physics Research Section A: Accelerators, Spectrometers, Detectors and Associated Equipment*, 292(1):12–20, June 1990. ISSN 0168-9002. doi:[10.1016/0168-9002\(90\)91729-U](https://doi.org/10.1016/0168-9002(90)91729-U).

BIBLIOGRAPHY

- [87] E. Öz, F. Batsch, and P. Muggli. [An accurate Rb density measurement method for a plasma wakefield accelerator experiment using a novel Rb reservoir](#). *Nuclear Instruments and Methods in Physics Research Section A: Accelerators, Spectrometers, Detectors and Associated Equipment*, 829:321–325, Sept. 2016. ISSN 01689002. doi:[10.1016/j.nima.2016.02.005](https://doi.org/10.1016/j.nima.2016.02.005). arXiv: 1511.08763.
- [88] R. B. Palmer. [Interaction of Relativistic Particles and Free Electromagnetic Waves in the Presence of a Static Helical Magnet](#). *Journal of Applied Physics*, 43(7):3014–3023, July 1972. ISSN 0021-8979. doi:[10.1063/1.1661650](https://doi.org/10.1063/1.1661650).
- [89] H. L. Pécseli. *Waves and Oscillations in Plasmas*. CRC Press, Boca Raton, 1st edition, Sept. 2012. ISBN 978-1-4398-7848-4.
- [90] K. Pepitone, S. Doeberl, G. Burt, E. Chevallay, N. Chritin, C. Delory, V. Fedosseev, C. Hessler, G. McMonagle, O. Mete, V. Verzilov, and R. Apsimon. [The electron accelerator for the AWAKE experiment at CERN](#). *Nuclear Instruments and Methods in Physics Research Section A: Accelerators, Spectrometers, Detectors and Associated Equipment*, 829(Supplement C):73–75, Sept. 2016. ISSN 0168-9002. doi:[10.1016/j.nima.2016.02.025](https://doi.org/10.1016/j.nima.2016.02.025).
- [91] F. Pozzi, T. D. Matteo, and T. Aste. [Exponential smoothing weighted correlations](#). *The European Physical Journal B*, 85(6):175, June 2012. ISSN 1434-6028, 1434-6036. doi:[10.1140/epjb/e2012-20697-x](https://doi.org/10.1140/epjb/e2012-20697-x).
- [92] T. Pratchett. *Equal Rites*. Number 3 in Discworld. Gollancz, 1987. ISBN 0-575-03950-7.
- [93] D. P. Pritchau and R. H. Siemann. [Experimental Study of RF Pulsed Heating on Oxygen Free Electronic Copper](#). *Physical Review Special Topics - Accelerators and Beams*, 5(11):112002, Nov. 2002. doi:[10.1103/PhysRevSTAB.5.112002](https://doi.org/10.1103/PhysRevSTAB.5.112002).
- [94] A. Pukhov and J. Meyer-ter Vehn. [Laser wake field acceleration: the highly non-linear broken-wave regime](#). *Applied Physics B*, 74(4-5):355–361, Apr. 2002. ISSN 0946-2171, 1432-0649. doi:[10.1007/s003400200795](https://doi.org/10.1007/s003400200795).
- [95] J. B. Rosenzweig, D. B. Cline, B. Cole, H. Figueroa, W. Gai, R. Konecny, J. Norem, P. Schoessow, and J. Simpson. [Experimental Observation of Plasma Wake-Field Acceleration](#). *Physical Review Letters*, 61(1):98–101, July 1988. doi:[10.1103/PhysRevLett.61.98](https://doi.org/10.1103/PhysRevLett.61.98).
- [96] J. B. Rosenzweig, B. Breizman, T. Katsouleas, and J. J. Su. [Acceleration and focusing of electrons in two-dimensional nonlinear plasma wake fields](#). *Physical Review A*, 44(10):R6189–R6192, Nov. 1991. doi:[10.1103/PhysRevA.44.R6189](https://doi.org/10.1103/PhysRevA.44.R6189).
- [97] J. B. Rosenzweig, A. M. Cook, A. Scott, M. C. Thompson, and R. B. Yoder. [Effects of Ion Motion in Intense Beam-Driven Plasma Wakefield Accelerators](#). *Physical Review Letters*, 95(19):195002, Oct. 2005. doi:[10.1103/PhysRevLett.95.195002](https://doi.org/10.1103/PhysRevLett.95.195002).

- [98] J. B. Rosenzweig, G. Andonian, M. Ferrario, P. Muggli, O. Williams, V. Yakimenko, and K. Xuan. [Plasma Wakefields in the Quasi-Nonlinear Regime](#). *AIP Conference Proceedings*, 1299(1):500–504, Nov. 2010. ISSN 0094-243X. doi:[10.1063/1.3520373](https://doi.org/10.1063/1.3520373).
- [99] R. D. Ruth, P. Morton, P. B. Wilson, and A. Chao. [A Plasma Wake Field Accelerator](#). *Particle Accelerators*, 17(SLAC-PUB-3374):171–189, 1985.
- [100] F. Salin, P. Georges, G. Roger, and A. Brun. [Single-shot measurement of a 52-fs pulse](#). *Applied Optics*, 26(21):4528–4531, Nov. 1987. ISSN 1539-4522. doi:[10.1364/AO.26.004528](https://doi.org/10.1364/AO.26.004528).
- [101] K. Schindl. [Space charge](#). In *Proceedings of the Joint US–CERN–Japan–Russia School on Particle Accelerators*, pages 127–151, Montreux and CERN, Switzerland, May 1999. World Scientific. ISBN 978-981-02-3881-0. doi:[10.1142/9789812818003_0004](https://doi.org/10.1142/9789812818003_0004).
- [102] C. B. Schroeder, C. Benedetti, E. Esarey, F. J. Grüner, and W. P. Leemans. [Growth and Phase Velocity of Self-Modulated Beam-Driven Plasma Waves](#). *Physical Review Letters*, 107(14):145002, Sept. 2011. doi:[10.1103/PhysRevLett.107.145002](https://doi.org/10.1103/PhysRevLett.107.145002).
- [103] C. B. Schroeder, C. Benedetti, E. Esarey, F. J. Grüner, and W. P. Leemans. [Particle beam self-modulation instability in tapered and inhomogeneous plasma](#). *Physics of Plasmas*, 19(1):010703, Jan. 2012. ISSN 1070-664X, 1089-7674. doi:[10.1063/1.3677358](https://doi.org/10.1063/1.3677358).
- [104] A. Schwinn, S. Matthies, D. Pfeiffer, M. Arruat, L. Fernandez, F. Locci, and D. G. Saavedra. [FESA3 – The New Front-End Software Framework at CERN and the FAIR Facility](#). In *Proceedings of PCaPAC 2010*, pages 22–26, Saskatoon, Saskatchewan, Canada, 2010. JACoW. ISBN 978-1-63266-483-9. WECOAA03.
- [105] Y. Sentoku, K. Mima, P. Kaw, and K. Nishikawa. [Anomalous Resistivity Resulting from MeV-Electron Transport in Overdense Plasma](#). *Physical Review Letters*, 90(15):155001, Apr. 2003. doi:[10.1103/PhysRevLett.90.155001](https://doi.org/10.1103/PhysRevLett.90.155001).
- [106] G. Stancari, V. Previtali, A. Valishev, R. Bruce, S. Redaelli, A. Rossi, and B. S. Ferrando. [Conceptual design of hollow electron lenses for beam halo control in the Large Hadron Collider](#). *arXiv:1405.2033 [physics]*, May 2014. arXiv: 1405.2033.
- [107] J. J. Su, T. Katsouleas, J. M. Dawson, and R. Fedele. [Plasma lenses for focusing particle beams](#). *Physical Review A*, 41(6):3321–3331, Mar. 1990. doi:[10.1103/PhysRevA.41.3321](https://doi.org/10.1103/PhysRevA.41.3321).
- [108] T. Tajima and J. M. Dawson. [Laser Electron Accelerator](#). *Physical Review Letters*, 43(4): 267–270, July 1979. doi:[10.1103/PhysRevLett.43.267](https://doi.org/10.1103/PhysRevLett.43.267).
- [109] L. Tonks and I. Langmuir. [Oscillations in Ionized Gases](#). *Physical Review*, 33(2):195–210, Feb. 1929. doi:[10.1103/PhysRev.33.195](https://doi.org/10.1103/PhysRev.33.195).

BIBLIOGRAPHY

- [110] C. Torrence and G. P. Compo. [A Practical Guide to Wavelet Analysis](#). *Bulletin of the American Meteorological Society*, 79(1):61–78, Jan. 1998. ISSN 0003-0007. doi:[10.1175/1520-0477\(1998\)079<0061:APGTWA>2.0.CO;2](https://doi.org/10.1175/1520-0477(1998)079<0061:APGTWA>2.0.CO;2).
- [111] M. Turner. [First Observation of the Seeded Proton Bunch Self-Modulation in Plasma](#). PhD thesis, Technical University of Graz, Dec. 2017.
- [112] M. Tzoufras, W. Lu, F. S. Tsung, C. Huang, W. B. Mori, T. Katsouleas, J. Vieira, R. A. Fonseca, and L. O. Silva. [Beam loading by electrons in nonlinear plasma wakes](#). *Physics of Plasmas*, 16(5):056705, May 2009. ISSN 1070-664X, 1089-7674. doi:[10.1063/1.3118628](https://doi.org/10.1063/1.3118628).
- [113] UCLA Plasma Simulation Group. [QuickPIC-OpenSource](#). repository. GitHub repository, 2017. <https://github.com/UCLA-Plasma-Simulation-Group/QuickPIC-OpenSource>.
- [114] S. Van der Meer. [Improving the power efficiency of the plasma wakefield accelerator](#). Technical Report CERN/PS/85-65 (AA), CLIC Note No. 3, CERN, Geneva, Nov. 1985.
- [115] C. Van Loan. [Computational Frameworks for the Fast Fourier Transform](#). Frontiers in Applied Mathematics. Society for Industrial and Applied Mathematics, Jan. 1992. ISBN 978-0-89871-285-8. <https://epubs.siam.org/doi/book/10.1137/1.9781611970999>. DOI: 10.1137/1.9781611970999.
- [116] J.-L. Vay. [Simulation of beams or plasmas crossing at relativistic velocity](#). *Physics of Plasmas*, 15(5):056701, Feb. 2008. ISSN 1070-664X. doi:[10.1063/1.2837054](https://doi.org/10.1063/1.2837054).
- [117] J.-L. Vay and R. Lehe. [Simulations for Plasma and Laser Acceleration](#). *Reviews of Accelerator Science and Technology*, 09:165–186, Jan. 2016. ISSN 1793-6268. doi:[10.1142/S1793626816300085](https://doi.org/10.1142/S1793626816300085).
- [118] J.-L. Vay, C. G. R. Geddes, E. Esarey, C. B. Schroeder, W. P. Leemans, E. Cormier-Michel, and D. P. Grote. [Modeling of 10 GeV-1 TeV laser-plasma accelerators using Lorentz boosted simulations](#). *Physics of Plasmas*, 18(12):123103, Dec. 2011. ISSN 1070-664X. doi:[10.1063/1.3663841](https://doi.org/10.1063/1.3663841).
- [119] J. Vieira, Y. Fang, W. B. Mori, L. O. Silva, and P. Muggli. [Transverse self-modulation of ultra-relativistic lepton beams in the plasma wakefield accelerator](#). *Physics of Plasmas*, 19(6):063105, June 2012. ISSN 1070-664X, 1089-7674. doi:[10.1063/1.4725425](https://doi.org/10.1063/1.4725425).
- [120] J. Vieira, R. A. Fonseca, W. B. Mori, and L. O. Silva. [Ion Motion in Self-Modulated Plasma Wakefield Accelerators](#). *Physical Review Letters*, 109(14):145005, Oct. 2012. doi:[10.1103/PhysRevLett.109.145005](https://doi.org/10.1103/PhysRevLett.109.145005).
- [121] J. Vieira, L. D. Amorim, Y. Fang, W. B. Mori, P. Muggli, and L. O. Silva. [Self-modulation instability of ultra-relativistic particle bunches with finite rise times](#). *Plasma Physics and Controlled Fusion*, 56(8):084014, 2014. ISSN 0741-3335. doi:[10.1088/0741-3335/56/8/084014](https://doi.org/10.1088/0741-3335/56/8/084014).

- [122] J. Vieira, W. B. Mori, and P. Muggli. [Hosing Instability Suppression in Self-Modulated Plasma Wakefields](#). *Physical Review Letters*, 112(20):205001, May 2014. doi:[10.1103/PhysRevLett.112.205001](https://doi.org/10.1103/PhysRevLett.112.205001).
- [123] D. H. Whittum, W. M. Sharp, S. S. Yu, M. Lampe, and G. Joyce. [Electron-hose instability in the ion-focused regime](#). *Physical Review Letters*, 67(8):991–994, Aug. 1991. doi:[10.1103/PhysRevLett.67.991](https://doi.org/10.1103/PhysRevLett.67.991).
- [124] K. Wille. *The Physics of Particle Accelerators: An Introduction*. Clarendon Press, Oxford, New York, first edition, May 2001. ISBN 978-0-19-850549-5.
- [125] K. Yee. Numerical solution of initial boundary value problems involving Maxwell's equations in isotropic media. *IEEE Transactions on Antennas and Propagation*, 14(3):302–307, May 1966. ISSN 0018-926X. doi:[10.1109/TAP.1966.1138693](https://doi.org/10.1109/TAP.1966.1138693).

